Geochemistry, age and structural character of the Au-hosting Uunimäki gabbro, SW Finland

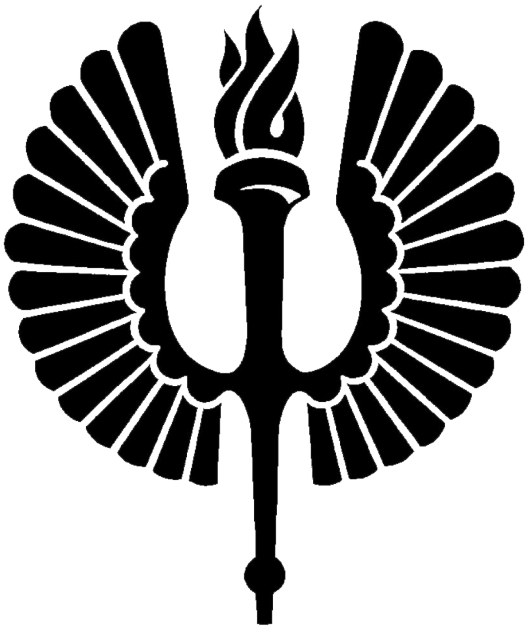

Tuomas Leskelä

University of Turku

Department of Geography and Geology

Geology section

March 2019

UNIVERSITY OF TURKU
Department of Geography and Geology, Geology section

LESKELÄ, TUOMAS: Geochemistry, age and structural character
of the Au-hosting Uunimäki gabbro, SW Finland

MSc thesis, 84 p. + 2 appendix pp.
Geology and mineralogy
March 2019

The western Häme Belt hosts several gold deposits, including the Uunimäki deposit, which is hosted by a gabbro. There are three main goals in this study: (i) age determination of the Uunimäki gabbro, (ii) geochemical classification of the gabbro, as well as comparison to other gold-hosting rocks in the western Häme Belt, (iii) structural characterisation of the Uunimäki area and its surroundings.

The age determination was performed with zircon U-Pb geochronology and yielded a concordia age of 1891 ± 5 Ma. This makes the Uunimäki gabbro one of the oldest plutonic rocks in the Häme Belt.

Geochemically, the Uunimäki gabbro is more mafic when compared to the two other gold-hosting intrusions in the area, the Jokisivu and Palokallio diorites. Major element geochemistry suggests that the Uunimäki gabbro is simply less fractionated. However, trace element geochemistry reveals that the gabbro has not formed during arc-type magmatism as other plutonic rocks in the Häme Belt. The gabbro has several characteristics atypical for arc-type rocks: (i) it lacks the typical negative Ta-Nb anomaly compared to N-MORB compositions, (ii) it is not enriched in large ion lithophile elements, (iii) the REE-pattern of is relatively unfractionated.

New field observations and structural measurements were collected from the western Häme Belt, and were used with geophysical maps to divide the study area into structural domains. The Uunimäki gabbro is located at the junction of three of these structural domains: (i) steep NE-plunging folds immediately to the south and northwest, (ii) an ENE-WSW-trending shear zone immediately to the north and northeast, (iii) a large N-S-trending shear zone to the west. The gabbro displays three distinct structural orientations, and has undergone deformation in several stages in both ductile and brittle regimes. The NW-SE-trending structures that are dominant in the Uunimäki gabbro are interpreted to have formed during re-activation of weakness zones caused by shearing along the ENE-WSW-trending shear zones.

The Uunimäki gabbro is interpreted to represent the primitive arc that formed in the early stages of the development of the Häme Belt, based on the age determination and geochemical signatures indicative of primitive magmatism with respect to its surroundings. The gabbro underwent deformation in several stages, including opening of NW-SE-trending fractures into which gold was precipitated. The fractures were later re-activated as shear zones that can be observed on the surface today.

Keywords: geochronology, geochemistry, structural geology, orogenic gold

TURUN YLIOPISTO
Maantieteen ja geologian laitos, geologian osasto

LESKELÄ, TUOMAS: Geochemistry, age and structural character
of the Au-hosting Uunimäki gabbro, SW Finland

Pro gradu – tutkielma, 84 s. + 2 liites.
Geologia ja mineralogia
Maaliskuu 2019

Hämeen vulkaanisen jakson länsiosissa on useita kultaesiintymiä, mukaan lukien Uunimäen kultaesiintymä, jonka isäntäkivi on gabro. Tällä tutkimuksella on kolme päätavoitetta: (i) Uunimäen gabron ikämääritys, (ii) gabron geokemiallinen luokittelu ja vertailu muihin kultaa isännöiviin kiviin Hämeen vulkaanisen jakson länsiosissa, (iii) Uunimäen alueen rakenteellinen tulkinta.

Uunimäen gabron ikämääritys suoritettiin zirkoni-mineraaleista in situ U-Pb-iänmääritysmenetelmää käyttäen. Gabron concordia-iäksi määritettiin 1891 ± 5 Ma, mikä tekee siitä yhden Hämeen vulkaanisen jakson vanhimmista kivistä.

Uunimäen gabro on mafisempi, kuin vertailuun käytetyt Jokisivun ja Palokallio kultapitoiset dioriitit. Pääalkuaineoksidien pitoisuuksien perusteella tämä johtuu Uunimäen gabron vähäisemmästä fraktioitumisasteesta. Hivenainegeokemia kuitenkin paljastaa, että gabro ei ole muodostunut samassa vulkaaniseen kaareen liittyvässä magmatismissa kuin muut syväkivet Hämeen vulkaanisella jaksolla. Gabrolla on useita geokemiallisia piirteitä, jotka eivät ole tyypillisiä vulkaanisen kaaren magmatismille: (i) sillä ei ole negatiivista Ta-Nb anomaliaa verrattuna keskimääräisiin N-MORB-pitoisuuksiin, (ii) se ei ole rikastunut suuren ionisäteen litofiileihin, (iii) sen REE-koostumus osoittaa vähäistä fraktioitumista.

Hämeen vulkaanisen jakson länsiosista kerättiin uusia kenttähavaintoja ja rakennemittauksia. Yhdistämällä ne alueen geofysikaalisiin karttoihin, tutkimusalueen rakenteet jaettiin alayksiköihin. Uunimäen gabro sijaitsee kolmen rakenteellisen alayksikön risteyskohdassa: (i) poimuakseliltaan koilliseen kaatuva poimutus on vallitseva rakennepiirre Uunimäen etelä- ja luoteispuolilla, (ii) ENE-WSW-suuntainen hiertovyöhyke kulkee Uunimäen pohjois- ja koillispuolilla, (iii) suuri N-S-suuntainen hiertovyöhyke kulkee Uunimäen länsipuolella. Gabrossa voidaan nähdä kolme selkeää rakennesuuntaa, ja se on deformoitunut useassa vaiheessa, sekä hauraassa että plastisessa ympäristössä. Hallitsevat NW-SE-suuntaiset rakenteet tulkitaan syntyneen ENE-WSW-suuntaisen hiertovyöhykkeen aiheuttamien heikkousvyöhykkeiden myöhemmässä uudelleenaktivoitumisessa.

Uunimäen gabro tulkitaan edustavan primitiivistä kaarimagmatismia, ja muodostuneen Hämeen vulkaanisen jakson varhaisessa kehitysvaiheessa. Tulkinta perustuu gabron ikämäärityksen tuloksiin, sekä sen primitiivisempään geokemialliseen koostumukseen suhteessa ympäristöönsä. Gabro on deformoitunut useassa vaiheessa, joissa luode-kaakko-suuntaisiin ruhjeisiin on saostunut kultaa. Ruhjeet ovat uudelleenaktivoituneet ja muodostaneet hiertovyöhykkeitä, jotka ovat nykyään osittain paljastuneena kallion pinnalla.

Avainsanat: geokronologia, geokemia, rakennegeologia, orogeeniset kultamalmit

Table of Contents

1. Introduction 1
   1.1 Orogens and shear zones 1
      1.1.1 Orogens 1
      1.1.2 Shear zones 2
   1.2 Orogenic gold 4
      1.2.1 Structural control 6
      1.2.2 Metamorphism, alteration and hydrothermal fluids 7
      1.2.3 Orogenic gold deposits in Finland 8
   1.3 Geological background 9
      1.3.1 Fennoscandian Shield 9
      1.3.2 Svecofennian Province 10
      1.3.3 The Häme Belt 12
      1.3.4 The Uunimäki area 16
2. Materials and methods 20
   2.1 Bedrock mapping 20
   2.2 Thin sections 22
   2.3 Whole-rock analysis 22
   2.4 Age determinations 22
   2.5 Geophysical maps 24
3. Results 25
   3.1 Petrography of the Uunimäki area 25
      3.1.1 The Uunimäki gabbro 25
      3.1.2 Granodiorites and quartz diorites 27
      3.1.3 Paragneisses 28
      3.1.4 Revised lithological map 30
   3.2 Geochemistry 32
      3.2.1 Major elements 34
      3.2.2 Minor elements 37
      3.2.3 Trace elements 39
   3.3 U-Pb zircon analyses 42
   3.4 Structural geology 47
      3.4.1 The Kankaanranta shear zone 50
      3.4.2 The Uunimäki area 61
4. Discussion 68
   4.1 Age of the Uunimäki gabbro 68
   4.2 Geochemistry of the Uunimäki gabbro 69
   4.3 Comparison of the Uunimäki gabbro to mafic volcanics in SW Finland 71
   4.4 Structural evolution 74
   4.5 The gold mineralisation in Uunimäki 75
   4.6 Hydrothermal alteration 76
5. Conclusions 77
6. Acknowledgements 77

References 79

1. Introduction

Several new gold prospects have been discovered in SW Finland since the beginning of the century, in addition to older deposits that are currently being mined (e.g. Jokisivu, Orivesi). This makes the area promising in terms of ore prospecting (e.g., Kärkkäinen et al. 2006, Saalmann et al. 2009). Many of these prospects were discovered by the Geolocigal Survey of Finland (GTK) during mapping of the mineral potential of southern Finland (Tiainen et al., 2017). There are three main types of ore mineralisations in the Häme Belt; i) the orogenic gold mineralisations such as in the Jokisivu gold mine, ii) the lithium pegmatites, such as the Somero-Tammela intrusions and iii) the epithermal porphyry-Cu-Au mineralisations. The Uunimäki gold deposit, detailed in this study, belongs to the first type and was first discovered in 2008 during mapping of mafic intrusives spatially associated with shear zones (Kärkkäinen et al., 2016). GTK conducted studies on the prospect between 2008-2016 with several methods including till geochemistry, bedrock mapping, and core drilling. In 2017, a two-year co-operative project between GTK and the University of Turku was started to continue the work in SW Finland.

In this study, three main goals were selected to gain new information on the geology of the area. The first goal is to compare the geochemical signatures of the gold-hosting Uunimäki gabbro to the nearby mafic intrusives hosting the Jokisivu gold deposit and and the Palokallio gold occurrence. Plutonic rocks with intermediate compositions were also sampled from the area surrounding the Uunimäki gabbro, to determine what similarities and differences the gold-hosting rocks and the non-mineralized rocks have. The second goal is to determine the age of the Uunimäki gabbro using U-Pb geochronology. The third goal is structural analysis of the Uunimäki area, which requires bedrock mapping in a wider scale, aiming at determining which deformation events have affected the gabbro, and the gold mineralisation it is associated with.

1.1 Orogens and shear zones

1.1.1 Orogens

Orogenies occur at destructive plate margins in convergent plate tectonic settings where intra-plate shortening, crustal thickening and topographic uplift take place (Kearey et al., 2009). Two types of orogens are identified by Kearey et al. (2009). *Noncollisional*

orogens develop in tectonic environments where oceanic and continental lithospheric converge, and subduction of the oceanic plate into the mantle leads to compression in the overriding continental plate. This type of orogen is also called the Andean-type orogen. The other type is a *collisional orogen*, where two continental plate margins, or an island arc collides with a continental margin. The thickness and buoyancy of these collisional plates restrict the subduction of material into the mantle and leads to compression in the plates. This type is also known as the Himalayan-type orogen. When an island arc system collides with a continental plate, it is also considered a collisional orogen. Orogens commonly begin as noncollisional, but eventually develop into collisional orogens as the ocean basins between plates close. This means that orogens are different phases of a long-term geological process (Cawood et al., 2009). Orogens that have grown over long periods of time without ocean closure, and therefore never becoming a collisional orogens, are sometimes called *accretionary orogens* (Kearey et al., 2009). The ancient composite Svecofennian orogen which serves as the backdrop of this study was formed in one accretionary event and several collisional orogenic events according to Lahtinen et al. (2005).

Lithospheric plates behave differently during orogenesis based on the strength and rheology of the plates (Kearey et al., 2009). If the continental plate is cool and strong, such as in the southern Andes, orogens are comparatively narrow (~100-400 km in width). If the continental plate is hot and weak, such as in the central Andes and Himalayas, strain can become distributed across areas 1000 km wide. The strength and rheology of the plates can be affected by processes such as magmatism, metamorphism, crustal thickening, crustal melting, sedimentation and erosion. After the orogenesis has ended, isostatic uplift of the crust and erosion alter the topography of the orogen. Eventually, only the overthickened, deformed roots of orogens, with high-grade metamorphic rocks, are exposed at the current erosional level.

1.1.2 Shear zones

According to Fossen (2010) a shear zone is a tabular zone in which the strain is notably higher than in the surrounding rock. A shear zone is separated from the wallrock by margins on both sides. Shear zones can be considered as deeper counterparts or extensions of brittle faults, in the sense that they displace material parallel to the wallrock and grow in width and length as displacement accumulates. The major difference between faulting

and shearing is that faulting is commonly a brittle feature and shearing is commonly a ductile feature. The brittle-ductile transition zone in the lithosphere lies at a depth of about 10-15 km, though this is dependent on the rock type under strain and temperature. Shear zones can occur at any scale at almost any tectonic regime, usually below the brittle-ductile transition zone and tend to have a high-strain core surrounded by a low-strain damage zone.

Shear zones can be normal, reverse, strike-slip or oblique, depending on the orientation of the strain applied to the bedrock and the effect of pre-existing structures (Fossen, 2010). Strike-slip shear zones tend to have steep dips, while extensional and contractional shear zones can have low-angle dips. A simplified classification of shear zone types can be made from the movement of the shear zone walls in relation to each other (Fig. 1). The main types of shear zones are pure shear zones, simple shear zones and subsimple shear zones. In simple shear zones, the walls of the zone move in opposite directions without moving towards or away from each other. In pure shear zones the walls of the zone move towards each other, flattening the shear zone area left in between, and creating displacement outwards along the edges. Subsimple shear zones either have both components present or have simultaneous compaction or dilation taking place. The shear zone type has a marked impact on the internal structures of the shear zone, which can then be used to make interpretations of the stress fields that led to the deformation. However, as shear zones are rarely formed in a homogenous stress field throughout its length, discontinuities and structural incompatibilities are formed, which can make interpretation of the structural regimes difficult. The effects of later deformation phases and erosion further complicate interpretation of ancient orogens.

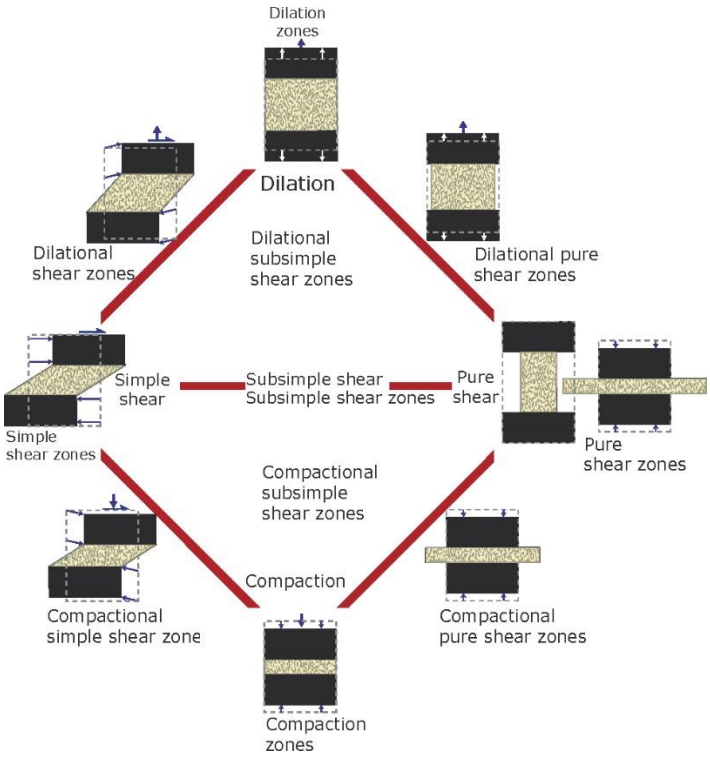

Fig. 1. Classification of shear zone types based on pure shear, simple shear, compaction and dilation components (Fossen, 2010).

The characteristic structures of shear zones are foliations and lineations (Fossen, 2010). Foliation is developed along the strike of the shear zone, and in well-developed ductile shear zones, reorient pre-existing structures to the same orientation. Lineations are developed along with the foliations and are visible on foliation surfaces. In ideal cases the strectch lineation on the shear plane indicates the shear direction. The kinematics of shear zones can be determined through kinematic indicators that showcase dextral (right-handed) or sinistral (left-handed) structures in both meso- and microscales.

1.2 Orogenic gold

Gold deposits can be formed in many different environments, and they are classified into several ore types, some of which have a significant overlap. The term ‘orogenic gold’ has been proposed to cover many of these ore types (Böhlke, 1982; Groves et al., 1998). Other names for these types of deposits include ‘lode gold’ (e.g., McCuaig & Kerrich, 1998), ‘gold-only’ (Hodgson et al., 1982) and ‘synorogenic gold’ (Goldfarb et al., 1998).

According to Groves et al. (1998), orogenic gold deposits have formed in compressional to transpressional settings at convergent plate margins in accretionary and collisional orogens. They are associated with metamorphic terranes of all ages. The gold itself is

most commonly located in quartz-dominated vein systems with up to 3-5% sulfide minerals and up to 5-15% carbonate minerals, but it can also occur in sulfidized wallrocks. The sulfide minerals present are dependent on the host rock; metasedimentary country rocks typically contain arsenopyrite while metamorphosed igneous rocks contain pyrite or pyrrhotite. The ratio of gold/silver in these deposits ranges from 10 (common) to 1 (rare). Other elements that may exhibit enrichment in the gold-bearing quartz veins are As, B, Bi, Hg, S, Sb, Te and W, with Cu, Pb and Zn enrichments only slightly exceeding the background concentrations (McCuaig & Kerrich, 1998; Groves et al., 1998). P-T conditions of gold mineralisations vary extensively, as they can occur in middle-to-upper crust at depths of ~5-20 km (Groves, 1993). Gebre-Mariam et al. (1995) divided Late Archean orogenic gold deposits into three subgroups based on the formation depth: epizonal (<6 km), mesozonal (6-12 km), and hypozonal (>12 km). According to Groves et al. (1998) this classification can be used for younger orogenic gold deposits as well (Fig. 2). The epi-, meso- and hypozonal deposits form a continuous series of elevating P-T conditions and metamorphic facies, and a single geological zone may contain deposits of all three subgroups. Orogenic gold deposits may have vertical continuity from a few hundred meters to several kilometers (Groves, 1993).

The ages of orogenic gold deposits correlate with thermal events related to the growth of new continental crust (Goldfarb et al., 2001). Major occurrences of orogenic gold seems to be concentrated on three distinct time periods: Late Archean (3.0 – 2.5 Ga), early Proterozoic (2.1 – 1.8 Ga) and Phanerozoic (570 Ma and younger).

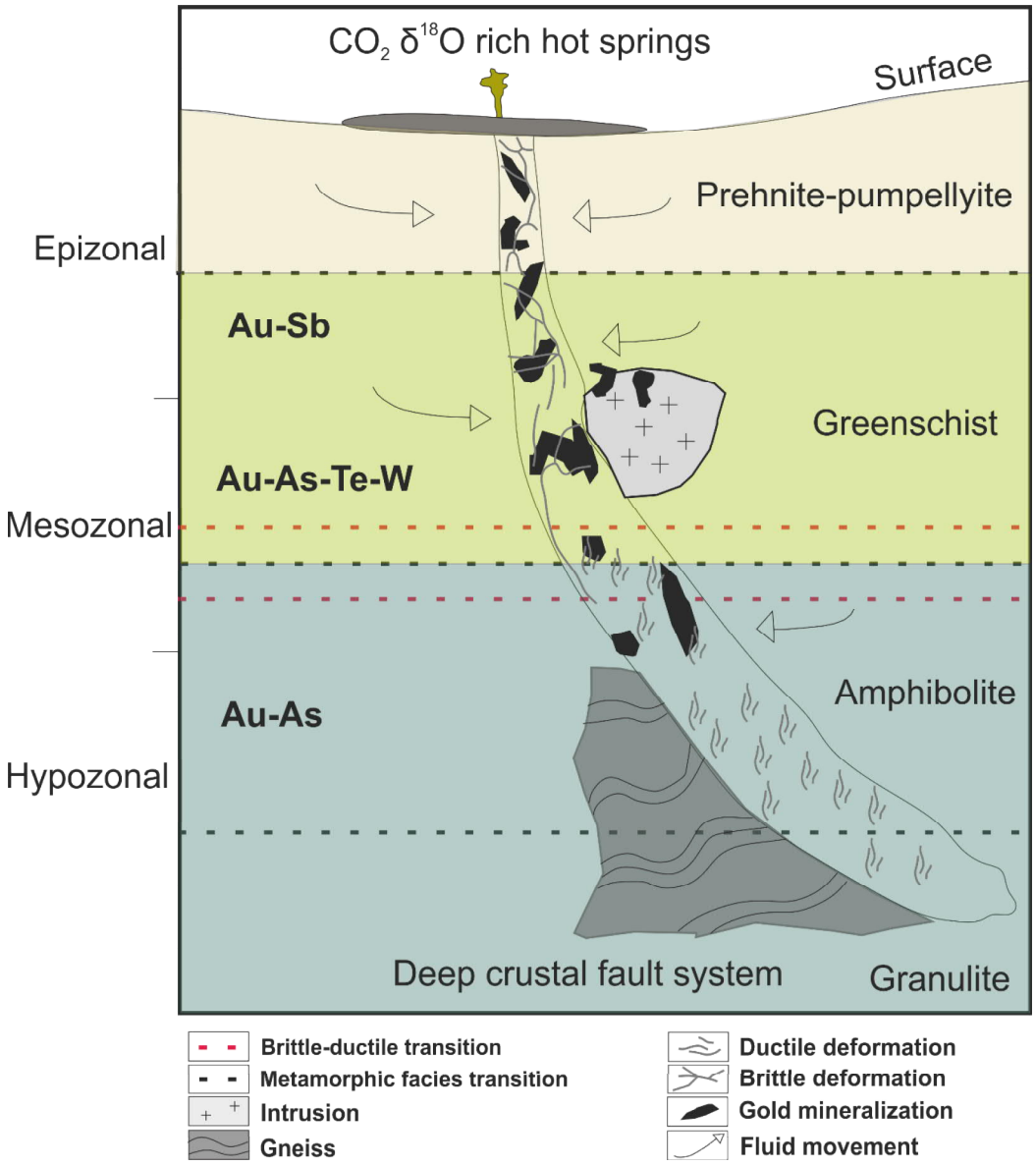

Fig. 2. Schematic view of orogenic gold forming environments. Note the change in Au-associated elements with increasing depth. Modified after Goldfarb & Groves (2015).

1.2.1 Structural control

Orogenic gold deposits are controlled by the structural features of the bedrock. They are most commonly found in second or third order structures near large-scale compressional structures (Groves et al., 1998). The major shear and fault zones associated with compressional structures are thought to work as channels where orogenic-gold forming fluids may flow. The controlling structures often represent the transitional area of ductile-brittle deformation in the crust (McCuaig & Kerrich, 1998). In the upper, more brittle parts of the crust, the gold-bearing veins more commonly appear as breccia (Groves, 1993). Gold-bearing veins formed in the lower crust, in ductile conditions, most commonly appear as parallel quartz veins and shear zones (Groves, 1993). Orogenic

events during and after mineralisation may create additional faulting and fracturing of the gold-hosting structures (Groves et al., 1998).

1.2.2 Metamorphism, alteration and hydrothermal fluids

Orogenic gold deposits are strongly associated with greenschist to lower amphibolite facies rocks (Groves, 1993; Groves et al., 1998). Mineralisation typically occurs at syn- to post-peak-metamorphism (McCuaig & Kerrich, 1998). Groves (1993) suggested that the timing of gold mineralisation in relation to metamorphism depends on the depth of mineralisation, with the metamorphic peak being closer to mineralisation in deeper deposits.

Gold is transported as a reduced sulphur complex in low-salinity, near-neutral H2O-CO2 ± CH4 fluids (Groves et al., 1998). $Au(HS)_2$- is the most common gold transporting sulphur complex in these conditions, though in slightly more acidic conditions $AuHS_0$ is also stable (Benning & Seward, 1996). Metamorphic and/or magmatic fluids derived from the lower crust/upper mantle are thought to be the source of these orogenic gold-forming fluids (e.g., Robb, 2005; Tomkins, 2013). These fluids move upward in the crust during earthquake events (Sibson et al., 1988) through major fault and shear zones that may have been suture zones between accreted terranes in the crust (Groves et al., 1998). If there are syngenetic sulfide minerals disseminated in the newly formed crust, sulfur may be released into the hydrothermal fluids, allowing the fluid to leach and transport gold from the rocks along its flow path (Goldfarb et al., 2001).

The exact source rocks of orogenic gold is not known, and is a very diffucult subject to study (Tomkins, 2013). Source rocks such as hydrated mafic rocks (e.g., Phillips & Powell, 2010) and carbonaceous metasedimentary rocks (e.g., Gaboury, 2013) have been suggested. It is unlikely that the source rocks have very high concentrations of gold, so it must be leached from a large area so that the high concentrations found in many orogenic gold deposits can be achieved. There are several theories how gold precipitates as temperature and pressure decrease, and the mechanisms by which it occurs may vary from place to place (Tomkins, 2013). Wallrock alteration occurs when hydrothermal fluids interact with wallrocks, and chemical reactions occur as the rock attempts to reach a new equilibrium with the elements brought in by the fluids. The extent of alteration is determined by several factors, including chemical and physical attributes of the fluid and

wallrock, the phase equilibria in the wallrock, the prevalent P-T conditions, and the amount of fluid that reacts with the wallrock (McCuaig & Kerrich, 1998). As a result of alteration, the wallrock can exhibit lateral zoning. Mikucki et al. (1998) consider fluid-rock interactions and wallrock sulphidisation to be the most important precipitation mechanisms at all crustal levels. Boiling, fluid mixing and chemisorption of pyrite and arsenopyrite are some of the other precipitation mechanisms suggested (Tomkins, 2013).

1.2.3 Orogenic gold deposits in Finland

Orogenic gold deposits form the overwhelming majority of all gold deposits in Finland (Eilu et al., 2003). They were mainly formed during and immediately after the metamorphic peak during the main accretionary phase of the Svecofennian orogeny at 1.89 – 1.86 Ga (Eilu et al., 2003). The host rocks of gold mineralisations have undergone metamorphism under lower-greenschist to upper-amphibolite facies P-T conditions and are structurally controlled by second or third order shear or fault splays from larger structures (Eilu et al., 2003). This is in line with other known orogenic gold deposits in Precambrian shields around the world (Groves et al., 1998). The areas with the most potential for discovery of new orogenic gold deposits are the late Archean and Paleoproterozoic greenstone belts in Eastern Finland and Lapland (Eilu et al., 2003). Orogenic gold deposits in Finland that are currently mined are the Suurikuusikko, Pahtavaara, Pampalo, Laiva and Jokisivu deposits. The Saattopora deposit was also mined until 1995. Several other orogenic gold deposits are known and are being prospected for possible mining activity, including the Satulinmäki, Kedonojankulma, Riukka, Uunimäki and Ritakallio deposits in the Häme Belt alone (Saalmann et al., 2007; Tiainen et al., 2017). Host rocks of the orogenic gold deposits in Finland are most commonly mafic intrusives and sedimentary rocks (Eilu et al., 2003). In addition to the orogenic gold mines, gold has also been mined from other types of gold deposits such as Orivesi and Haveri, and as side products of base metal mines.

1.3 Geological background

1.3.1 Fennoscandian Shield

The bedrock of Finland is part of a Precambrian shield of Archean and Proterozoic rocks in NE Europe called the Fennoscandian Shield which as a crustal segment, it is part of the East European Craton. (Gorbatschev & Bogdanova 1993; Bogdanova et al. 2008; Nironen, 2017). The East European Craton is separated from its surroundings by the Timanian fold belt in the north, the Norwegian Caledonides in the west, and the Trans-European Suture Zone in the south. Fennoscandia within the East European Craton is bounded by Sarmatia to the SE and Volgo-Uralia to the NE (Fig. 3).

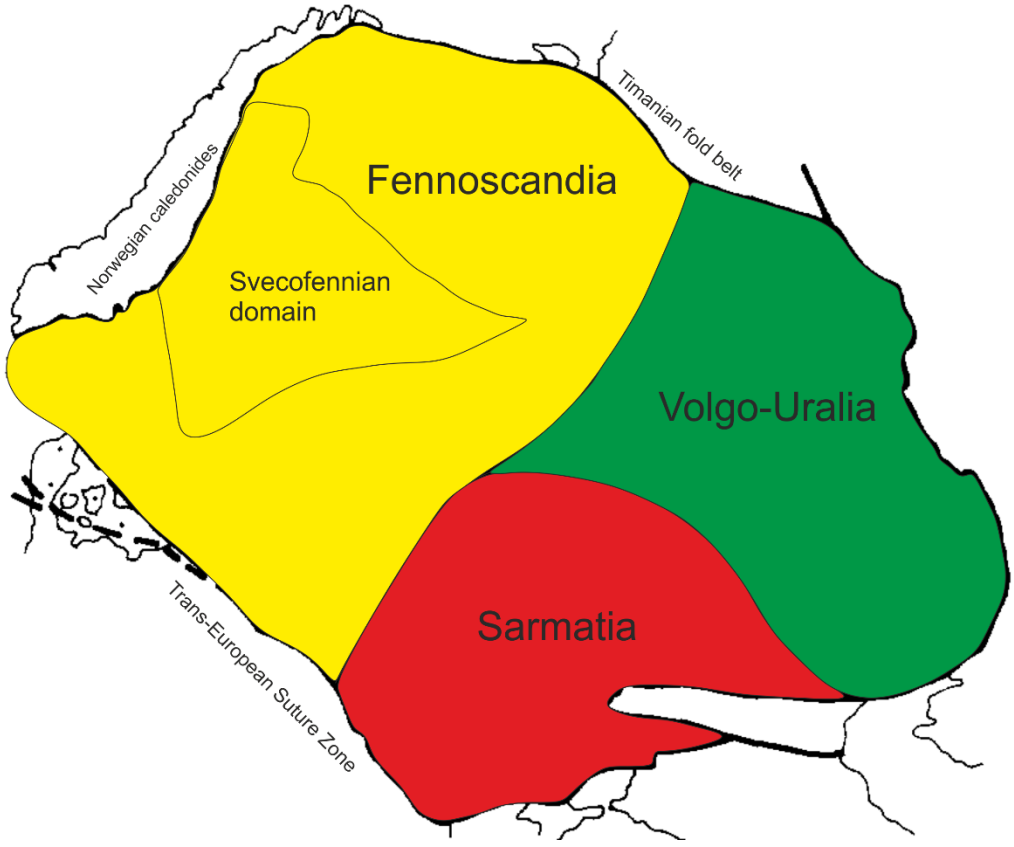

Fig. 3. The East European Craton. Modified after Gorbastchev & Bogdanova (1993).

The Shield can be further divided into four clearly distinct areas: the Archean, Svecofennian, Sveconorwegian domains and the Transscandinavian Igneous Belt (Vaasjoki et al., 2005). Large parts of northern and eastern Finland belong to the Archean domain (mostly >2.5 Ga) and consist of two major Archean blocks: the Karjala and Kola cratons. The central and southern parts of Finland belong to the Svecofennian domain

mostly formed at 1.93-1.80 Ga, though later intrusions by 1.65-1.54 Ga rapakivi granites and sedimentation during the Paleozoic and Mesozoic brought additional components into the bedrock of southern Finland. Much of the sedimentary cover was removed through five glaciation periods in the Pleistocene, leaving the bedrock relatively well exposed.

1.3.2 Svecofennian Province

The Paleoproterozoic Svecofennian Province is separated from the Archean Karelia-craton in the NE by a complex NW-SE suture zone (Fig. 4) and consists of several terranes and lithotectonic units in Finland and Sweden. In the contemporary geological map of Finland by Nironen et al. (2016), the Svecofennian Province in Finland is divided into several terranes: the Savo Belt, the Vaasa Complex, the Central Finland Granitoid Complex, the Tampere, Pirkanmaa, Häme and Uusimaa Belts (Fig. 4).

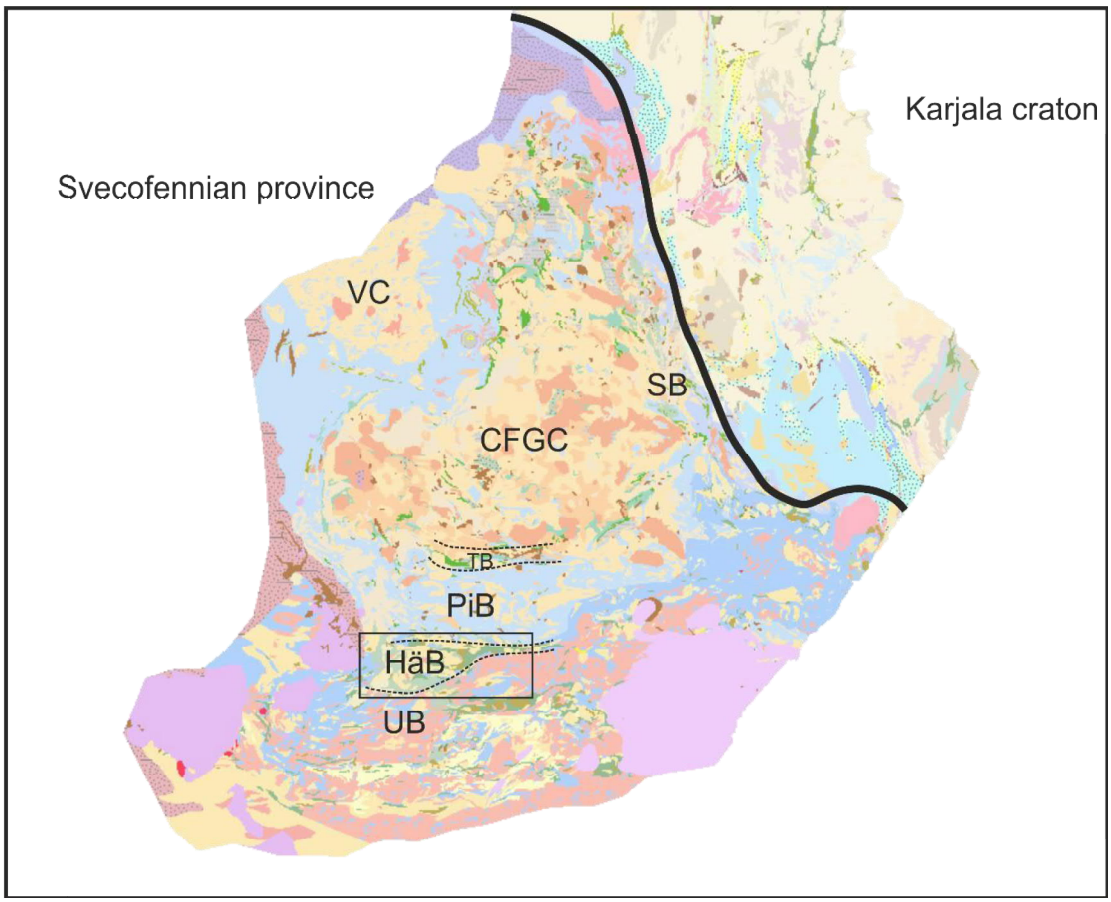

Fig. 4. The Southern Svecofennian province in the generalized geological map of Finland. The thick black line represents the interpreted suture zone (Raahe-Laatokka) between the Svecofennian province and Karjala craton. UB = Uusimaa Belt, HäB = Häme Belt, PiB = Pirkanmaa Belt, TB = Tampere Belt, CFGC = Central Finland Granitoid Complex, VC = Vaasa Complex, SB = Savo Belt. Modified after Korsman et al. (1997).

The oldest rocks of the Svecofennian Province in Finland are the 1.92 Ga primitive island arc rocks in the Savo belt (Mikkola et al., 2018). The rocks of the Central Finland Granitoid Complex, the Vaasa Complex, the Tampere Belt and the Pirkanmaa Belt are metasedimentary rocks, volcanic-arc type rocks, intruded by ultramafic-mafic plutonic rocks, granitoids and gabbros (Nironen, 2017). Together, they form the western Finland arc complex. The Häme and Uusimaa Belts form the southern Finland arc complex. They consist of varying metavolcanic rocks, metasedimentary rocks, syn-volcanic mafic intrusions, and younger plutonic rocks. Two possible models explaining the formation of the Svecofennian orogen (Fig. 5), one by Lahtinen et al. (2005) and the other by Hermansson et al. (2008), are discussed here.

According to the model by Lahtinen et al. (2005) the Svecofennian orogen formed as a result of collision and accretion of several microcontinents and volcanic arcs onto the Archean craton at ~1.92 – 1.79 Ga. The model proposes that two subduction zones, in the west and south respectively, operated at high angles, resulting in a very complicated tectonic setting as a result of repeated accretions (Fig. 5). According to this model, there were five orogenic phases; Lapland-Kola, Lapland-Savo, Fennian, Svecobaltic and Nordic; that partially overlap temporally and spatially. These orogenic phases are divided by orogenic collapses, extensional phases and a subduction switchover. The most voluminous of these orogenic stages, the 1.89 – 1.87 Ga 'Fennian' stage, is interpreted to have formed the Häme Belt, which is the setting of this study. The end of the Svecofennian orogeny would take place at ~1.79 – 1.77 Ga with a large-scale orogenic collapse.

The model by Hermansson et al. (2008) suggests that there was only one active subduction zone during the entire Svecofennian orogeny. In this model, the cyclic tectonic evolution of compression and extension in the Svecofennian Orogen is explained by alternating hinge retreat and hinge advance of the subduction zone (Fig. 5). Following a period of hinge retreat and extension in the back-arc at 1.91-1.89 Ga, the hinge migration is interpreted to have changed its direction. This led to compression in the back-arc, resulting in voluminous calc-alkaline arc magmatism at 1.89 – 1.87 Ga: the time period when the plutonic rocks of the Häme Belt were formed.

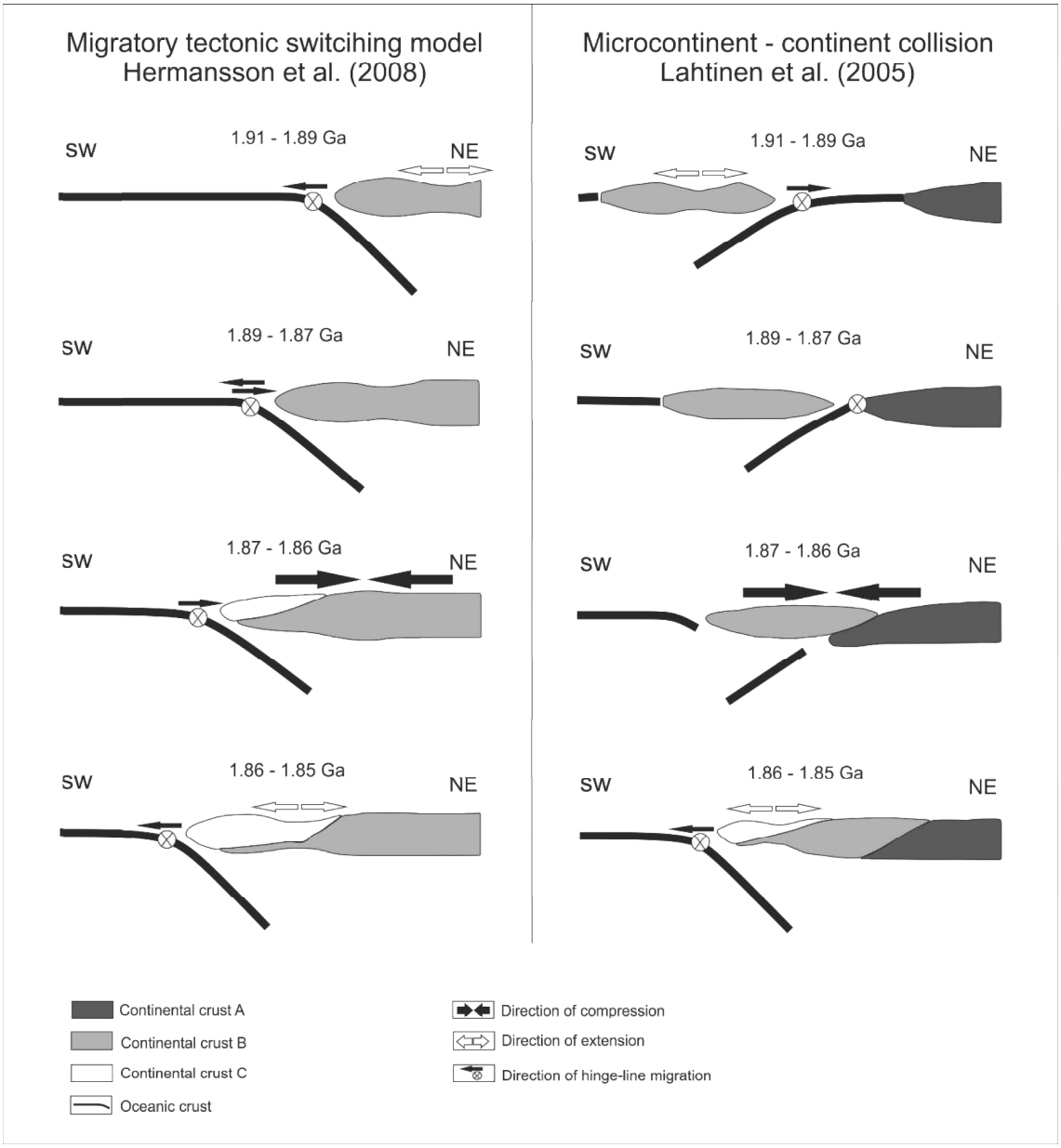

Fig. 5. The two models explaining the cyclic tectonic evolution of the Svecofennian province. Continental crust A-C are correspond with lithotectonic units in Sweden, but are applicable for the evolution of the Svecofennian province in Finland. A: Ljusdal domain, B: Bergslagen domain, C: Småland domain. Modified after Hermansson et al. (2008).

1.3.3 The Häme Belt

The bedrock of the E-W trending Häme Belt in SW Finland was primarily formed at 1.89 – 1.87 Ga, during the 'Fennian' stage of the Svecofennian orogeny (Lahtinen et al., 2005). It consists of various types of volcanic and sedimentary rocks (Nironen 1999, Kähkönen 2005) that have undergone metamorphism under amphibolite facies conditions (Hölttä & Heilimo, 2017). The supracrustal rocks are intruded by syn-tectonic plutonic rocks of gabbroic, dioritic, granodioritic and tonalitic composition (Nironen 1999, Kähkönen 2005, Mäkitie et al. 2016) and late- to post-tectonic (1.83 – 1.79 Ga) granites, migmatites

and pegmatites (Nironen et al. 2016). Supracrustal and plutonic rocks are approximately equally voluminous in the area (Mäkitie et al., 2016). Volcanic rocks of the Häme Belt were divided into three groups by Sipilä & Kujala (2014): the Forssa, Loimaa and Renkajärvi suites. Rocks of the Forssa volcanic suite have a calc-alkaline affinity and their composition ranges from basaltic to rhyolitic, with andesitic being the most common. Rocks of the Loimaa suite also have a calc-alkaline affinity, but have undergone metamorphism in a higher temperature than the Forssa suite rocks. They consist mostly of amphibolites and hornblende-gneisses. Rocks of the Renkajärvi suite have an N-MORB-affinity, and consist of mafic and intermediate volcanic rocks. Plutonic mafic rocks are often associated with the volcanic rocks (Peltonen, 2005). The most common plutonic rock in the Häme Belt is deformed granodiorite (Mäkitie et al., 2016). Epiclastic sediments are less common than in other areas of the Svecofennides (Sipilä & Kujala, 2014).

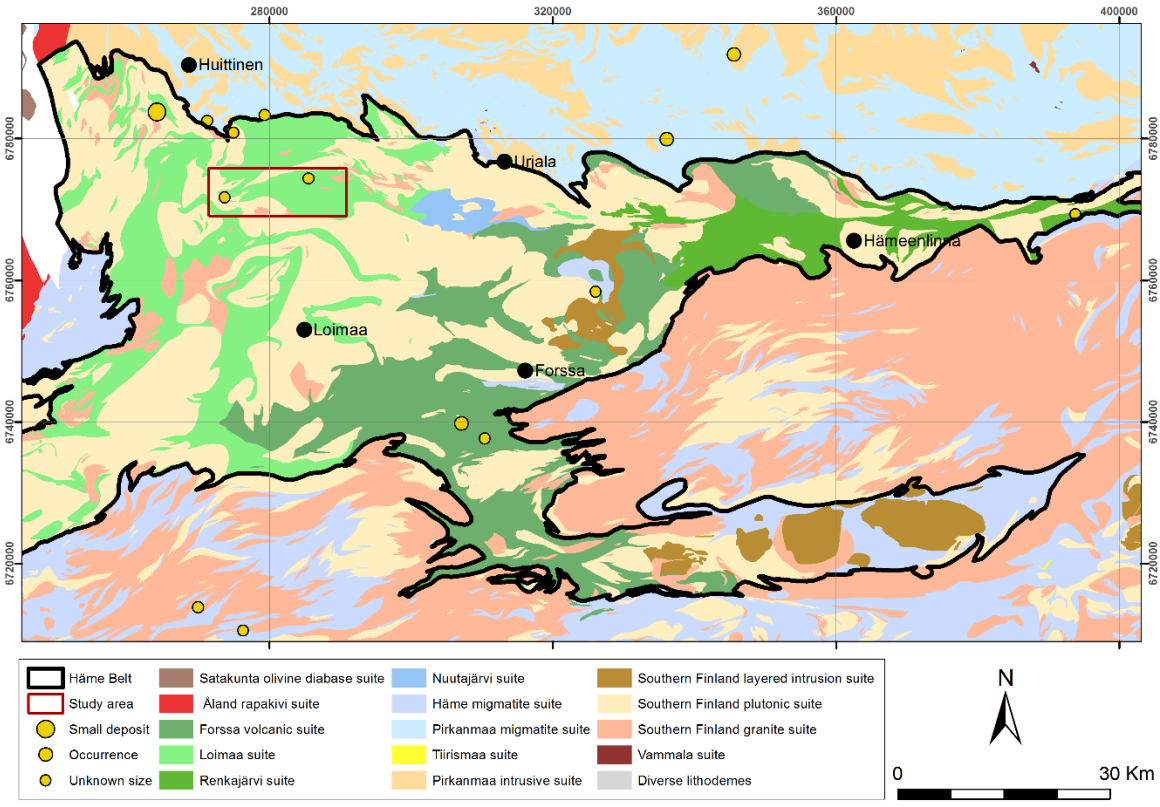

Fig. 6. General geology of the Häme Belt, modified after Korsman et al. (1997). The study area in Figs. 19, 20 & 34 marked with a red rectangle. Locations of significant gold deposits and prospects after Tiainen et al. (2017).

The Häme Belt is situated between the Uusimaa Belt to the south and the Pirkanmaa Belts to the north (Nironen et al. 2017). Major E-W trending shear zones, the Nuutajärvi SZ

and the Somero SZ may act as dividing boundaries between the Belts (Nironen et al. 2017), but terrane boundaries are not sharp and are difficult to constrain (Kähkönen 2005, Sipilä et al. 2011). According to Väisänen (2002), the evolution of the Häme Belt took place in three stages: pre-collisional, collisional, and post-collisional (Fig. 7). In the pre-collisional phase at 1.89 Ga, the Häme Belt is interpreted as a rifted remnant arc. It is separated from the northwards verging subduction zone by a back-arc basin, the Uusimaa arc and the forearc basin. During the collisional phase as the subduction progressed, the Häme Belt was sutured onto the Pirkanmaa belt to the north at 1.88-1.86 Ga. This has caused the penetrative foliation in the Häme Belt. Deformation continued in the post-collisional stage, as convergence towards the north continued. Penetrative foliation and folding overprinted some of the older structures, which were then overprinted by late orogenic shear zones. The shear activity in the Häme Belt is interpreted to have occurred after peak metamorphism (Lahtinen et al. 2005, Saalmann et al. 2010). The shearing is characterized mostly by NE-SW and NW-SE trending shear zones throughout the Belt, and N-S trending shear zones in the west.

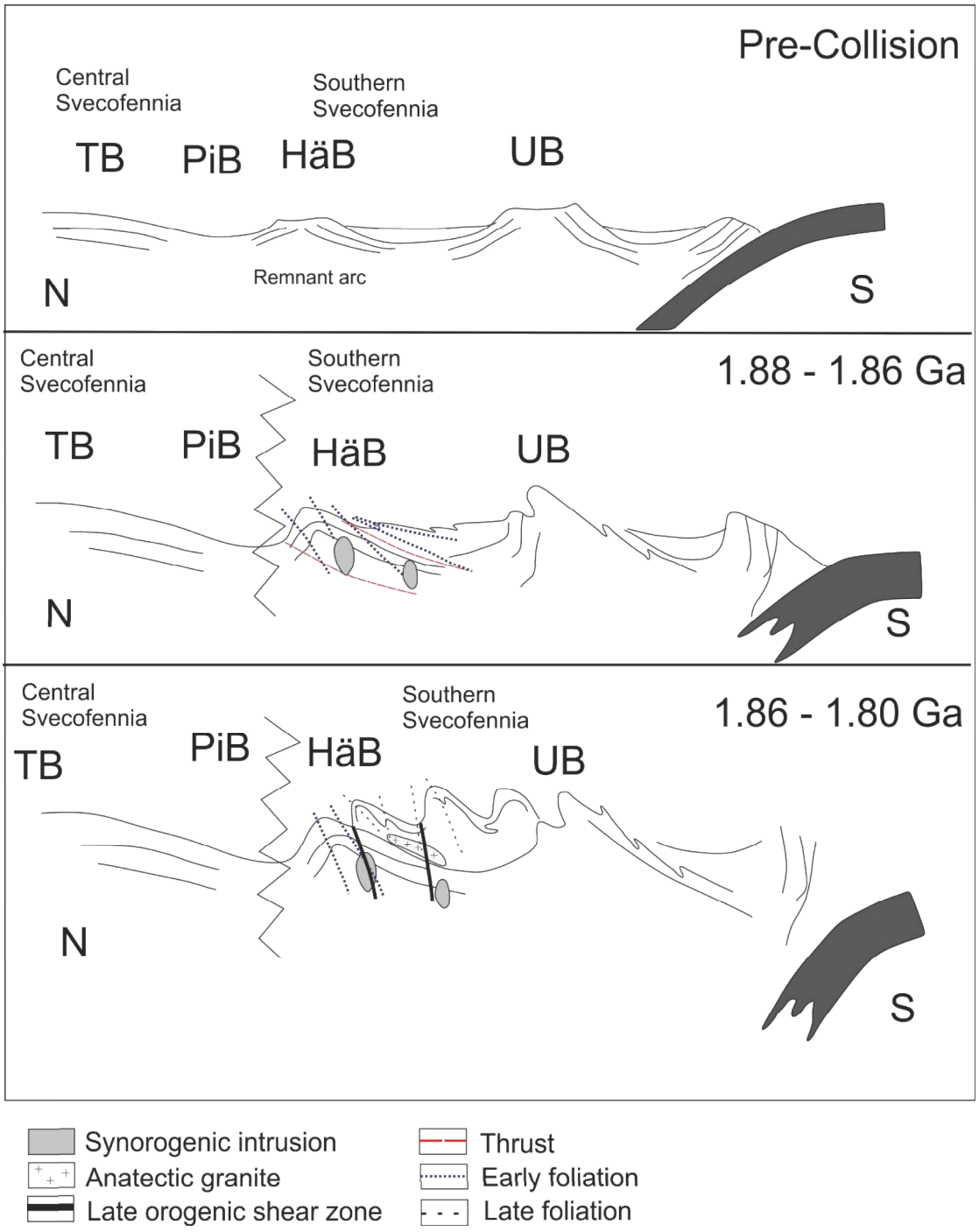

Fig. 7. Three-stages of development for the Central and Southern Svecofennian provinces. Not to scale, emphasis on structures of the Häme Belt area. Pirkanmaa and Häme Belts separated by suture zone. TB = Tampere belt, PiB = Pirkanmaa belt, HB = Häme Belt, UB = Uusimaa belt. Modified after Väisänen (2002).

The Häme Belt hosts different types of ore deposits (Tiainen et al., 2017). The most significant ore mineralisations include a VMS-type Zn-Pb-Ag deposit, a porphyry Cu-Au deposit, several orogenic gold deposits, Fe-Ti deposits in gabbro intrusions, and LCT-type pegmatites. The orogenic gold mineralisations are attributed to be structurally controlled by shear zones of various ages (Saalmann et al. 2009, Saalmann et al. 2010,

Mertanen & Karell 2011, Mertanen & Karell 2012). Rasilainen & Eilu (2016) mathematically estimated that 17.5 undiscovered Cu, Zn, Ni and Au mineralisations exist within the Häme Belt. Ore prospecting is still ongoing.

1.3.4 The Uunimäki area

Uunimäki is located in the northwestern part of the Häme Belt, in the village of Pikku-Vampula in the municipality of Loimaa. The gold deposit was discovered by GTK in the autumn of 2008, during mapping of gold potential in mafic intrusions intersected by fault and shear zones (Kärkkäinen et al., 2016). During initial mapping, three shear zones with quartz veins and arsenopyrite were discovered, indicating possible Au-mineralisation. Till samples were collected for heavy mineral separation from a nearby depression, yielding microscopic grains of native gold and scheelite (Kärkkäinen et al., 2015). Further mapping was carried out in 2011 and 2012. Rock fragments were collected in 2012 and 2014 during percussion drilling for till geochemical surveys. A total of 36 diamond drill holes have been drilled in the area in 2009-2014 (Fig. 8), with a total of 3425 m of drill cores. The drill cores showed that ilmenite and pyrrhotite are the most common ore minerals in the Uunimäki area.

The bedrock of the area consists of mica gneisses, mafic volcanic rocks, granitoids and mafic intrusions (Kärkkäinen et al., 2016). The gold itself is hosted by the Uunimäki gabbro, which has undergone metamorphism in the amphibolite facies, indicated by the replacement of pyroxenes by amphiboles. Mineralogy of the gabbro shows alteration characterized by albitisation, sulfidisation, chloritisation, sericitisation and the formation of epidote, quartz veins and carbonate veins (Kärkkäinen & Tiainen, 2016).

Gold-rich (>1 ppm) sections (Table 1) were discovered in 27 of the 36 new holes drilled during 2009-2014 (Fig. 8; Kärkkäinen et al., 2016). The highest concentrations of gold/m were found in holes R8 (15.0 ppm), R23 (35.2 ppm) and R25 (38.4 ppm). Most of the drilling was done in NW Uunimäki, and drilled towards the SW with an azimuth of 225 and a dip of 45. Holes R315 and R13 were drilled towards NE; these holes did not contain gold-rich sections. The gold was found to be in association with silicates and sulfides; thin pyrrhotite vein networks and pure quartz veins with native gold have the highest gold concentrations. Gold occurs as complex grains with Bi, Bi-sulfide, Bi-Te minerals and arsenopyrite as well as individual grains (Kärkkäinen et al., 2015). Gold was found to be

concentrated into the seemingly unaltered gabbro near sheared and fractured parts of the gabbro.

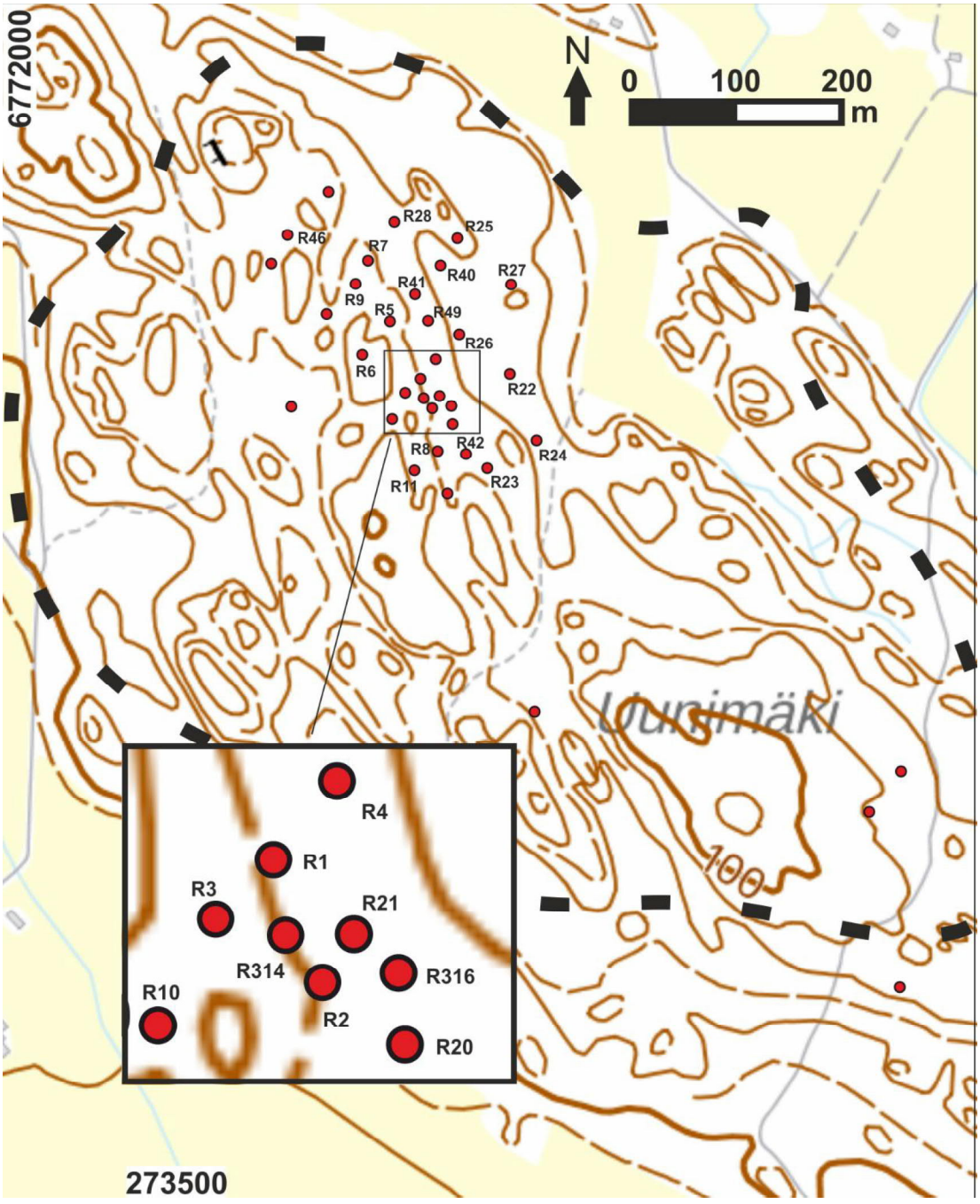

Fig. 8. Map of Uunimäki with GTK drilling locations from 2009 to 2014 marked with red circles. Outline of the Uunimäki gabbro drawn with a dashed black line. Drill holes with at least 1 m sections of gold-rich rock (>1 ppm) labeled. Modified after Kärkkäinen et al. (2016).

Table 1. Gold-rich drilling sections (>1 ppm) at Uunimäki. Listed is the total length of mineralized rock along with the highest Au-concentration per meter from each drill hole (Kärkkäinen et al. 2016).

Hole	**Total length of the mineralized intersection (m)**	**Grade of the highest 1 m intersection (ppm)**
R314	8	12.2
R316	1	3.3
R1	4.9	8.5
R2	10	2.9
R3	1	1.3
R4	1	2.9
R5	10	9.7
R6	10	8.1
R7	5	1.4
R8	14	15.0
R9	2	1.5
R10	1	1.0
R11	1	1.9
R20	1	8.6
R21	1	8.8
R22	1	1.2
R23	1	35.2
R24	1	1.3
R25	17	38.4
R26	1	3.4
R27	9	5.9
R28	1	3.3
R40	7	5.2
R41	4	10.1
R42	1	1.3
R46	1	10.8
R49	12	8.7

The gold mineralisation is interpreted to be related to a complex network of fracture and shear zones, where NW-SE-trending fractures and shears have been the structures controlling gold mineralisation (Kärkkäinen et al., 2016). The 3D-model of the Uunimäki

prospect based on the chemical analyses from the 32 drill holes in NW Uunimäki as shown in Fig. 9 (Kärkkäinen et al., 2016). The total volume of mineralized rock based on the model is 630 000 m^3, totaling 1.88 Mt of mineralized rock with an average grade of 1.1 ppm Au.

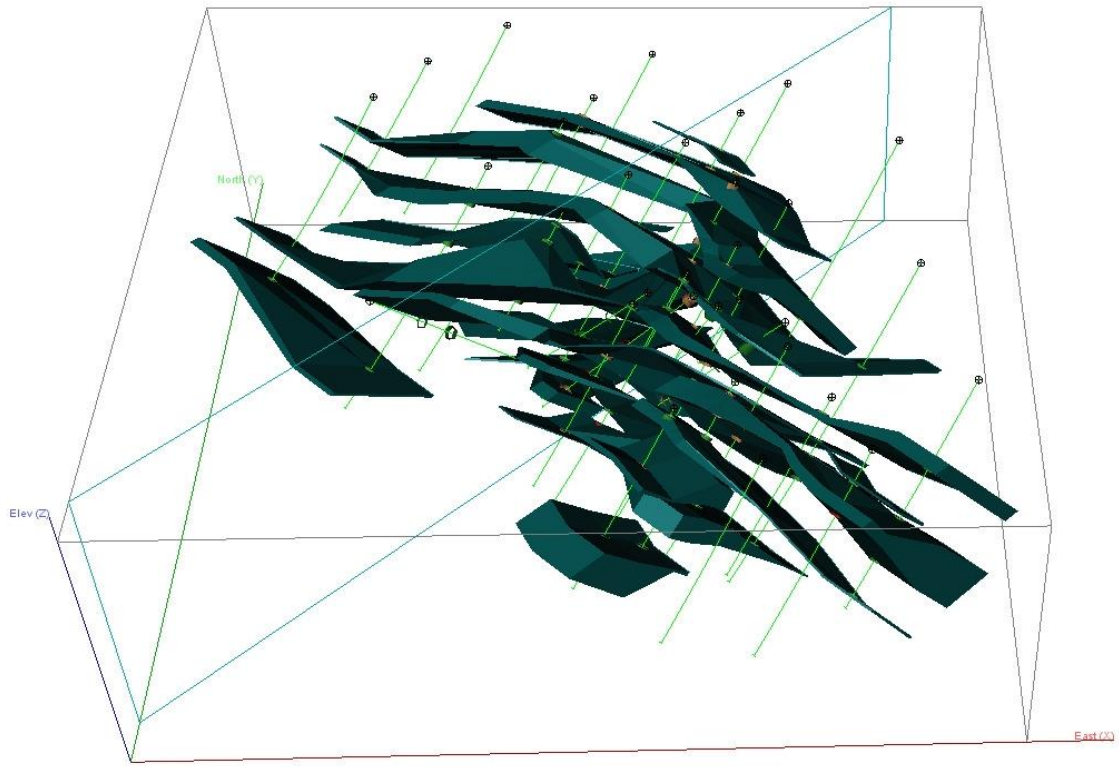

Fig. 9. 3D-model of the Uunimäki gold mineralisation (Kärkkäinen et al., 2016). Light green lines represent drill holes, while turquoise polygons represent rock interpreted as mineralised. North is upwards.

2. Materials and methods

The materials for this study consist of bedrock observations and analyses made on samples collected from the field. Bedrock maps and geophysical maps provided by GTK were used during field mapping and structural analysis. The collected samples were prepared for thin section study, geochemical analyses and an age determination.

2.1 Bedrock mapping

During the summer of 2017, 89 new bedrock observations from the Uunimäki region and 72 new observations from the ENE-WSW-trending shear zone, called the Kankaanranta shear zone from now on, were made (Fig. 10). All observations were linked to the Kapalo-database used by GTK, using the GIS-software ArcMap. Panasonic Toughbook field laptops, which have built-in GPS receivers provided by GTK were used in the acquisition of field data. The used coordinate system was EUREF-FIN-TM35FIN based on the Universal Transverse Mercator projection which uses the GRS80 datum. All observed outcrops had their rock type, grain size, colour of the erosion surface and structural features recorded. 119 field photos were taken from the Uunimäki area and the Kankaanranta shear zone, and several field sketches were drawn to help recollection of outcrops at a later time.

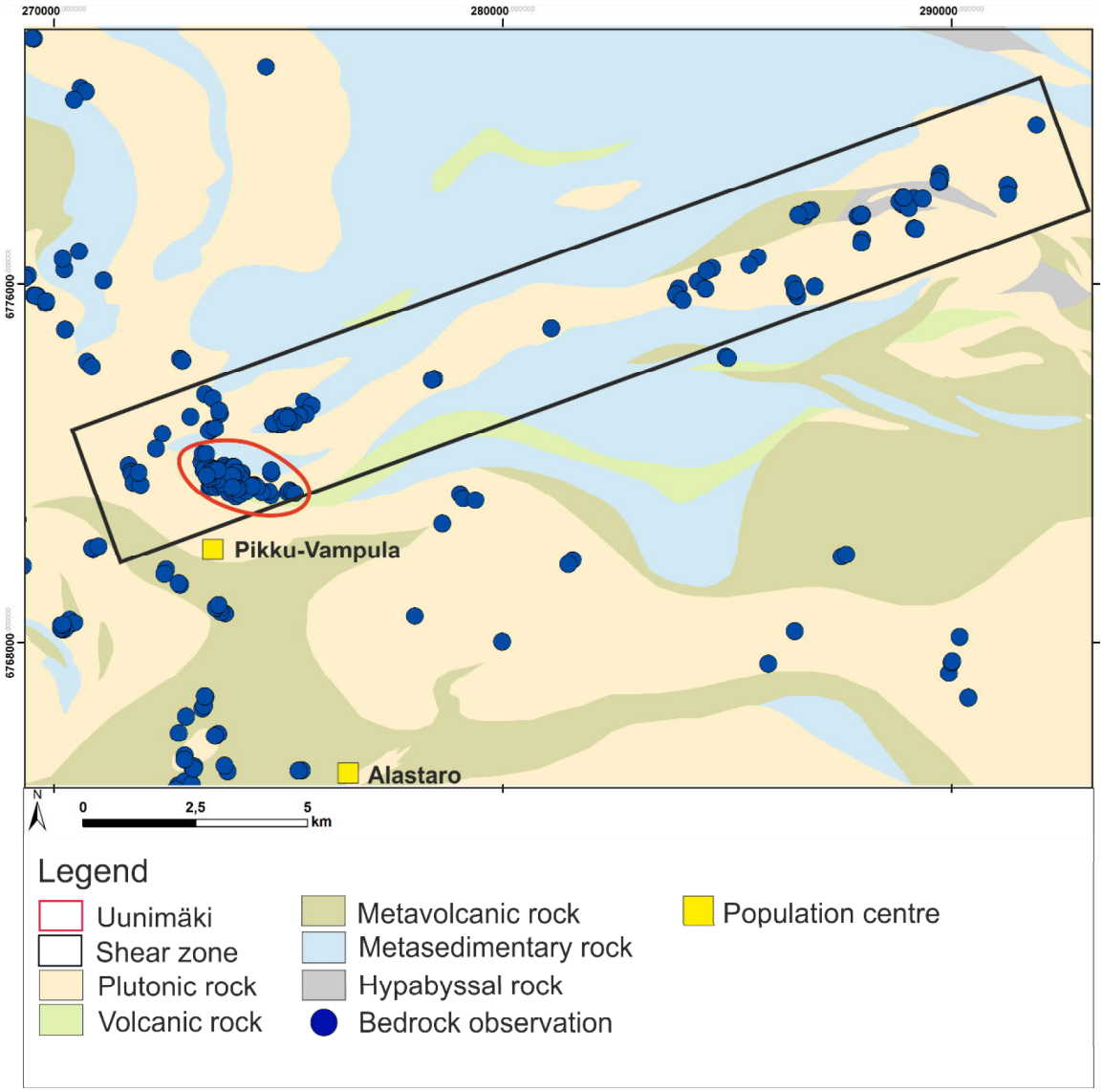

Fig. 10. Outlines of the study areas in the western Häme Belt. Note that Uunimäki lies at least partially within the Kankaanranta shear zone. Modified after Kallioperä-Bedrock of Finland 1:200 000.

Structural observations were measured with a geological compass. All measurements had their magnetic declinations corrected later, with +7 degrees added to them. 110 of the observations made in the Uunimäki area and Kankaanranta shear zone included tectonic measurements, most of which were foliations and lineations. Fold axes, axial planes and faults were also measured whenever possible. Additionally, 27 samples were collected from the Uunimäki region with a rock hammer, with 8 of the samples being oriented. 23 oriented samples were collected from the Kankaanranta shear zone for microscale analysis of the kinematics of the shear zone. Oriented samples, which were collected whenever rocks showed mylonitic or other types of sheared textures, had a north arrow and horizontal lines drawn onto them to preserve information of their original position in

the bedrock Some of the samples were collected not only for later analysis, but for also determining the rock type and comparing them with other collected samples.

2.2 Thin sections

A total of 30 thin sections were prepared from the study area, 10 of which are from the Uunimäki gabbro, and 18 from the Kankaanranta trending shear zone immediately to the north of Uunimäki. A thin section was also made from a paragneiss sample in order to constrain the peak-metamorphic paragenesis of the Uunimäki area. Thin sections were used to determine the mineralogy and textures of the rocks, as well as the shear senses of oriented samples, to allow interpretation of the kinematics of the deformation.

2.3 Whole-rock analysis

20 rock samples were collected from the Uunimäki gabbro and its surrounding areas. The samples were initially prepared in the laboratories of the University of Turku and sent to Acme Analytical Laboratories Ltd. in Vancouver for geochemical analysis. Total whole rock characterisation was performed by ICP-MS. Additionally, ICP-ES/MS analysis was performed after samples were leached in hot modified aqua regia for Mo, Cu, Pb, Zn, Ni, As, Cd, Sb, Bi, Ag, Au, Hg, Tl and Se.

2.4 Age determinations

A single rock sample (TALE-2017-17.1) from the Uunimäki gabbro was selected for zircon U-Pb single grain age dating (Fig. 11). The sample was selected due to showing no clear signs of deformation or hydrothermal alteration so that the zircons would be as undisturbed as possible.

Zircons were separated from the gabbro in the laboratories of the University of Turku by crushing, panning, hand magnet separation, heavy liquid separation, Franz magnetic separation and hand picking. The hand-picked zircons were placed to an epoxy mount, which was then polished so that the interiors of the zircons were exposed. A total of 158 zircon grains were BSE-imaged with a scanning electron microscope at the Top Analytica laboratories in Turku. 32 zircon grains were selected for spot analysis based on the BSE-images. Zircons with no substantial cracks or metamict domains were preferred.

Fig. 11. Relatively undeformed Uunimäki gabbro from the age sampling site TALE-2017-17 (N: 6771790, E: 274010.)

A Nu Plasma AttoM single collector ICP-MS connected to a Photon Machine Excite laser ablation system in the Finnish Geosciences Research Laboratory at the Geological Survey of Finland in Espoo was used for U-Pb dating analysis of the Uunimäki gabbro. Ablation conditions were as follows: beam diameter: 25 µm, pulse frequency: 5 Hz, beam energy density: 2.5 J/cm^2. Each U-Pb measurement was preceded by 5 pre-ablation pulses with a diameter of 25 µm, followed by on-mass background measurement for 15 seconds, then ablation with a stationary beam for 30 seconds. Three calibration standards were used: GJ-1 (609±1 Ma; Belousova et al., 2005), an in-house Paleoproterozoic standard A382 (1876±2 Ma; Huhma et al., 2012), and an in-house Archean standard A1772 (2712±1 Ma; Huhma et al., 2012). All of the three standards were run at the beginning and end of the analyses, and at regular intervals during the sessions. Data was corrected for background, laser-induced elemental fractionation, mass discrimination and drift in ion counter gains, yielding U-Pb isotope ratios by calibration to the concordant reference zircons mentioned above. The raw data reduction was executed with the program Glitter (Van Achterberg et al., 2001). Further data reduction for common lead correction and error propagation was performed using an in-house Excel spreadsheet. The Isoplot-extension in Microsoft Excel (Ludwig, 2003) was used to plot concordia-diagrams, calculate concordia ages and weighted average ages for the reduced U-Pb data.

2.5 Geophysical maps

Aeromagnetic geophysical maps both in greyscale and pseudocolour were used to plan the field work, and to help interpreting large scale structures of the study area. The shear zones that are one of the primary interests of this project appear continuous linear structures in the aeromagnetic maps. The abundance of mafic volcanics where the magnetism has been preserved makes interpreting both large and small structures easier, as they are easily identifiable in the pseudocolour map (Fig. 12). Some of the mafic intrusions, such as the Uunimäki gabbro, are visible in the pseudocolour map, helping to determine the extent and boundaries of the intrusions at the ground level.

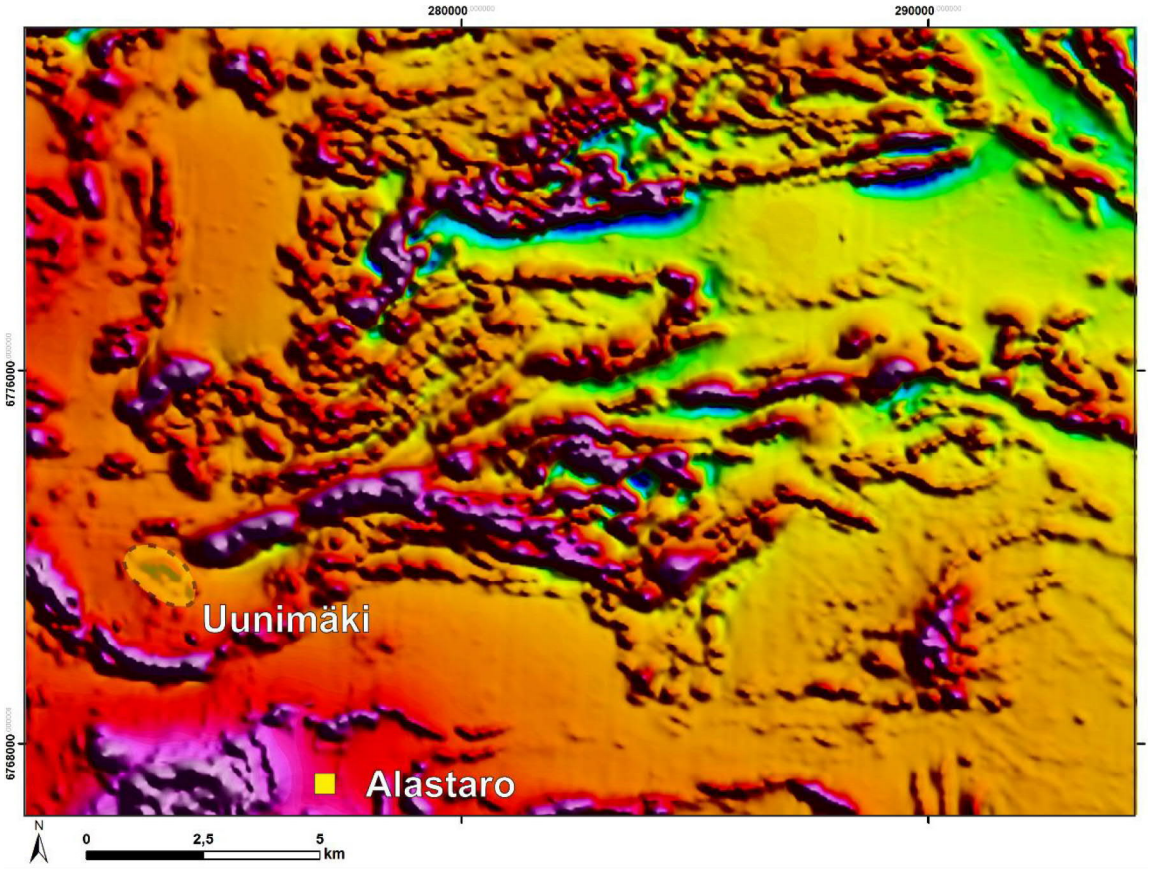

Fig. 12. Pseudocoloured aeromagnetic anomaly map with shading towards NW. Uunimäki area outlined with a dashed black line and shaded with yellow. The Kankaanranta shear zone can be seen in the middle of the map as an ENE-WSW-trending zone with a negative magnetic anomaly. Map provided by GTK.

3. Results

3.1 Petrography of the Uunimäki area

There are four main rock types in the Uunimäki area: gabbro, quartz diorite, granodiorite and paragneiss. The gabbro is surrounded most sides by granodiorite or quartz diorite. The exception is its SE margin, where it has a contact with paragneiss. The paragneiss is also common as enclosures within granodiorite or quartz diorite. The granodiorites and quartz diorites are very similar, and geochemistry in chapter 3.2 suggests there is little difference between them.

3.1.1 The Uunimäki gabbro

The Uunimäki gabbro is exposed as a 1000 x 700 m large oval-shaped intrusion and is clearly distinguishable from aeromagnetic maps. The colour of the Uunimäki gabbro is dark-gray, and it is most commonly medium-grained and equigranular (Fig. 13), though in some outcrops finer grained gabbros could also be observed. The gabbro rarely shows a strong mineral orientation but deformation has concentrated into shear bands and shear zones of varying sizes. The colour near the sheared areas commonly shift to a paler shade of gray. The Uunimäki gabbro is crosscut by quartz veins, hornblende-rich mafic veins, quartz-feldspar veins, carbonate veins and (rarely) pegmatite dykes. Magmatic layering is visible on some outcrops, and the gabbro contains cumulus-textured peridotitic enclaves, visible in outcrops and drill cores (Kärkkäinen et al., 2016).

Fig. 13. Left: Deformed gabbro crosscut by rusted quartz veins. TALE-2017-203. N: 6771836, E: 274025. Right: Fresh surface of the gabbro in hand specimen.

Mineralogically, the Uunimäki gabbro is not a gabbro *sensu stricto*, but a hornblende-gabbro where pyroxene has been replaced by hornblende (Fig. 14). The primary minerals are therefore plagioclase, amphibole and biotite. Accessory minerals include ilmenite, and in rare cases, pyrrhotite. Zircons are not common but are present as enclosures in some biotite grains (Fig 14B). Using the Michel-Levy method, the maximum extinction angles of suitable plagioclase grains determined from five thin sections ranged between 30-35°, giving an An content of An_{55}-An_{60}: labradorite. This is most likely not the original igneous composition of the plagioclase as the gabbro has undergone metamorphism. The amphibole is mostly hornblende. Alteration in the Uunimäki gabbro can be seen in the occurrence of sericite, chlorite, epidote and titanite. The sericitisation of plagioclase is the most common form of alteration and is visible in every thin section made from the gabbro (Fig. 14A) Biotite and amphibole have begun to alter to chlorite on the edges of many mineral grains.

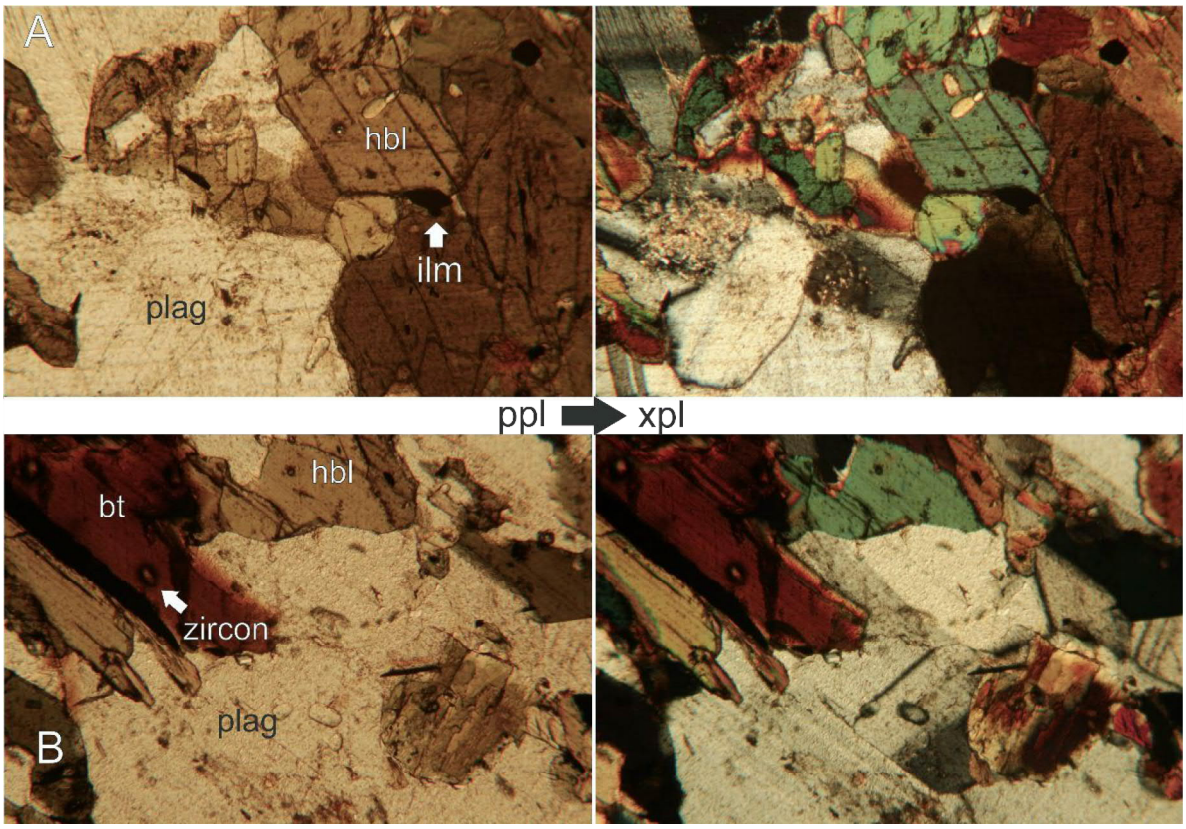

Fig. 14. Microphotographs of the Uunimäki gabbro. ***A)*** *Plagioclase has been partially altered to sericite. From an equigranular gabbro sample TALE-2017-117.1.* ***B)*** *Zircon enclosures with pleochroic halos in biotite. From the age sample TALE-2017-17.1.*

3.1.2 Granodiorites and quartz diorites

Though the geochemical classification in Fig. 19 determines the rock types as granodiorites and diorites, the rocks all have >5% of quartz. Therefore, two groups separated by geochemical classification are from here on considered granodiorites and quartz diorites. They are medium-grained, equigranular, and their colour ranges from dark-gray and brownish-gray to gray. The quartz diorites usually have a slightly larger percentage of mafic minerals, giving them a darker colour. Their primary minerals are plagioclase, biotite and quartz. In the granodiorites K-feldspar is also a primary mineral. Amphiboles are present as accessory minerals, with opaque minerals rarely being present. The granodiorites and quartz diorites display a strong orientation, and commonly have mafic enclaves elongated in that orientation. Quartz veins are sometimes present along the main foliation orientation, with rare aplite and pegmatite veins crosscutting the dominant structural features. Granodiorite and quartz diorite outcrops near the Uunimäki gabbro often have a heavily deformed look and are intruded by quartz veins (Fig. 15).

Fig. 15. Quartz diorite near the Uunimäki gabbro intruded by foliation-parallel quartz and quartz-feldspar veins. TALE-2017-122. N: 6771915, E: 273995.

The composition of the plagioclase in the quartz diorites and granodiorites was determined using the Michel-Levy method. There was no systematic difference in plagioclase composition between quartz diorites and granodiorites. The maximum extinction angles of suitable plagioclase grains ranged between 20-30°, giving an An-content of An_{35}-An_{50}: andesine. Biotites are elongated and have apatite and zircon inclusions. K-feldspar grains, when present, are often clearly coarser than the rest of the grains, making the rock locally porphyritic (Fig. 16).

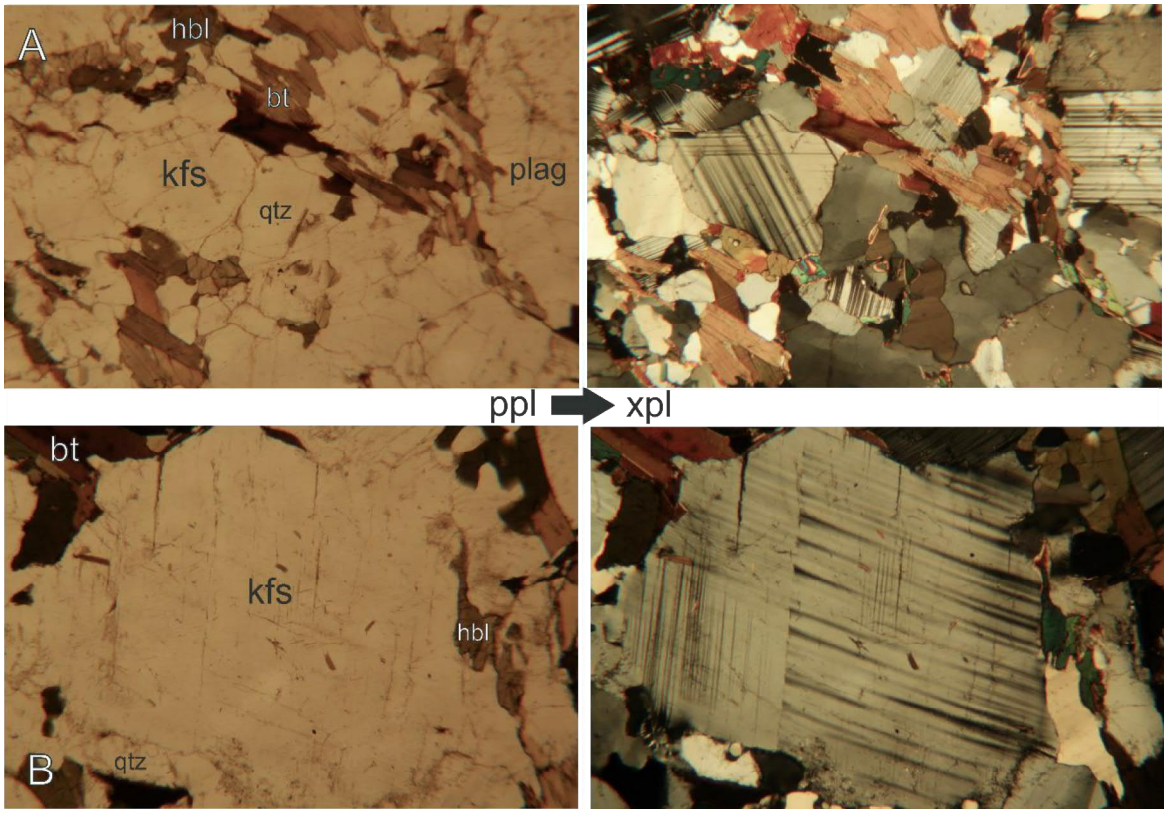

Fig. 16. Microphotographs of granodiorite from the Uunimäki area. ***A)*** *Equigranular granodiorite, from sample TALE-2017-72.1.* ***B)*** *K-feldspar porphyritic granodiorite, from sample TALE-2017-79.1.*

3.1.3 Paragneisses

The primary minerals of the paragneisses are biotite, quartz and plagioclase and the grain size is ~2-5 mm. It is clear from field observations that the composition of the paragneisses has varied quite a bit in the area, as the degree of migmatitisation varies from none to >50%. A paragneiss observation immediately to the north of the shear zone had two leucosome generations; one that was folded along with the paragneiss, and a later one that has intruded into the axial plane of the folding (Fig. 17). The direction of the fold axis in the folded paragneiss and leucosome is NE-dipping, and fits into the North fold structural domain outlined in chapter 3.4.

Fig. 17. A paragneiss with two generations of leucosomes near the Uunimäki gabbro. TALE-2017-7. N: 6 773 360, E: 275 570.

The sample TALE-2017-13.1 was taken from a partially migmatitic paragneiss inclusion within a quartz diorite intrusion in order to determine the conditions of peak metamorphism in the area. The metamorphic mineral paragenesis of the sample is biotite-cordierite-garnet, indicating upper-amphibolite to lower-granulite facies conditions (Fig. 18).

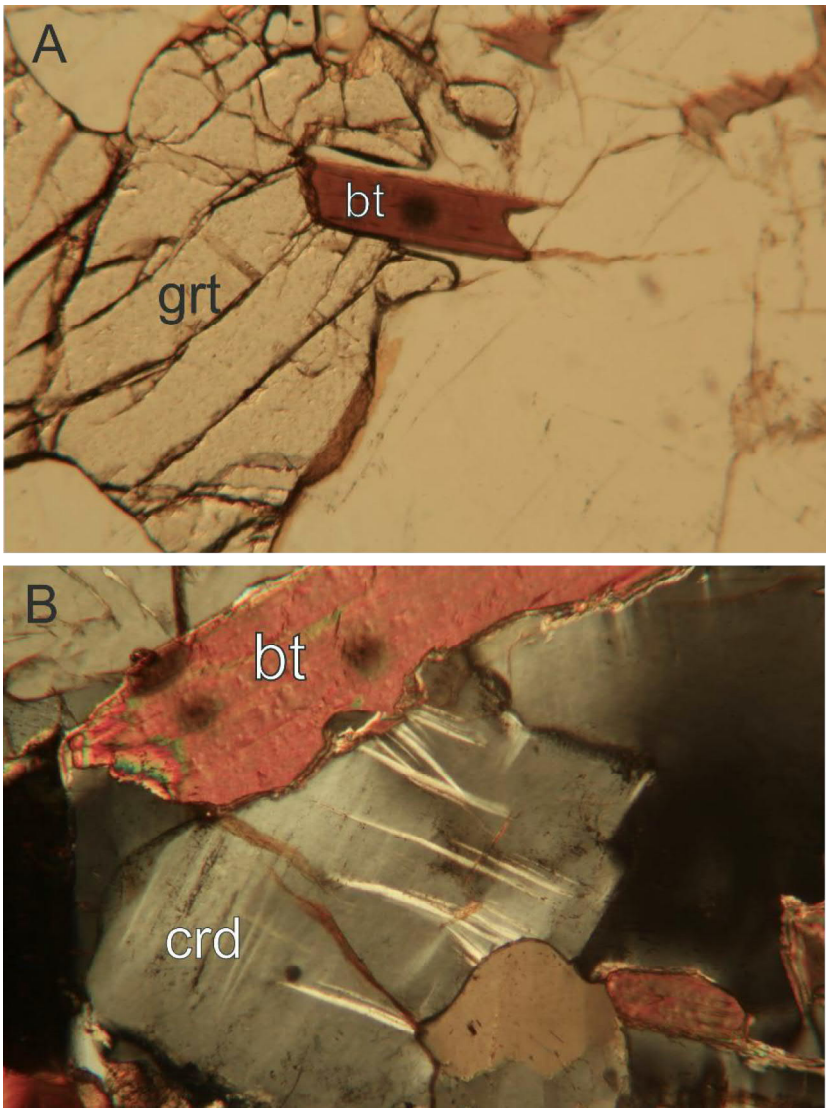

Fig. 18. Microphotographs of the biotite-cordierite-garnet paragneiss from sample TALE-2017-13.1. ***A)*** *garnet with biotite under plane-polarized light,* ***B)*** *cordierite with biotite under cross-polarized light.*

3.1.4 Revised lithological map

A revised version of the lithological map of the area was modified from Bedrock of Finland-DigiKP 1:50 000 (Fig. 19), based on new bedrock observations and structural measurements (Fig. 20). The boundaries of the Uunimäki gabbro were changed; the outcropped extent of the gabbro is smaller than in the previously drawn maps. Gabbro lenses to the SW of Uunimäki were removed, as only granodiorite was observed at the outcrops. The tonalite to the NW of Uunimäki was merged with the granodiorite and quartz diorite it was in contact with, as there were no apparent differences in the rocks. The porphyry granodiorite to the SE of Uunimäki was merged with the granodiorite and quartz diorite. While outcrops of porphyry granodiorite were found, they do not follow the boundaries previously drawn on the map, and do not crop out systematically enough

to separate as their own unit in this scale. Gabbro lenses to the SE of Uunimäki were removed or changed to diorite. Those that were removed could not be observed in the field at all, or were too small to consider their own units in this scale. Some gabbro lenses in the eastern end of the study area were also changed to diorite. The contacts between diorite and paragneiss were re-drawn in the western end of the area to fit field observations better. Several lithological units were merged for the sake of simplicity and lack of systematic differences: pegmatite-granite and granite units were merged to granite, hornblende-gneiss and amphibolite were merged to amphibolite, while volcanic conglomerate, uralite-porphyry, plagioclase-porphyry and mafic volcanics were merged to mafic volcanics.

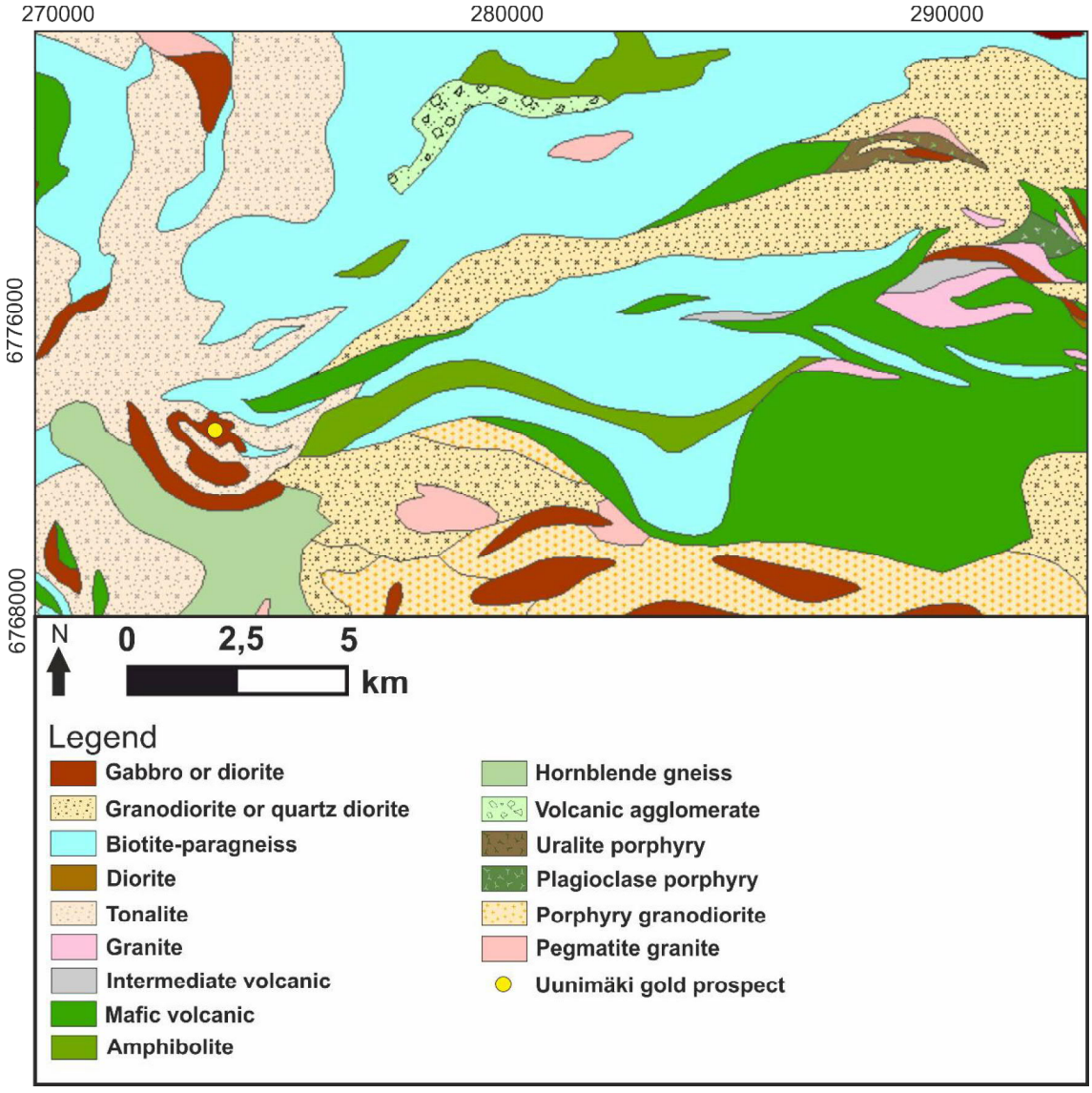

Fig. 19. Original lithological map of the study area. Bedrock of Finland-DigiKP 1:50 000.

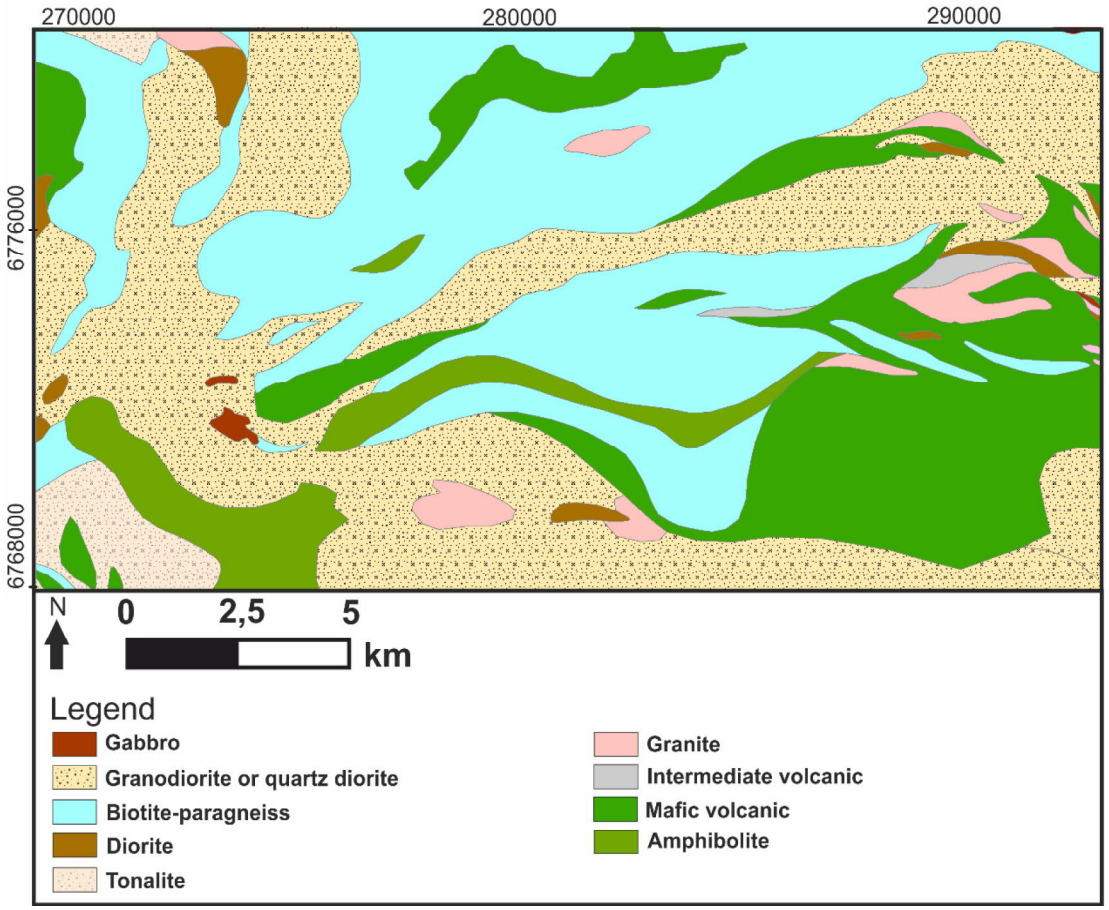

Fig. 20. Revised lithological map of the study area. Modified from Bedrock of Finland-DigiKP 1:50 000.

3.2 Geochemistry

Eighteen samples that were collected from the study area were analysed and are used for geochemical comparison (Table 2). The samples include eight samples of the Uunimäki gabbro, granodiorites and quartz diorites from near Uunimäki and five samples of the Jokisivu diorite. The samples were mostly selected for analysis for looking as homogenous as possible, and with no veins crosscutting the sample. Some of the samples were, however, collected from near contacts with other rock types or close to shear zones, and two of the diorite samples from Jokisivu were visibly altered.

Table 2. List of rock types and samples collected for geochemical analysis.

Rock type	Number of samples	Sample #
Uunimäki gabbro	8	TALE-2017-16.1 TALE-2017-17.1 TALE-2017-107.1 TALE-2017-108.1 TALE-2017-117.1 TALE-2017-129.1 TALE-2017-182.2 IJPI-2017-159.2
Uunimäki area quartz diorite or granodiorite	5	TALE-2017-12.1 TALE-2017-14.1 TALE-2017-72.1 TALE-2017-79.1 IJPI-2017-159.1
Jokisivu diorite	5	JKKA-2017-26.1 JKKA-2017-26.2 JKKA-2017-26.3 JKKA-2017-27.1 JKKA-2017-27.2

Previously published geochemical analyses from twelve drill core samples from the nearby Palokallio gold prospect are also used for comparison (Voipio, 2008). Both the Jokisivu and Palokallio deposits are hosted by mafic intrusive rocks with similar structural control. The sampled sites are concentrated on the NW part of the studied area (Fig. 21). The full list of results from the geochemical analyses can be seen in Appendix 1.

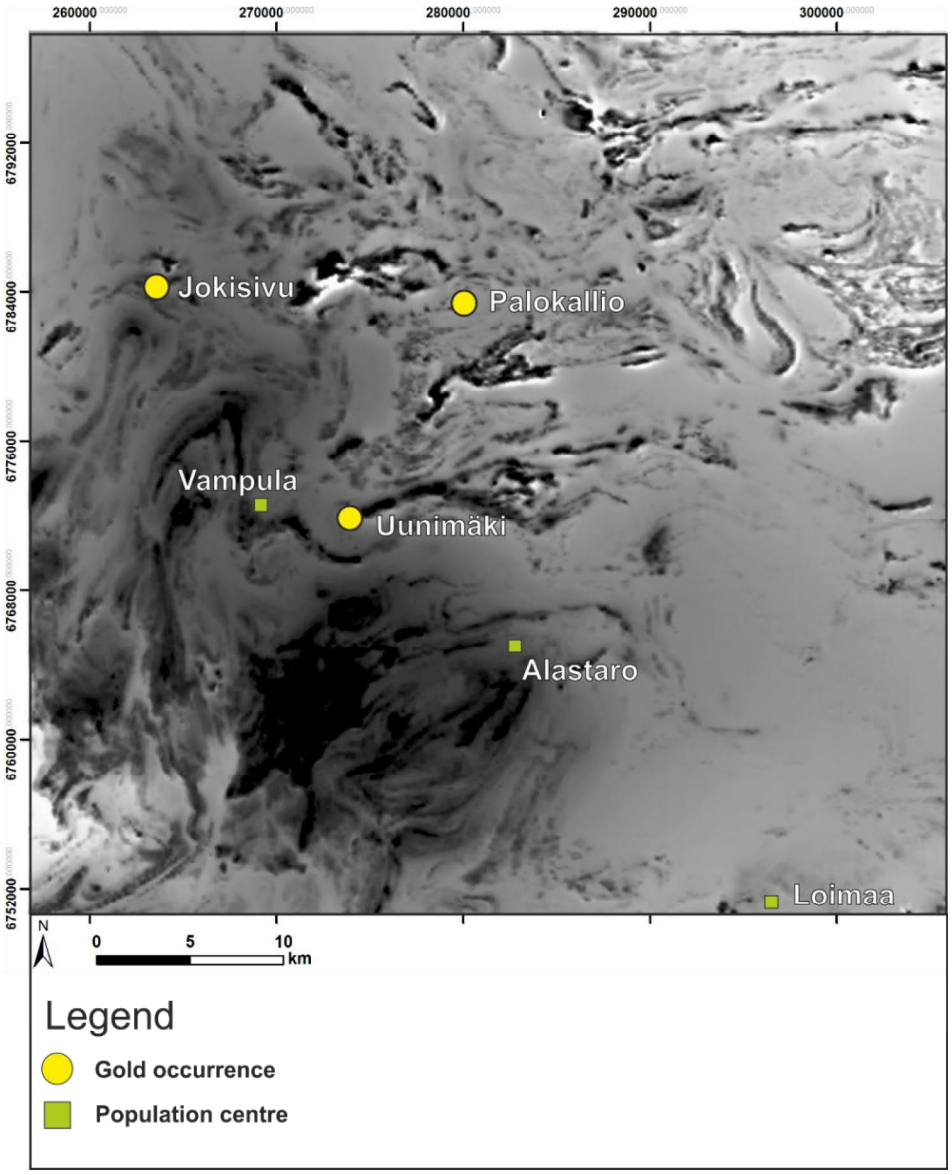

Fig. 21. Map of the western Häme Belt with sampled gold occurrences noted. Greyscale aeromagnetic anomaly map provided by the Geological Survey of Finland used as background.

3.2.1 Major elements

The mafic plutonic rocks of the Uunimäki are classified as gabbros in the Total Alkali vs. Silica (TAS)-diagram (Middlemost, 1994) due to their low SiO_2 content, and relatively low concentrations of Na_2O and K_2O (Fig. 22). Two of the samples show slightly elevated SiO_2-contents in comparison to the rest; these samples are the collected north of the main Uunimäki gabbro but interpreted to be a part of the same intrusion.

Four of the granitoid samples that were collected from outcrops near the Uunimäki gabbro are classified as diorites in TAS-diagram. However, as the samples contain >5% quartz,

they are considered quartz diorites. Additionally, two of the samples contain enough k-feldspar to be considered granodiorites. One sample is classified as a monzonite (TALE-2017-12.1), but it is also considered a quartz diorite as i) its SiO_2-content of 56.99-wt% is within the limits of what is classified as a diorite, ii) the high Na_2O+K_2O-content which causes the sample to plot into the monzonite-field instead of the diorite-field is due to alteration rather than original magmatic composition and iii) aside from signs of alteration, the rock looks similar to the other two quartz diorites that were sampled. The geochemistry of the granodiorite and quartz diorite samples will be detailed as a single group, unless there is a significant systematic difference between geochemical contents between the samples of the two rock types.

The samples from Jokisivu plot neatly into the gabbroic diorite field, while the Palokallio samples plot into the gabbroic diorite, diorite, monzodiorite and monzonite fields. The four groups form a fairly continuous series with alkali content slightly increasing along with increasing silica.

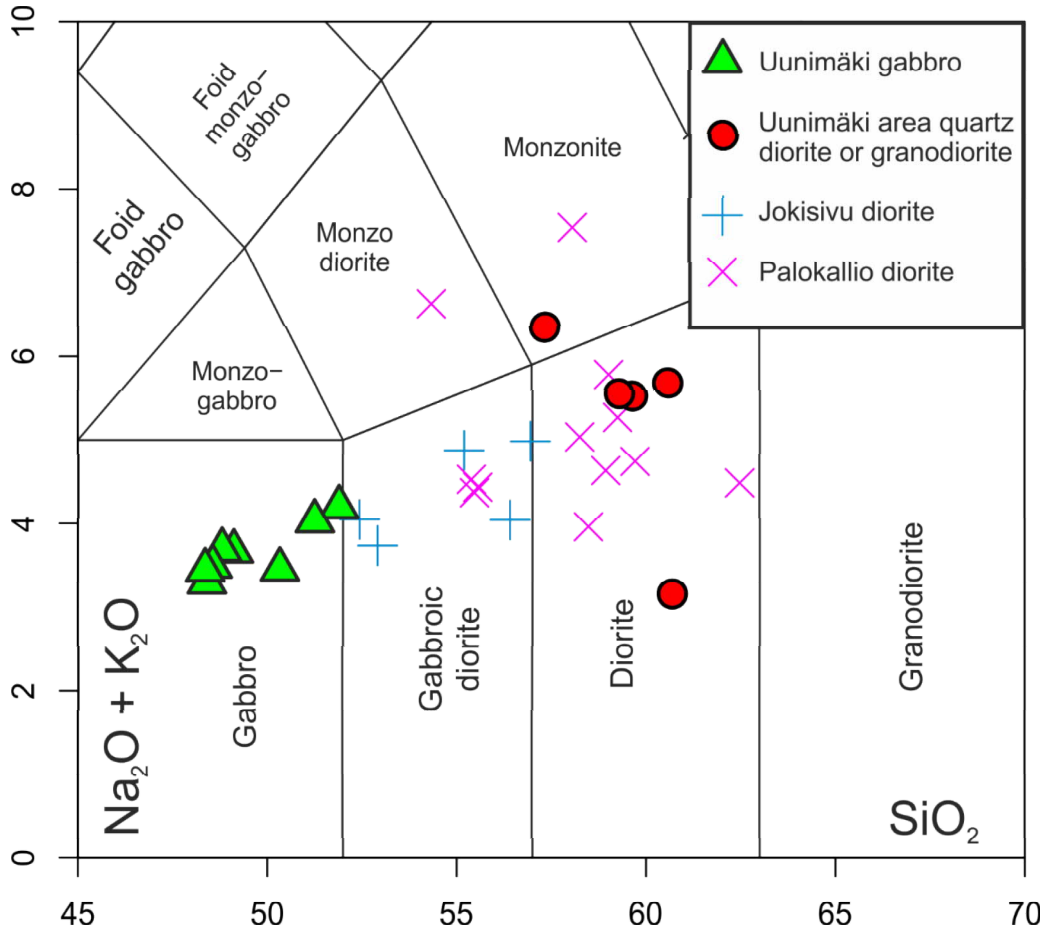

Fig. 22. Geochemcial classification of the collected samples in the Total Alkali vs. Silica -diagram for plutonic rocks according to Middlemost (1994). Samples from Jokisivu and Palokallio are shown for comparison.

The SiO_2-content of the Uunimäki gabbro varies between 48.03-51.57 wt-% (Fig. 23). The Uunimäki gabbros contain high contents of CaO (8.40-9.93 wt-%). The sample with the highest CaO is crosscut by amphibole veins. The MgO content of the Uunimäki gabbros varies between 4.16-5.29 wt-% and Fe_2O_3 is abundant at 11.59-13.97 wt-%. The Al_2O_3 content is standard (16.86-18.68 wt-%) and does not significantly vary from Jokisivu or Palokallio. K_2O-content of the samples is very low at 0.49-1.35 wt-%; the two samples (TALE-2017-182.2 and IJPI-2017-159.2) with the highest contents have most likely undergone alteration as they are collected near the contact of a shear zone. Regardless of alteration, the gabbro samples belong in the calc-alkaline series according to the SiO_2 vs K_2O diagram (Peccerillo & Taylor, 1976). The Na_2O-content is standard at 2.64-3.16 wt-% with little variance between samples. P_2O_5 content is low at 0.19-0.29 wt-%, and consequently no apatite grains are visible in thin sections. TiO_2 is high at 1.30-1.92 wt-%, causing crystallisation of ilmenite.

The SiO_2-content of the quartz diorite and granodiorite samples vary between 56.99-60.14 wt-%. In four of the samples Al_2O_3 content is between 15.35-17.84 wt-%, but one sample (TALE-2017-12.1) has an Al_2O_3 content as high as 19.67 wt-%. Fe_2O_3-content ranges between 6.15-8.62 wt-%. The MgO content varies between 1.67-4.40 wt-%. CaO-content ranges between 4.60-6.21 wt-%. Na_2O-content for four of the samples varies between 3.03-3.97 wt-%, but one sample (IJPI-159.1) has only 1.32 wt-% Na_2O. K_2O-contents of the samples are between 1.67-2.48 wt-%. TiO_2 contents are between 0.64-1.12 wt-%. P_2O_5 contents of the samples are predictably low, ranging between 0.12-0.29 wt-%.

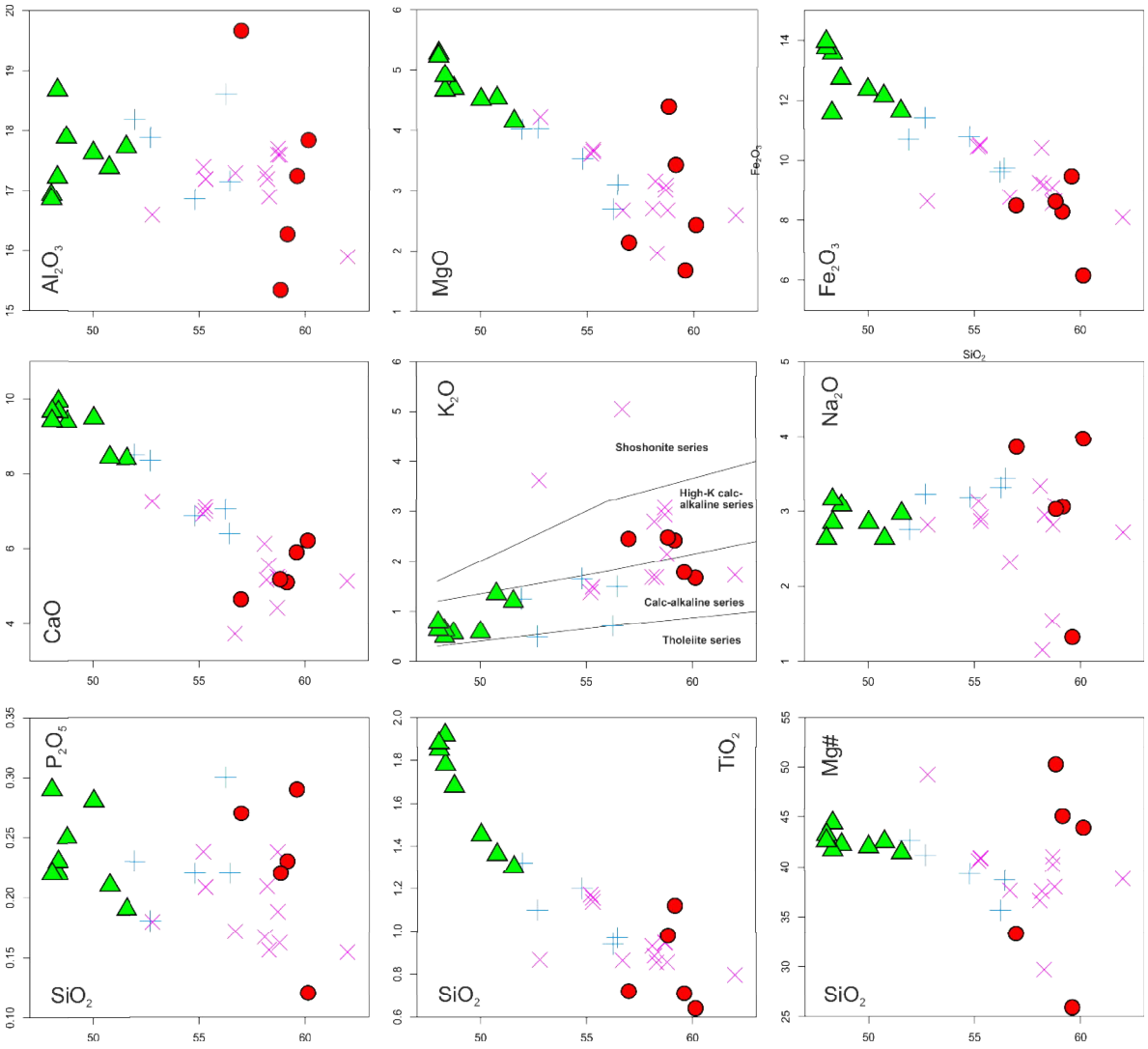

Fig. 23. Major element vs. Silica diagrams from the rocks of the Uunimäki area. Palokallio and Jokisivu samples shown for comparison. Symbols as in Fig. 21.

3.2.2 Minor elements

In the Uunimäki gabbro, Rb contents are between 7.0-16.1 ppm, except for the two altered samples that have contents of 36.8 and 42.5 ppm respectively (Fig. 24). Ba-content is between 173-291 ppm, also slightly elevated in the altered samples. Sr-content is between 302.7-445.2 ppm. Ni-content of the Uunimäki gabbro is low (7.1-15.5 ppm), as is the Cr-content (5-14 ppm). Nb-content is between 8.9-11.7 ppm. There is some variation in the Zr-content, which varies between 59.3-124.5 ppm. Y-content is 19.2-26.2. F-content ranges between 257-432, except for the altered sample IJPI-2017-159.2, which has a F-content of 627.

The Rb-content of the granodiorite and quartz diorite samples is between 48.7-127.4 ppm Ba-contents are between 390-532 ppm. Sr-contents are between 315.9-421.3 ppm. There is considerable variation in Ni-content, as it ranges between 3.4-41.4 ppm, just as there is in Cr-content (6-106 ppm). Two samples have anomalously low Ni- and Cr-contents (TALE-2017-12.1 and IJPI-2017-159.1), and one sample has anomalously high contents in Ni and Cr (TALE-2017-14.1). Nb-content is between 10.9-17.4 ppm, except in sample TALE-2017-14.1, which has 42.9 ppm of Nb. Zr-content varies between 167.4-240.9 ppm. Y-content is between 15.3 -31.9 ppm. F-content is between 442-485 ppm., except in sample TALE-2017-14.1, where it is 820 ppm.

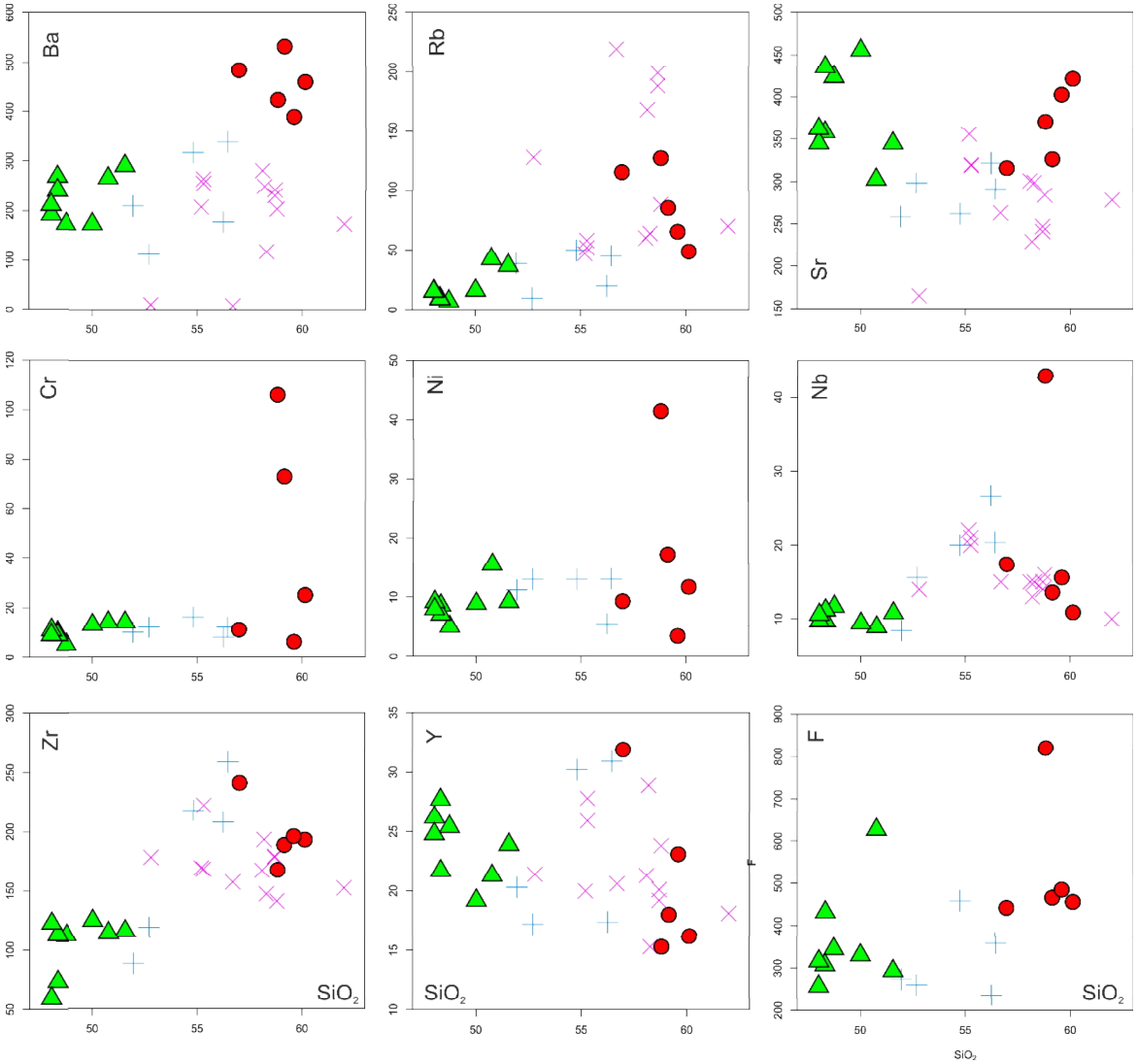

Fig. 24. Minor element vs. Silica diagrams from the collected samples. Palokallio and Jokisivu samples shown for comparison. Symbols as in Fig. 21.

3.2.3 Trace elements

The REE-pattern of the Uunimäki gabbro is relatively gently sloping (Fig. 25) (Boynton, 1984). The LREE are only slightly enriched (La_N/Yb_N = 3.41-4,′.77), (La_N/Sm_N = 1.62-2.41), (Gd_N/Yb_N = 1.47-1.94). There is no clear Eu-anomaly in the samples (Eu/Eu* = 0.89-1.14). There is some variation in the total REE-content of the samples (REE_{tot} = 71.4 – 103.4). Geochemical alteration has not affected the abundances of the REE in the gabbro.

The REE-slope of the quartz diorites and granodiorites is steeper than in the gabbro. One sample, TALE-2017-12.1 is clearly anomalous as it is enriched in the HREE, so it is not included in the REE-calculations. The granodiorites and quartz diorites are clearly enriched in LREE, and not enriched in HREE (La_N/Yb_N = 4.78-12.61) (La_N/Sm_N = 1.83-4.03), (Gd_N/Yb_N = 1.44-2.04). There is no Eu-anomaly in either the quartz diorite (Eu/Eu* = 0.90-1.00) or granodiorite samples (Eu/Eu* = 1.07-1.10).

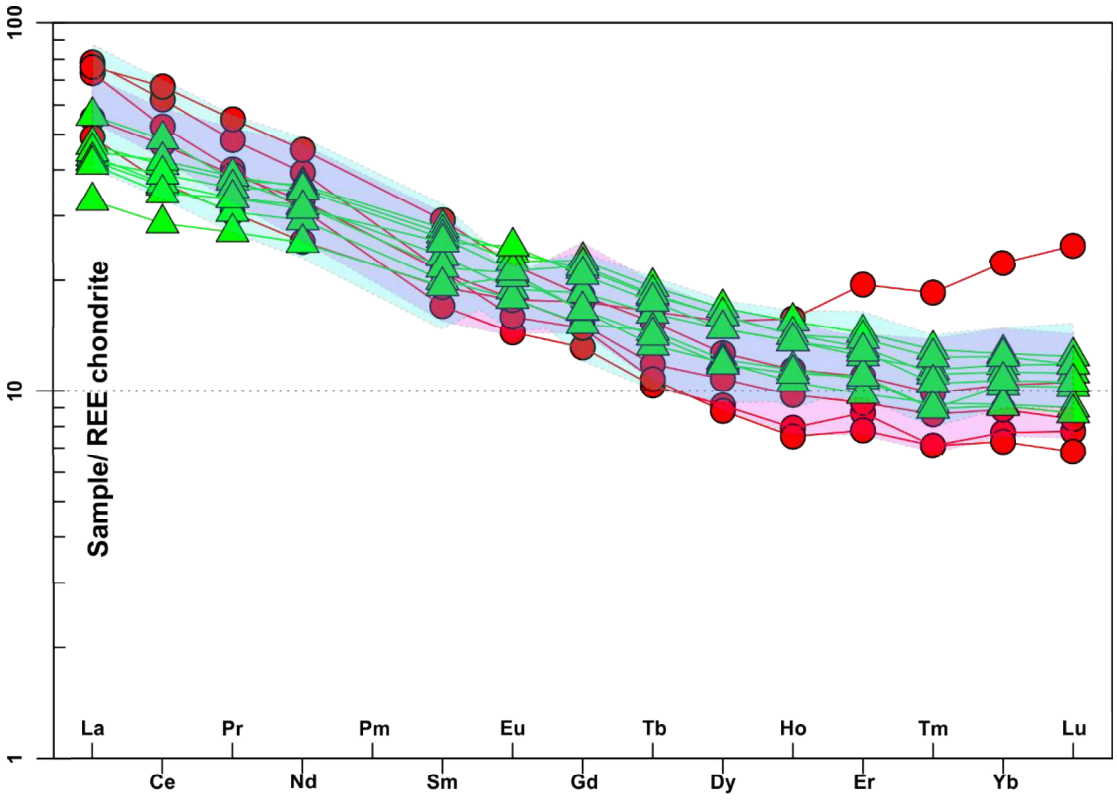

Fig. 25. Spider-diagram of the REE-contents of the collected and reference samples based on Boynton (1984). Symbols otherwise as in Fig. 21, except the Jokisivu sample range in a light blue shade, and the Palokallio samples in a pink shade.

The Uunimäki gabbro is not enriched in fluid-mobile elements (Rb, K, Sr, Ba) and Th-content is low, apart from two samples (TALE-2017-182.2 and IJPI-2017-159.2) that show clear enrichment in these elements (Fig. 26). The two samples are the altered samples previously mentioned in this chapter. The negative Ta-Nb anomaly, which is common in subduction zone rocks, is not present. There is a slight negative Zr-Hf in relation to Sm. The gabbro is slightly enriched in Ti and Yb.

The granodiorites and quartz diorites are slightly enriched in fluid-mobile elements (Sr, K, Rb, Ba). There is a slightly negative Ta-Nb-anomaly in the samples, and a significant negative Ti-anomaly, which is indicative of subduction-related rocks. On the other hand, there is a very slight positive Zr-Hf-anomaly in the samples, which is atypical for subduction-related rocks.

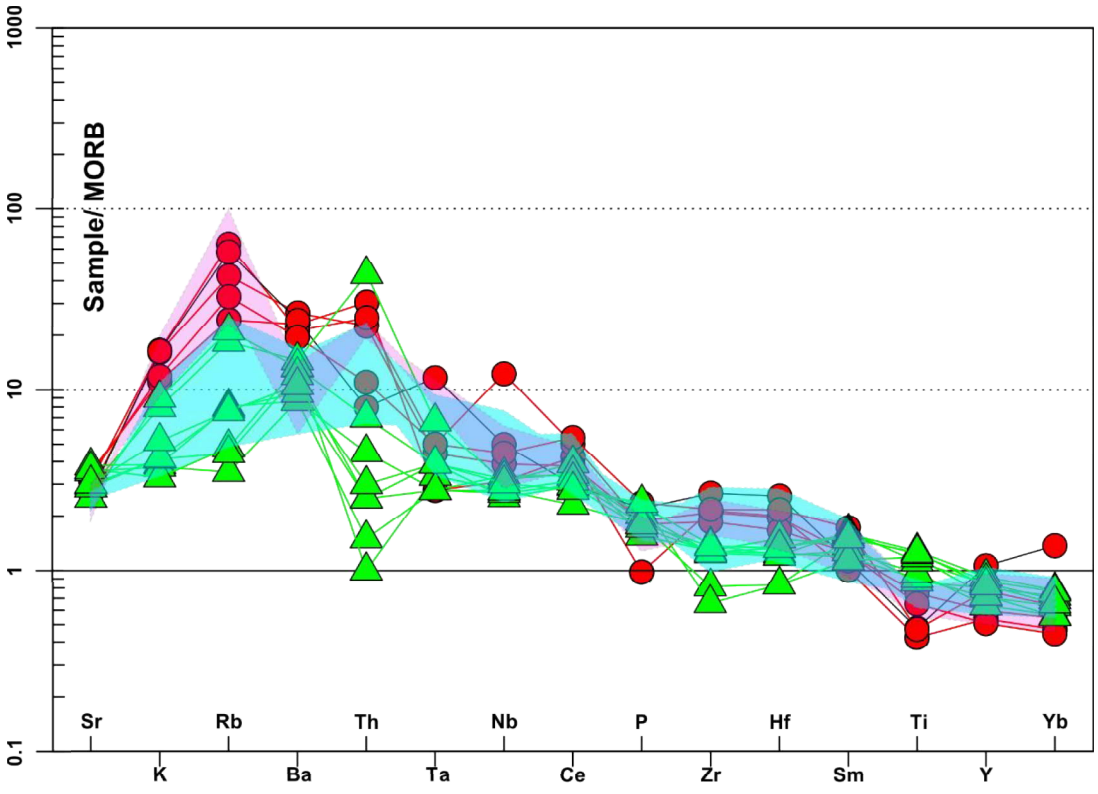

Fig. 26. MORB-normalized Spider-diagram of the collected and reference samples based on Pearce (1983). The Jokisivu sample range is in a light blue shade, while the Palokallio sample range is in a pink shade.

Most of the gabbro samples fall into the MORB-OIB array in the diagram by Pearce (2008) (Fig. 27). This contrasts with the diorites from Jokisivu and Palokallio, with the quartz diorites and granodiorites surrounding the Uunimäki gabbro, which plot into the

volcanic arc array. Two altered samples are clear outliers in these ratios, sample TALE-2017-182.2, where Th-content is eightfold to the rest of the gabbro samples, and TALE-2017-12.1, the altered quartz diorite containing garnet and where Th has been depleted.

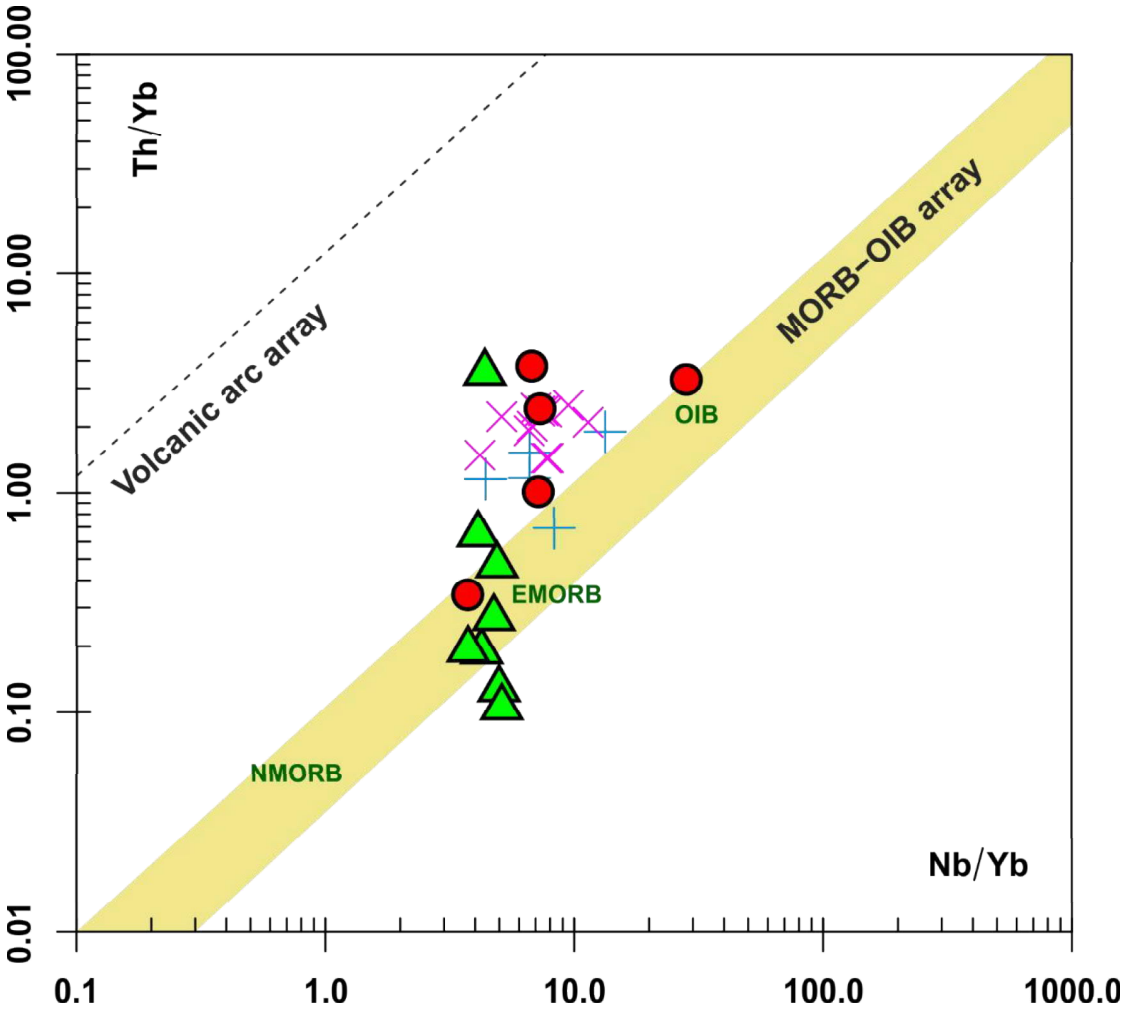

Fig. 27. Collected and reference samples in the geotectonic Nb/Yb vs. Th/Yb -diagram according to Pearce (2008). Symbols as in Fig. 21.

According to the magma series discrimination for different tectonic environments based on trace element geochemistry by Wood et al. (1979), the Uunimäki gabbro has an E-MORB or within-plate tholeiitic signature based on its Zr/Hf-Nb/Ta-Th-content (Fig. 28). The sample with an anomalously high Th-content (TALE-2017-182.2) predictably plots closer to Th, and shows a calc-alkaline basalt signature. The quartz diorites and granodiorites do not plot neatly into the diagram, with one of the samples having a within-plate alkaline signature, while two of the samples have an E-MORB or within-plate tholeiitic signature, and the remaining two have a calc-alkaline basalt signature. The Jokisivu and Palokallio diorites have a calc-alkaline basalt nature based on this discrimination.

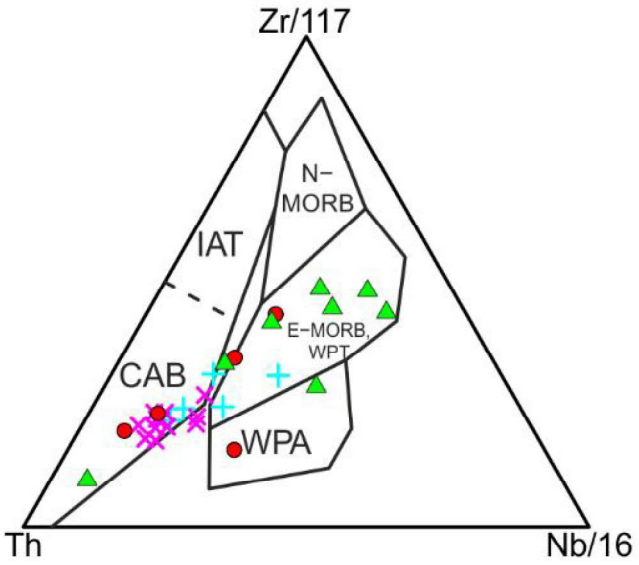

Fig. 28. Geotectonic discrimination diagram for igneous rocks based on Zr-Nb-Th composition (Wood, 1979). The Palokallio samples do not have Hf and Ta measurements, so Zr and Nb were used in their place.

None of the samples collected are enriched in Au or Ag. Three of the gabbro samples, TALE-2017-107.1, TALE-2017-129.1 and IJPI-159.2, are enriched in As. Two samples, TALE-107.1 and TALE-108.1, show enrichment in Cu. None of the samples are particularly enriched in B, Bi, Hg, S, Sb, Te or W; other common pathfinder elements for gold.

3.3 U-Pb zircon analyses

The zircons separated from the Uunimäki gabbro are most commonly prismatic grains (Fig. 29), typical for zircon crystals in gabbros (Corfu et al., 2003). Their colour ranges from completely transparent to light brown. As most of the grains are prismatic and elongated, their length is mostly 50-200µm, but only 15-50µm in width. Only a few of the zircons are wider than 50µm. The inner structures of the zircon grains are very homogenous; very few crystals show oscillatory zoning or cores and there are no visible inclusions. Cracks are common; it was the most common reason for some zircons not to be suitable for spot analysis.

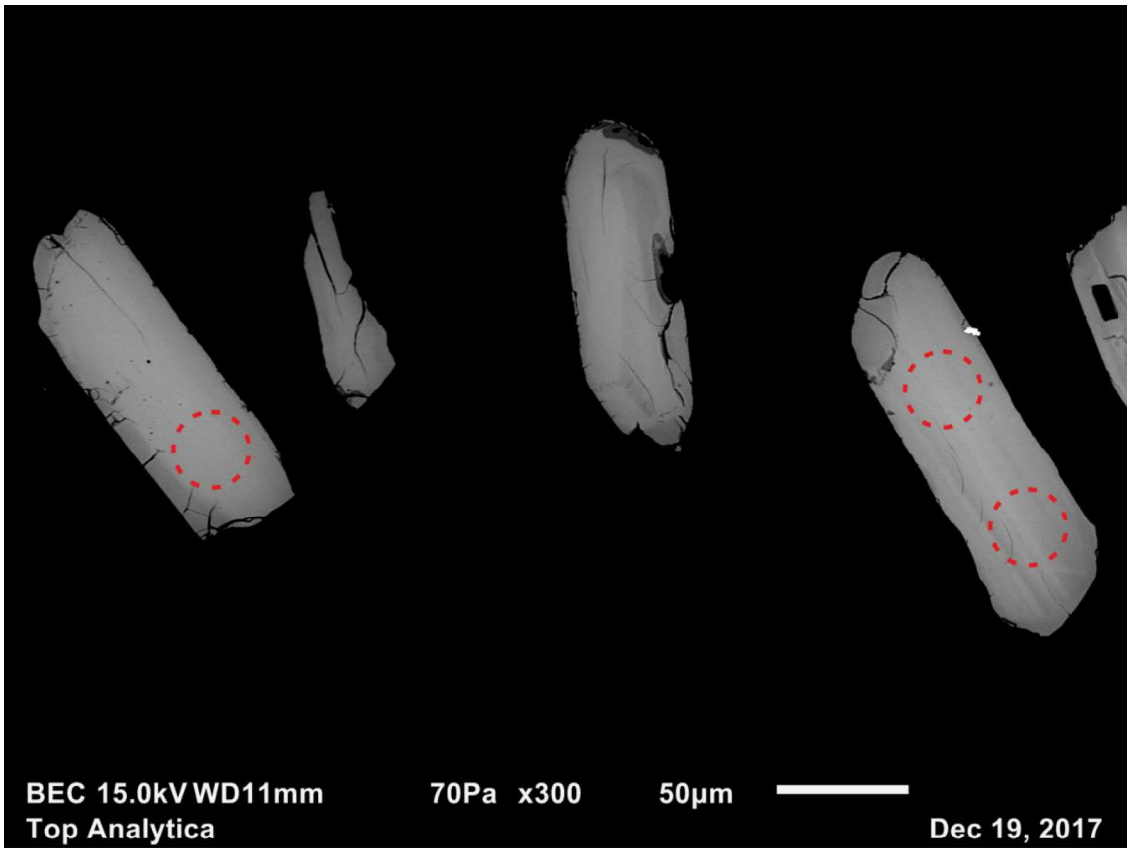

Fig. 29. Close-up BSE-image of zircon grains separated from the Uunimäki gabbro. Dashed red lines represent sites selected for spot analysis.

34 analyses were performed from 32 grains. Four different age populations were found from the analyses (Fig 30A). 1) An older population containing two zircons yielded $^{207}Pb/^{206}Pb$ ages of 1920 and 1917 Ma and most likely represent inherited crystals (Fig. 31A). 2) The largest population contains 24 zircons and yielded a concordia age of 1891 ± 5 Ma (Fig 30B). The $^{207}Pb/^{206}Pb$ age of the largest population is 1894 ± 5 Ma (Fig. 31B). 3) A younger population that contains 6 zircons yielded a condordia age of 1864 ± 10 Ma (Fig. 30C). 4) The youngest population consists of two zircons and yielded $^{207}Pb/^{206}Pb$ ages of 1845 and 1835 Ma (Fig. 31A). No textural differences can be recognized between the zircon populations (Fig. 32). The full list of results from the U-Pb analyses can be seen in Appendix 2.

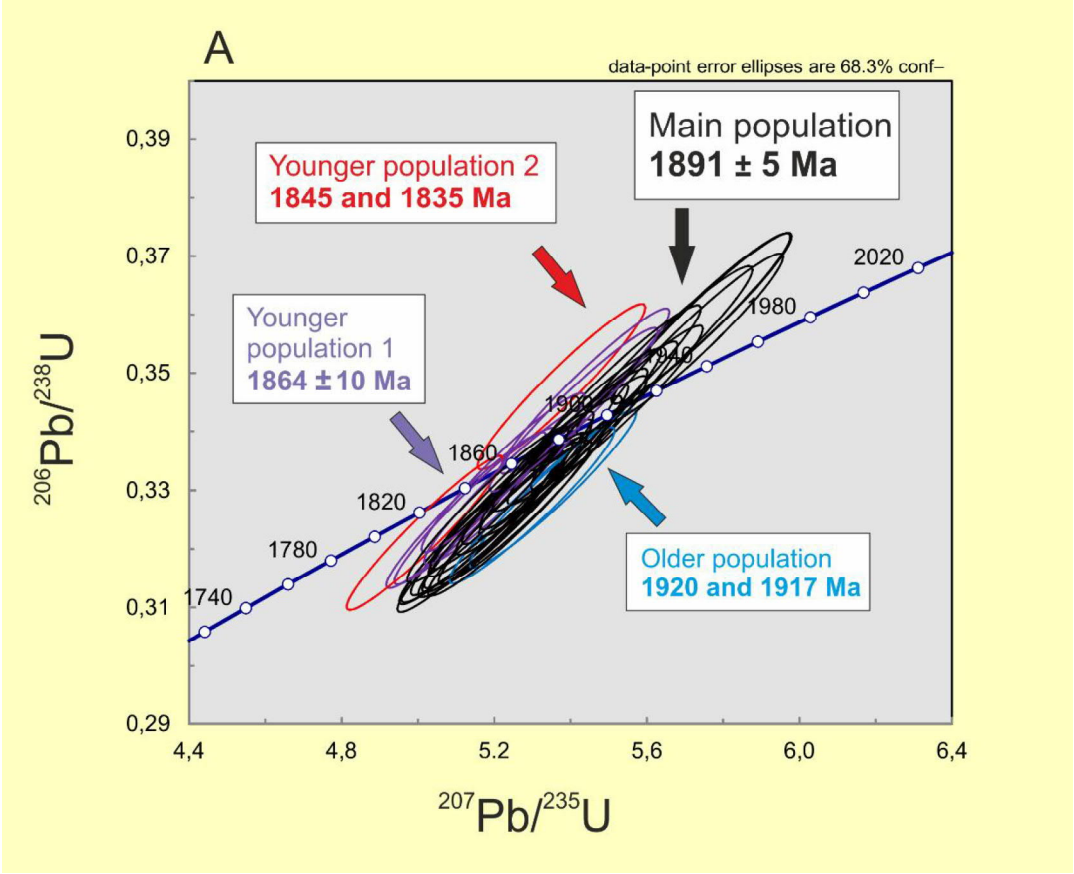
A
data-point error ellipses are 68.3% conf–
Main population
1891 ± 5 Ma
Younger population 2
1845 and 1835 Ma
Younger
population 1
1864 ±10 Ma
Older population
1920 and 1917 Ma
2020
1980
1940
1900
1860
1820
1780
1740
0,39
0,37
0,35
0,33
0,31
0,29
4,4
4,8
5.2
5,6
6,0
6,4
206Pb/238U
207Pb/235U

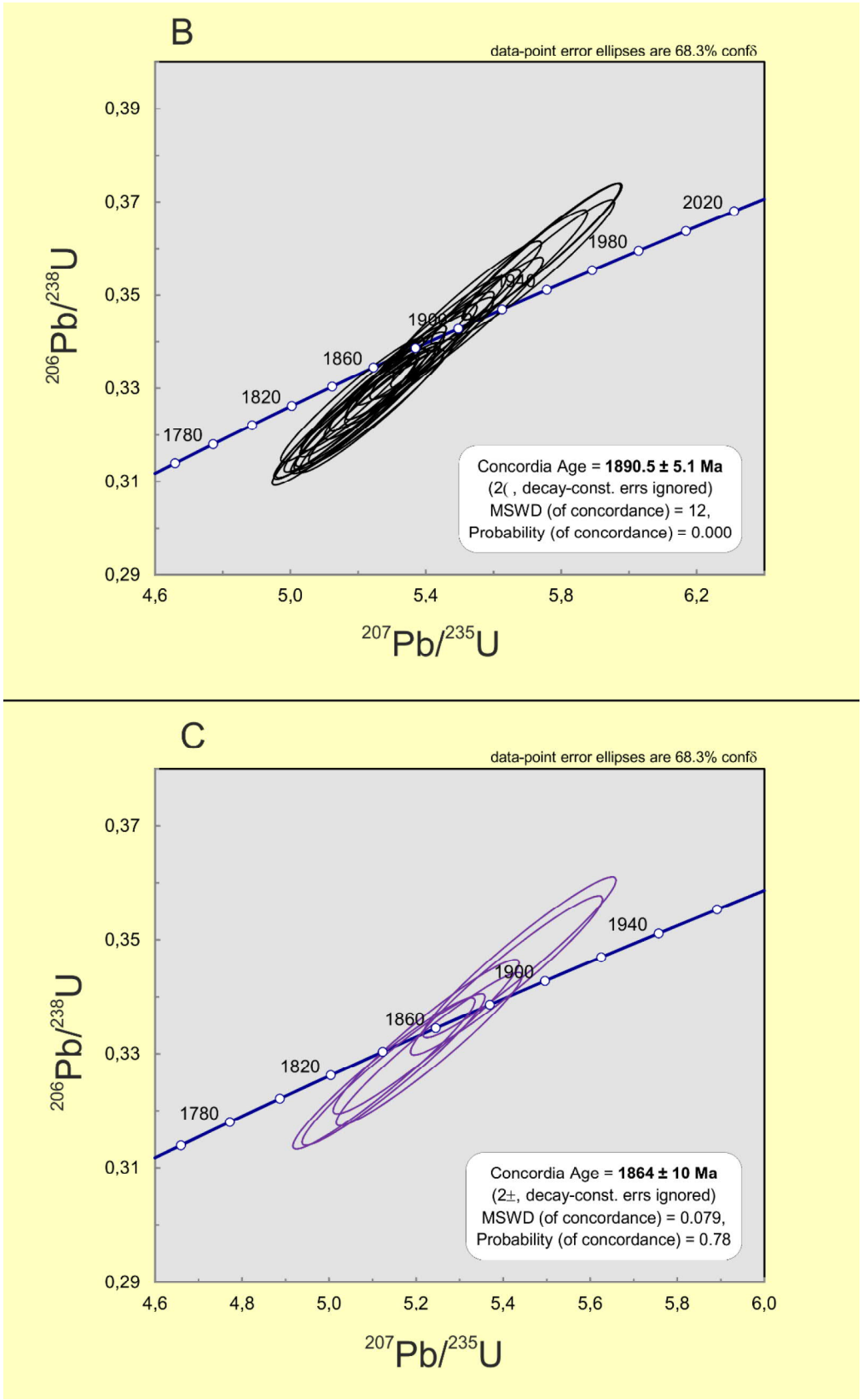

Fig. 30. Condordia ages for the zircons separated from the Uunimäki gabbro. ***A)*** *All of the zircons with four populations noted.* ***B)*** *Concordia age for the main population of zircons.* ***C)*** *Concordia age for the 1864 ± 10 Ma population of zircons.*

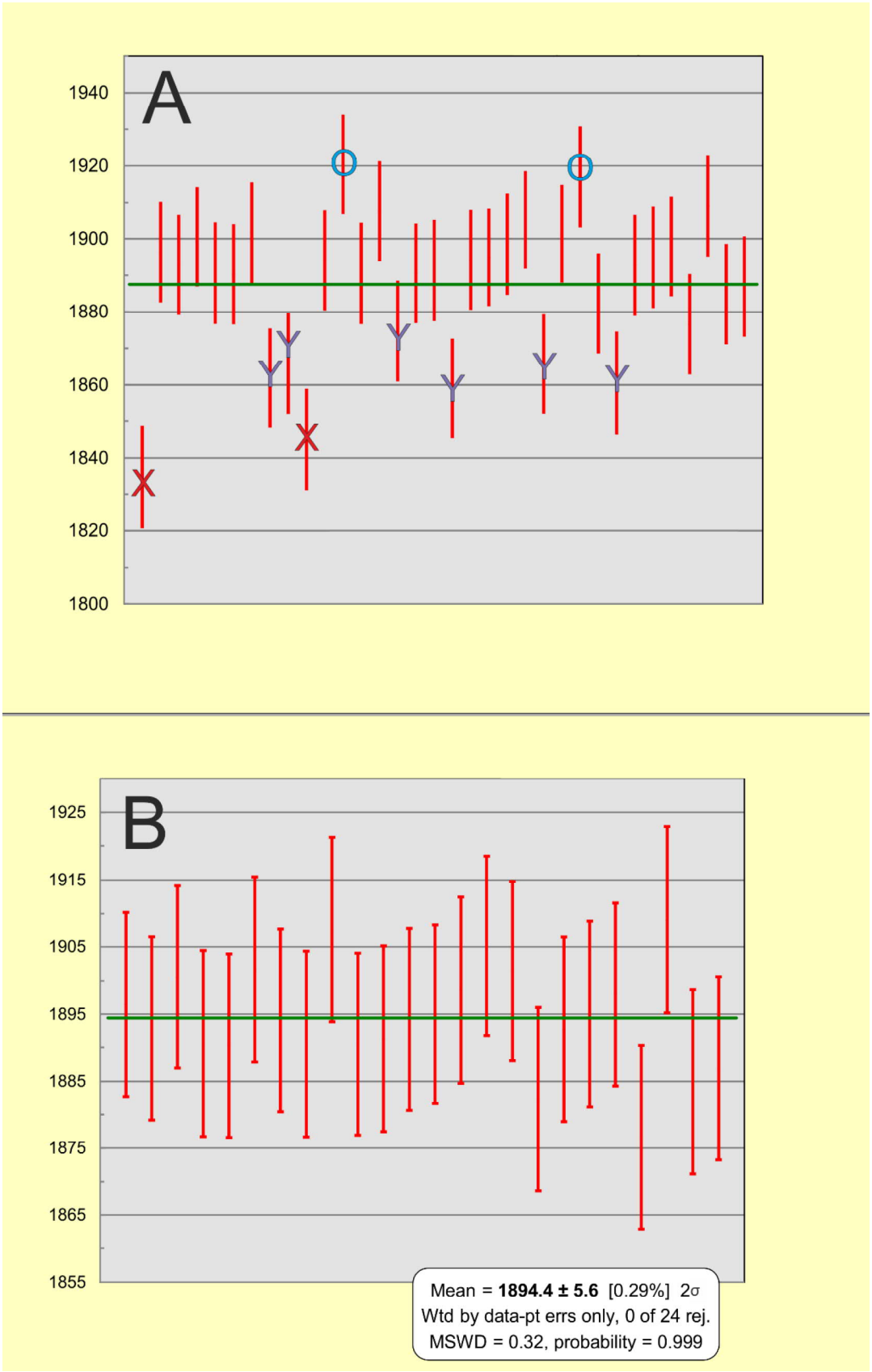

Fig. 31. ***A)*** *$^{207}Pb/^{206}Pb$ weighted average ages for all of the analyses from the Uunimäki gabbro. Analyses representing an older population marked with a blue O and analyses representing younger populations marked with a purple Y or red X.* ***B)*** *$^{207}Pb/^{206}Pb$ weighted average ages for the interpreted magmatic population of zircons from the Uunimäki gabbro.*

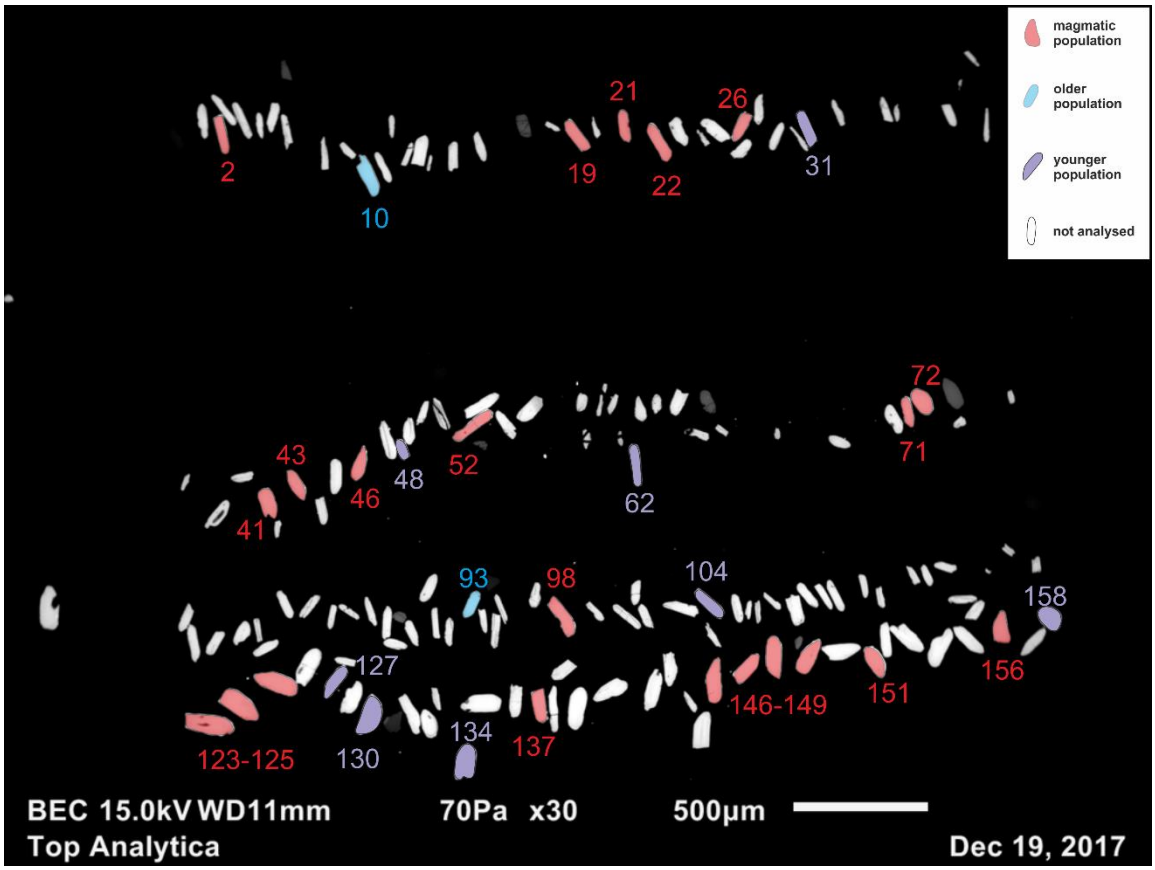

Fig. 32. BSE-image of the zircons separated from the Uunimäki gabbro. Zircons representing the magmatic population marked with red, zircons from the older population marked with blue, zircons from younger populations marked with purple, and zircons not analysed are white. Reference numbers of analysed zircons marked above or below the respective grain.

3.4 Structural geology

The structural domains of the western Häme Belt were delinated based on aeromagnetic signatures of the crust, previously existing observations and structural data, as well as new field observations and the acquired structural data. Six subareas were identified based on dominant structures: the Alastaro shear zone (N-S trending), the Kankaanranta shear zone (ENE-WSW trending), the North fold, the Alastaro fold, the Oripää fold and the Uunimäki area (Fig. 33). The western termination of the structurally mapped area is roughly bound by the Alastaro shear zone, which is likely linked to other major shear zones in SW Finland; the NE-SW-trending Kolinummi shear zone in the south (Väisänen & Skyttä, 2007), and the NW-SE-trending Kynsikangas shear zone in the north (e.g. Pietikäinen, 1994; Reimers et al., 2018). The Alastaro shear zone is characterized by

penetrative ductile dip-slip type shearing, steeply-dipping planar and linear structures,

and W-block up kinematics (Pitkälä, in prep.). The Kankaanranta shear zone is also characterized by dominantly dip-slip type shearing and steeply dipping planar structures. However, the ductile shearing is not as penetrative as in the Alastaro shear zone, and the associated stretching lineations show a wider range of trends and plunges indicating the setting is not just dip-slip dominated in the same way as the Alastaro shear zone is. There is also a pronounced dextral strike-slip component present as indicated by gently-plunging lineations associated with dextral kinematic indicators observed from the western part of the shear zone. Regional folding dominates the structural environment outside the shear zones. The folded domains occur within a loosely defined NW-SE trending zone, where the orientation of the fold axes exhibits a gradual shift from NNE-plunging in the North fold to E-dipping in the Oripää fold, with the Alastaro fold in between having an incoherent orientation. The interpreted structural evolution of the western Häme Belt is discussed in more detail in the MSc thesis of Iiro Pitkälä (Pitkälä, in prep.).

The target of this investigation, the Uunimäki area, is spatially located near the junction of the Alastaro and Kankaanranta shear zones, and showcases a complex environment with three distinct structural orientations. To explain how these orientations have formed, we must first examine the Kankaanranta shear zone and its splays as the Uunimäki gabbro is located immediately to the south of the western termination of the shear zone.

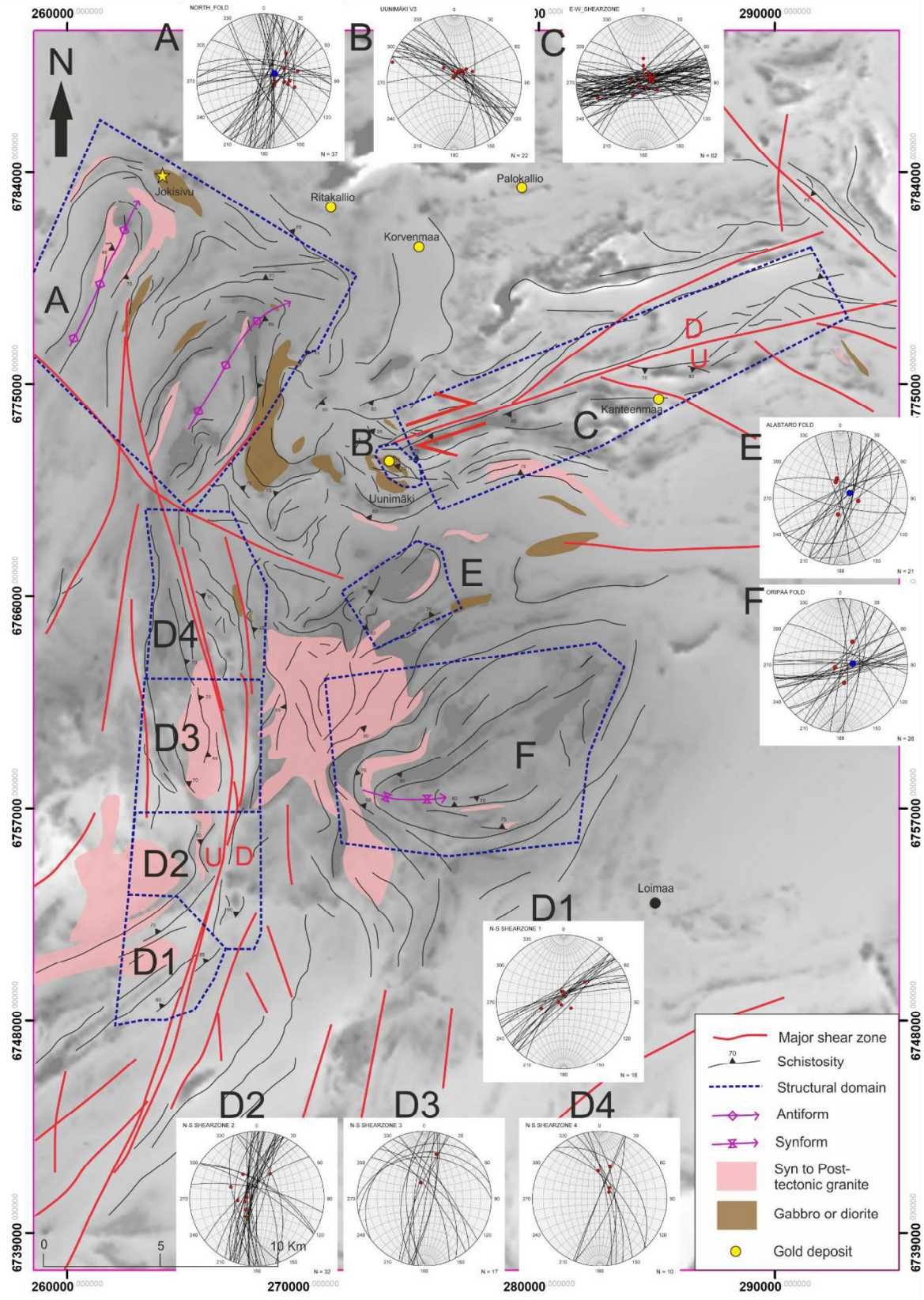

Fig. 33. Subdivision of the structural domains within the western Häme Belt, with a greyscale aeromagnetic anomaly map provided by GTK serving as the background. Stereographic projections of the structures of each subarea on the sides of the map: planar structures marked by great circles, linear structures marked by red dots. The blue dot marks the statistical fold axis for folded domains, calculated from foliation measurements. A: North fold, B: Uunimäki, C: Kankaanranta shear zone, D1-4: Alastaro shear zone, E: Alastaro fold, F: Oripää fold. Note that Uunimäki lies within the damage zone of the Kankaanranta shear zone. From Pitkälä (2019).

3.4.1 The Kankaanranta shear zone

The ENE-WSW-trending Kankaanranta shear zone has an outcropping length of ~20 km, with an approximately 20 m thick core surrounded by a zone of several hundreds of metres of influence characterized by shear-zone parallel foliation on both sides of the core (Fig. 34). In the east, it is possibly linked to the E-W trending Nuutajärvi shear zone, whereas in the west, the shear zone terminates abruptly into a structural domain characterized by NE-plunging lineations and folds with no clear evidence for distinct shear zones. Direct age relationships between folding and shearing could not be determined on any outcrop in the field. However, the westernmost outcrop of the Kankaanranta shear zone crosscuts the folded domain in such a way the regional folding-related NE-dipping foliations can be observed on of either side of its influence zone. Additionally, the secondary structures attributed to the Kankaanranta shear zone crosscut the folded areas. Therefore, the Kankaanranta shear zone is interpreted as younger than the folded domains surrounding it at its western termination. The Kankaanranta shear zone being late-orogenic fits previous models of E-W trending shear activity in the western Häme Belt by Väisänen (2002), Lahtinen et al. (2005) and Saalmann et al. (2010).

The shear zone is clearly visible in aeromagnetic geophysical maps (Fig. 10). Sheared fabrics and mylonitic rocks were observed in the field along a ~20 km long and ~200 m wide area, though the structural trends of the bedrock are parallel to the shear zone in a much wider area. Shear zone-parallel foliations were measured as far as 2 km from the shear zone core. Foliation measurements in the shear zone have dip directions of 140-170° and 330-350° and have steep-to-vertical (70-90°) dips. Measured dip directions in the shear zone mostly dip to the SE, but sometimes towards NW when the dip is sub-vertical. The dips become steeper with proximity to the interpreted shear zone core. The steepest dips (>85°) were measured from near the western and eastern terminations of the shear zone, with gentler dips in the middle. This may be due to the shear zone core only being exposed at few outcrops; the dip of the foliations in the shear zone core is likely sub-vertical throughout the zone. Lineations in the area are dominantly steep, ranging between 60-80° in plunge, indicating that the shear zone has more of dip-slip than strike-slip character. An exception to this is the Tirmanmäki area (Fig. 33), where a slickenside lineation was measured with a plunge of 18°. Plunge directions of the lineations in the shear zone are variable and can be divided into three groups: ENE-plunging (50-80°), SE-plunging (115-150°) and SW-plunging (210-240°). The ENE-plunging lineations occur

within and near the core of the shear zone, and are thus interpreted to represent the relative movement between the two sides of the shear zone. In contrast, the SE-plunging and WSW-plunging lineations become more common as distance from the shear zone core increases (Fig. 33). All fold axis measurements made from the shear zone plunge to the ENE.

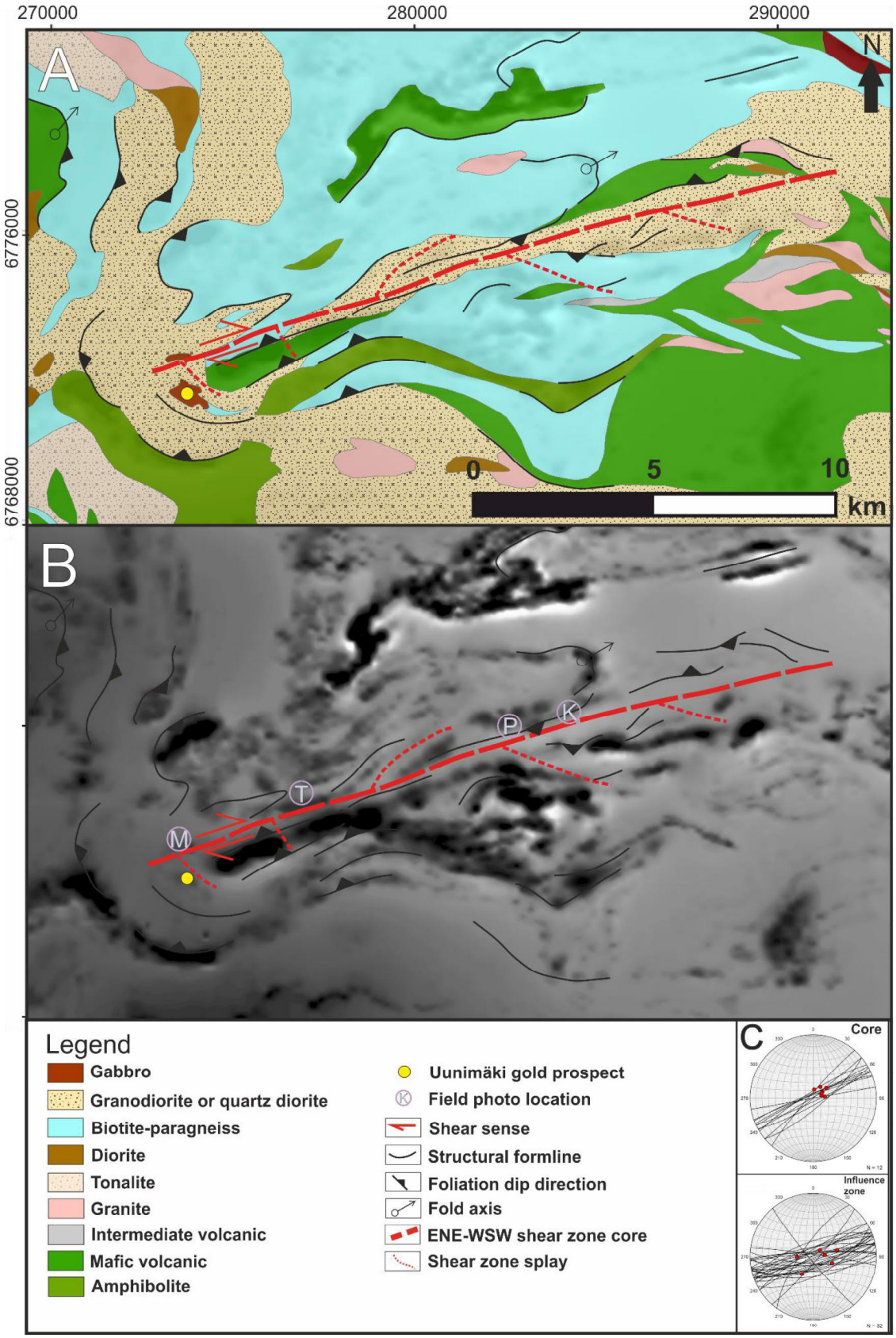

Fig. 34. Structural formline maps of the Kankaanranta shear zone. ***A)*** *Revised lithological map of the study area with structural formlines. Modified after Bedrock of Finland-DigiKP 1:50 000.* ***B)*** *Aeromagnetic map of the study area provided by GTK with structural formlines and field photograph locations noted. M = Metsäsiankallio, T = Tirmanmäki, P = Palokangas, K = Kankaanranta.* ***C)*** *Stereographic projections of tectonic measurements from the shear zone divided into two groups, core and influence zone, based on strain intensity. Great circles represent planar structures while red dots represent linear structures.*

3.4.1.1 Mesoscale kinematics of the Kankaanranta shear zone

Outcrops with exposed mylonites are not common, and the presence of sheared rocks appears to be dependent on rock type. Large sections of the shear zone as inferred from the aeromagnetic geophysical map are located in areas interpreted as biotite-paragneiss or metavolcanics, which are practically not cropping out. Though some paragneisses are present in areas just outside the most intensely sheared rocks, the only areas where the shear zone core itself can be mapped in the field are the areas where younger intrusives (gabbro, quartz diorite or granodiorite) are the dominant rock type.

Overall, the mylonites in the shear zone show a predominantly dextral sense of shear on horizontal outcrop surfaces in mesoscale. Shear sense indicators that were determined in the field were asymmetric folding, shear bands, and feldspar porphyroclasts (Fig. 35). As the lineations are mostly subvertical, thin section studies are required to reliably determine the true sense of the shear from the mylonites. The best mylonite outcrops are at Metsäsiankallio (N: 6772845, E: 274195), Tirmanmäki (N: 6773370, E: 275570), Palokangas (N: 6776050, E: 284400) and Kankaanranta (N: 67766580, E: 285670).

Metsäsiankallio (M in Fig. 34) is the westernmost outcrop where the Kankaanranta shear zone can be observed. The mylonite can be observed along a contact between fine-grained gabbro and migmatitic garnet-biotite-paragneiss (Fig 35C). Dextral shear bands were observed in all parts of the mylonite. Leucosomes have formed sigma-clasts within the mylonite and display clear dextral senses of shear. The mylonite is cut by quartz veins ranging from 1 to 5 cm in thickness, and some have a rusty hue. Quartz veins within the paragneiss have asymmetric dextral folds. The measured shear foliation is 348/86, and the lineation is 073/73. There are small garnet grains within the gabbro near the contact.

At Tirmanmäki (T in Fig. 34), several outcrops of sheared rock can be observed. A sheared contact between amphibolite and garnet-biotite-paragneiss has quartz-feldspar veins that have formed sigma-clasts showcasing a dextral sense of shear, as well as asymmetric folding (Fig 35A). Dextral tension gashes have formed in the amphibolite. The biotite-paragneiss north of this contact is heavily sheared and characterized by chloritisized dextral and sinistral shear bands. Foliations and lineations vary heavily in the Tirmanmäki area. Foliations are sub-vertical with dips towards NNW and SSE. Lineations are mostly steep, with nearly down-dip geometries. However, lineations near

the contact of the paragneiss and amphibolite are subhorizontal, suggesting that the strike-slip component of the strain has been partitioned into thin zones along lithological boundaries.

The shear zone core is visible in the granodiorite at Palokangas (P in Fig. 34). Penetrative dextral shear bands and seams as well as tension gashes run through the outcrop (Fig. 35B). In the middle of the outcrop, the brownish, less deformed granodiorite shows a gradual transition into a pale greenish sheared mylonite. A pegmatite vein that otherwise crosscuts the granodiorite is deflected in the direction of the shear. The measured foliation is 161/74. A reliable lineation measurement could not be made.

The fault zone core is best exposed at the Kankaanranta (K in Fig. 34) outcrop which gives the name to the shear zone. The outcrop consists of quartz diorite with a high-strain texture and foliation-parallel mylonite seams, as well as a cracked and deformed pegmatite vein (Fig. 36). The orientation of the foliation is 343/85 with a down-dip geometry of the lineation. As the lineation in the outcrop is the steepest measured in the entire Kankaanranta shear zone, it is likely that the quartz diorite here has accommodated more of the dip-slip component of the shear zone than at other locations. Determining the sense of shear with any certainty was impossible in the field, as the outcrop did not have a proper vertical surface.

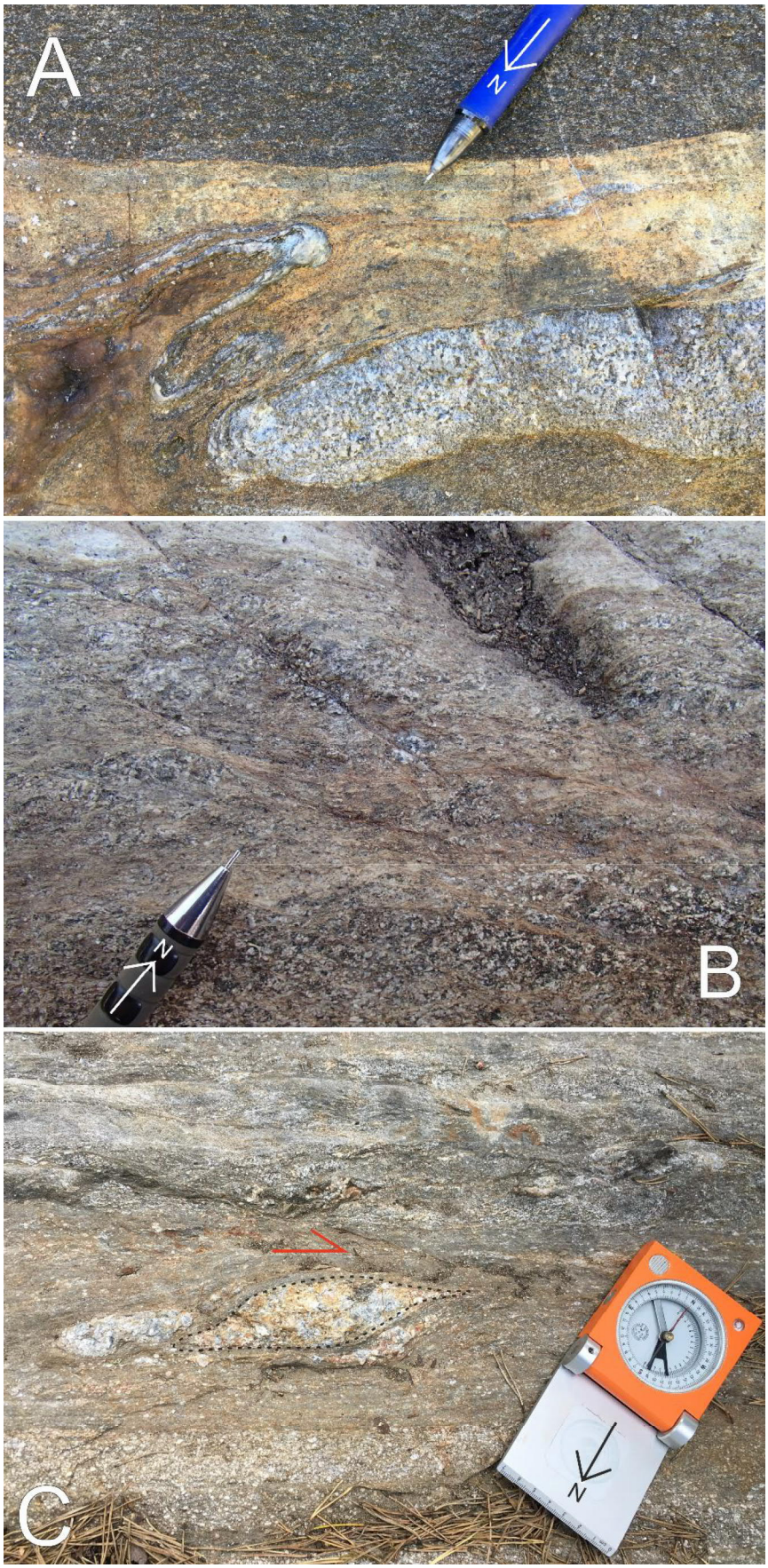

Fig. 35. Shear sense indicators from the Kankaanranta shear zone. ***A)*** *Asymmetric dextral folding in the sheared contact of amphibolite and paragneiss at Tirmanmäki. TALE-2017-11. N: 6773370, E: 275570.* ***B)*** *Dextral shear bands in heavily deformed granodiorite at Palokangas. TALE-2017-28. N: 6776050, E: 284400.* ***C)*** *Dextral sigma-clast framed by a leucosome aggregate within the mylonitic contact between gabbro and garnet-biotite-paragneiss at Metsäsiankallio. TALE-2017-182. N: 6772845, E: 274195.*

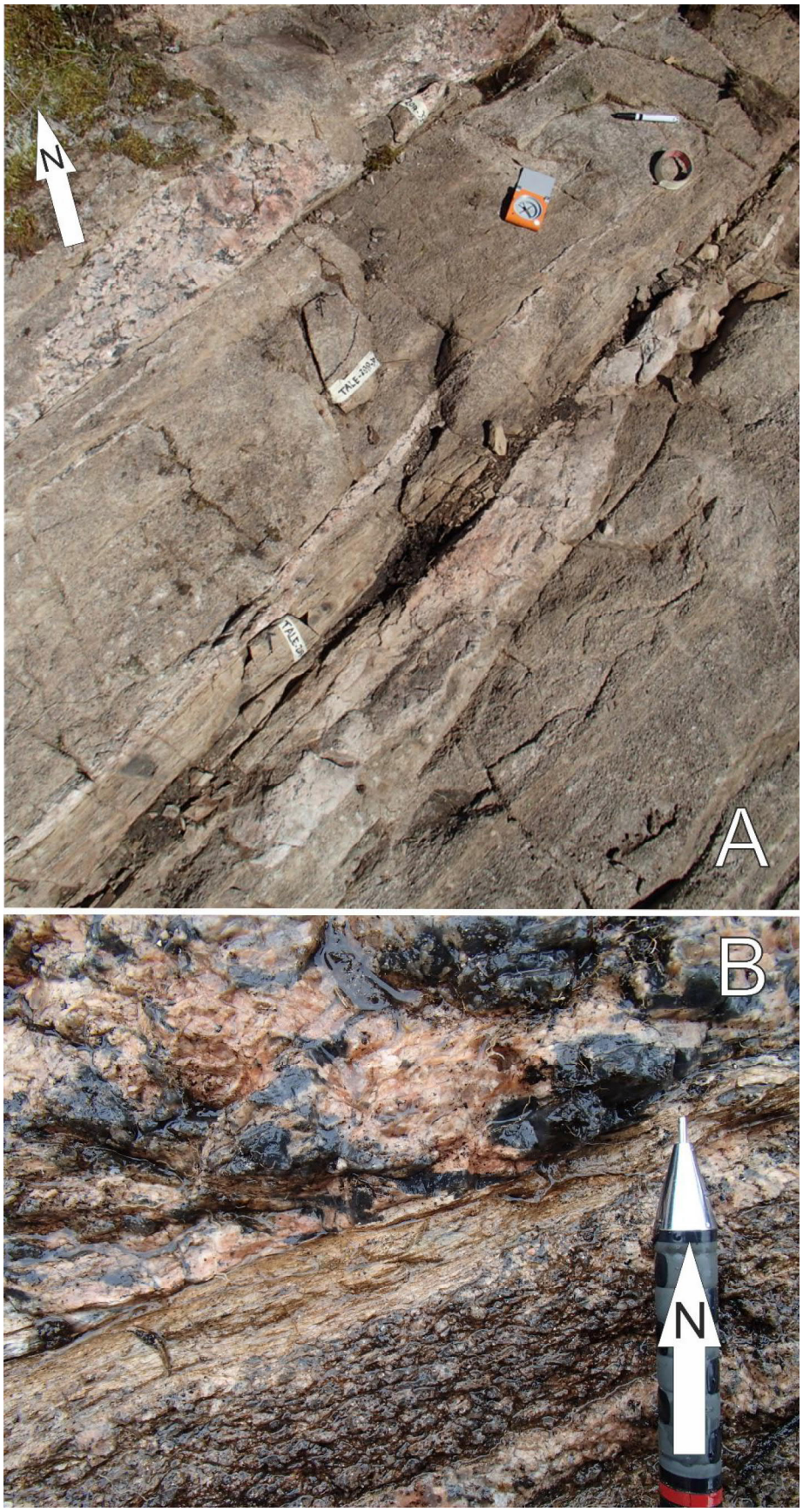

Fig. 36. The exposed shear zone core at Kankaanranta. TALE-2017-33. N: 6776585, E: 285675. ***A)*** *Overview of the shear zone core with foliation-parallel mylonite seams and a pegmatite vein that has broken off into smaller segments.* ***B)*** *Close-up of the sheared contact of the quartz diorite and pegmatite vein.*

3.4.1.2 Microscale kinematics of the Kankaanranta shear zone

The sampled rocks from the Kankaanranta shear zone display evidence of the development of asymmetric microstructures, such as delta- and sigma-clasts, shear bands and oblique foliation of quartz grains (Fig. 37). Two outcrops, Kankaanranta and Metsäsiankallio (for locations, see Fig. 34), yielded the best thin sections for kinematic determination. The kinematic evidence, which displays a predominantly dextral sense of shear, is in line with the mesoscale indicators observed at their respective outcrops. The orientation of the samples at outcrops compared with the kinematic indicators from thin sections suggests S-block up tectonics in the shear zone.

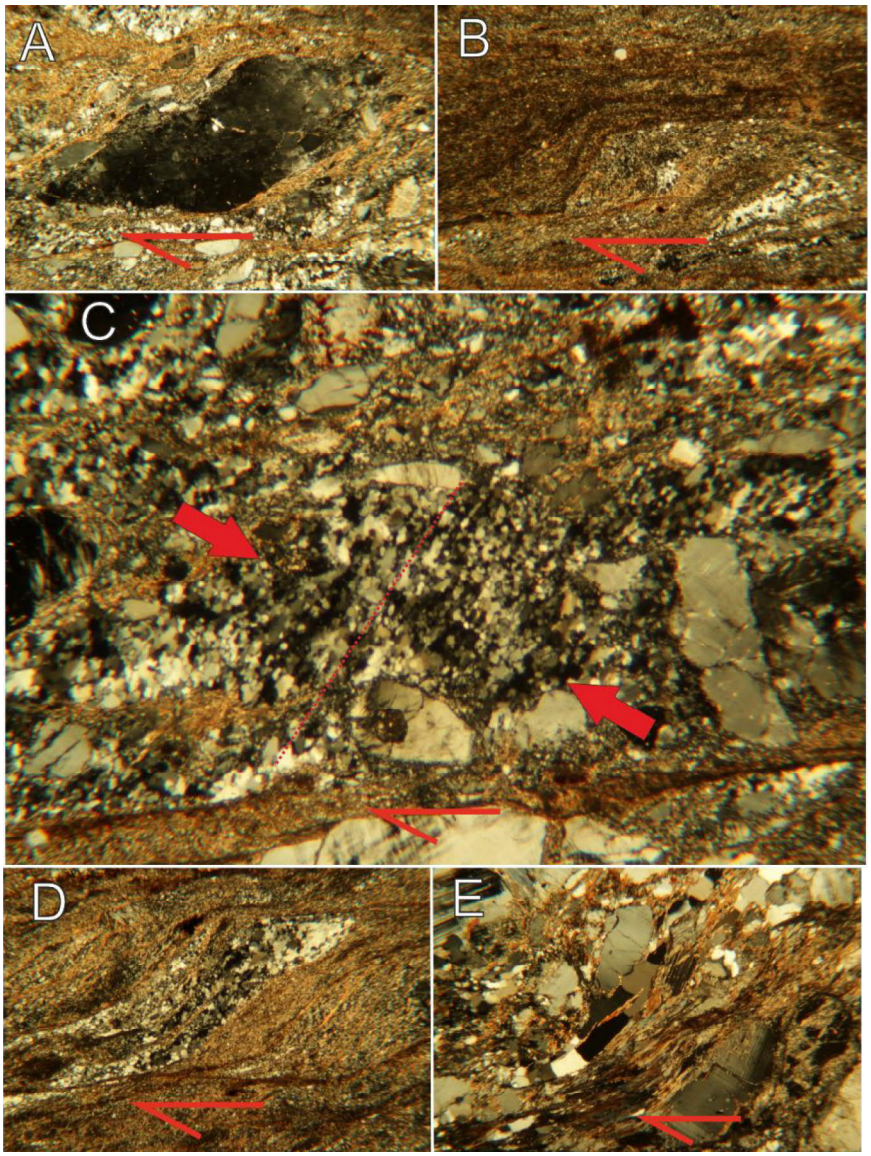

Fig. 37. Microphotographs of kinematic indicators from the Kankaanranta shear zone. ***A)*** *Dextral feldspar delta-shaped porphyroclast. From Kankaanranta, TALE-2017-33.1.* ***B)*** *Dextral delta-shaped poprhyroclast. From Kankaanranta, TALE-2017-33.1.* ***C)*** *Oblique foliation of quartz veins between two shear planes. From Kankaanranta, TALE-2017-33.1.* ***D)*** *Dextral shear bands visible in micas and ribbon-quartz. From Kankaanranta, TALE-2017-33.4.* ***E)*** *Dextral shear bands cutting through feldspar and quartz clasts. From Metsäsiankallio, TALE-2017-182.3.*

Dynamic recrystallization of quartz has taken place at variable temperatures in the shear zone. Recrystallized quartz behaves differently in Kankaanranta and Metsäsiankallio, despite their deformation appearing nearly identical in mesoscale. The differences in the behaviour of the quartz can be used to constrain the differences in their thermal conditions during dynamic quartz recrystallization.

Kankaanranta is located in the eastern part of the shear zone (for location, see Fig. 34). In the thin sections from the outcrop, the quartz appears as ribbon-quartz, which indicates a recrystallization type of SGR (subgrain rotation) (Fig. 38). The minimum temperature for SGR is 400°c (Stipp et al., 2002). The quartz grains outside the main zone of deformation have a uniform oblique foliation with respect to the main orientation of the ribbon-quartz (Fig. 37C). The quartz also exhibits some polygonisation due to progressive SGR recrystallization (Fig. 37D), though the degree of polygonisation differs in different parts of the thin sections. Both the polygonisation and formation of an oblique foliation suggests the thermal conditions have been on the higher end of the SGR spectrum. The lack of characteristic GBM (grain boundary migration) features, such as sutured grain boundaries, suggests that the SGR/GBM transition temperatures (480-530°c) have not been reached, however. The thermal conditions for the dynamic recrystallisation of quartz at Kankaanranta is therefore between 420 and 480°c.

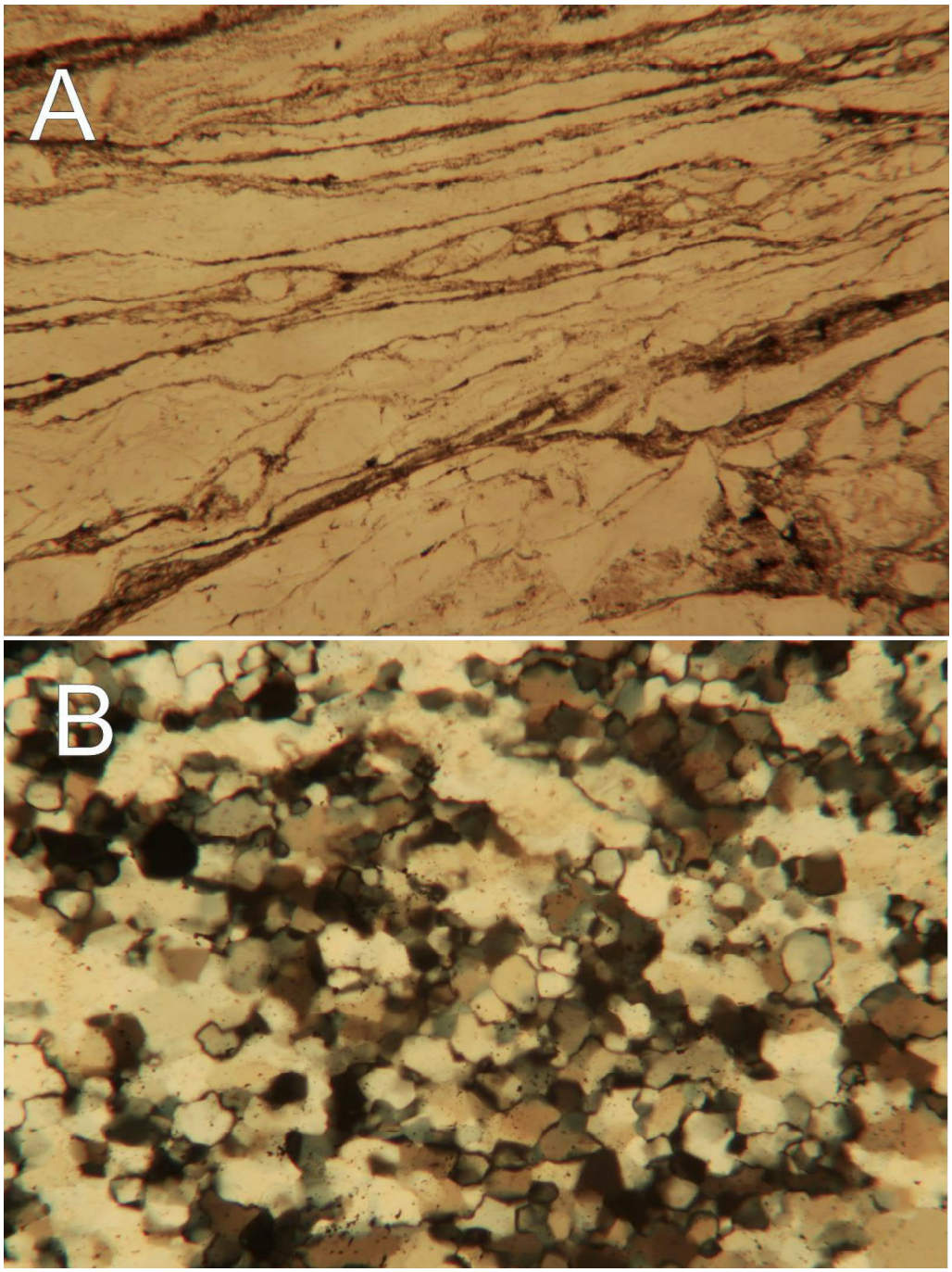

Fig. 38. Dynamic recrystallization of quartz at Kankaanranta. ***A)*** *Quartz as elongated ribbon-grains. TALE-2017-33.1.* ***B)*** *Subgrain rotation fabric with polygonisation of quartz grains. TALE-2017-33.3.*

Metsäsiankallio is located near the western tip of the shear zone as could be constrained in the field (for location, see Fig. 34). The behaviour of the quartz in the thin sections from the site suggests BLG (bulging recrystallization) as the dominant recrystallization type (Fig. 39). The transition from cataclastic flow to BLG recrystallization takes place at 300°c (Stipp et al., 2002). Quartz grains in the thin sections showcase serrated grain boundaries with recrystallized bulges, as well undulose and patchy extinction. The quartz grains have not been polygonised or formed ribbon-quartz, so it can be said that elements

of SGR recrystallization has not taken place in the quartz. The BLG-SGR transition is at 380-420°c. We can therefore constrain the recrystallization temperature of quartz at Metsäsiankallio at 300-380°c.

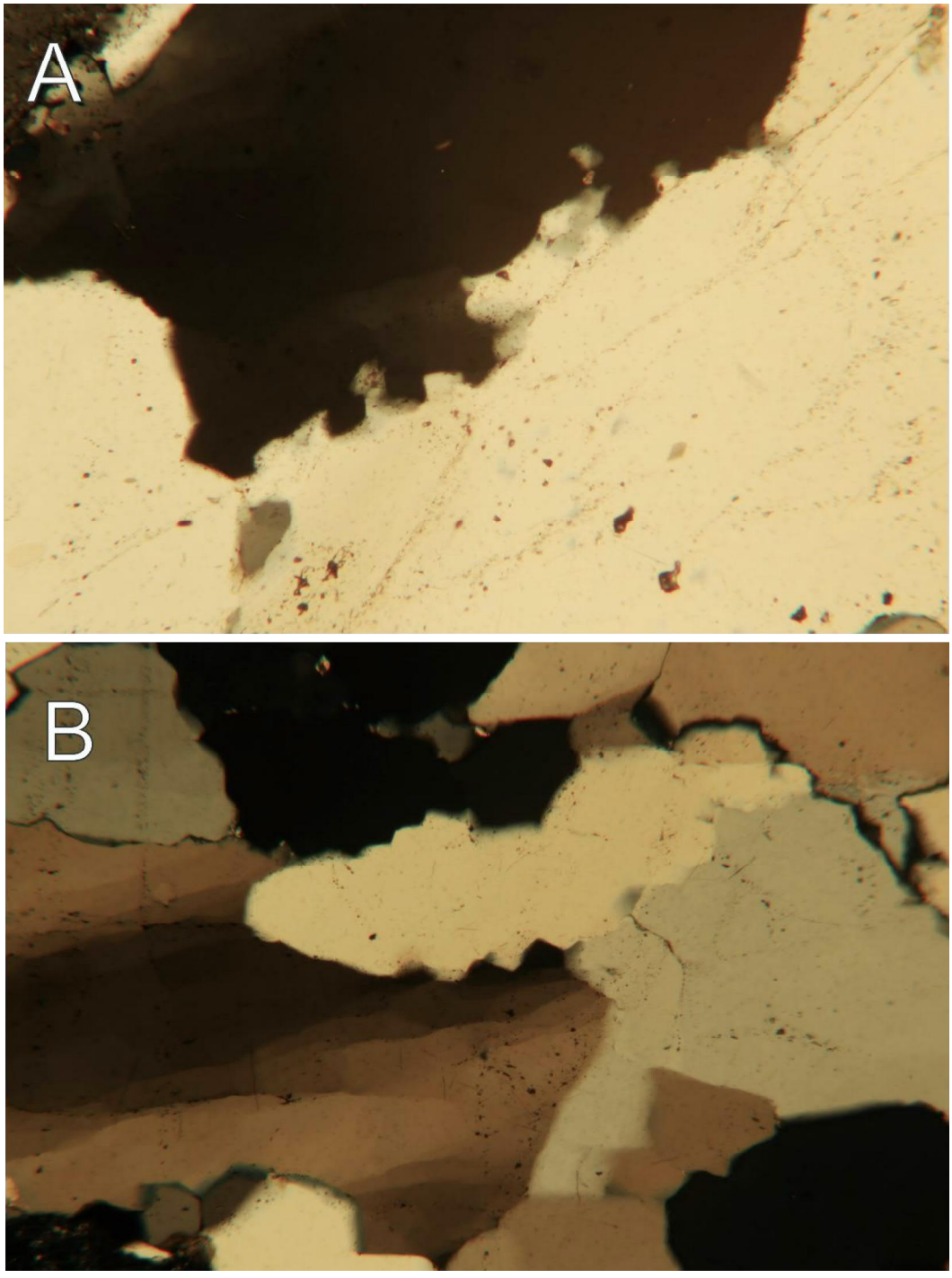

Fig. 39. Dynamic recrystallisation of quartz at Metsäsiankallio. ***A)*** *Recrystallised bulges in the quartz grain boundaries. TALE-2017-182.3.* ***B)*** *Recrystallized bulges, serrated grain boundaries and undulose extinction of quartz grains. TALE-2017-182.3.*

3.4.1.3 Splays of the main shear zone

NW-SE trending splays from the Kankaanranta shear zone create smaller areas of oblique deformation with respect to the main orientation of the shear zone (Fig. 34). The westernmost of these splays is named the Helmelä splay which bounds the Uunimäki gabbro from the NE side can be followed for a length of 1.5 km to the southeast from the shear zone (Figs. 34 & 43). Though the high-strain core of the Helmelä splay is not outcropped, a fairly continous zone of rock deformed with moderate intensity can be constrained on both of its sides. Foliations along the Helmelä splay dip towards NE (030-060°) with steep (70-85°) dips. Lineations plunge towards NNE (010-030°) with steep plunges (70-75°) indicating that the movement in the splay are mostly dip-slip as well. Small shear bands in the rocks with the highest deformation intensities indicate that the strike-slip component in the splay could have relative dextral movement. The relative motion of the dip-slip component is unclear. Rocks along any of the splays were not sampled, so there was no opportunity for study in the microscale.

3.4.2 The Uunimäki area

The Uunimäki gabbro crops out 800 m south of the western termination of the Kankaanranta shear zone (Fig. 34). The Helmelä splay of the Kankaanranta shear zone bounds the Uunimäki gabbro from the NE side, while structures on the western and southern sides of Uunimäki follow the regional folding trends. Uunimäki is thus situated within in the intersection of several different structural domains, which is reflected in the structural orientations present in area (Fig. 40). Although the Uunimäki gabbro has undergone several stages of deformation, most of the outcrops in the area contain only homogenous equigranular gabbro. Structural orientations at Uunimäki can be divided into three groups: NW-SE, ENE-WSW, and N-S. Overall the different structural trends of the Uunimäki area give the gabbro a mosaic-like structure, where the most intense deformation has been concentrated into a series of spaced shear zones located in the topographic depressions between major outcrops (Fig. 40). This can be seen in increasingly sheared textures and enhanced foliation intensity near the edges of outcrops (Fig. 42). The most intensely sheared gabbro in Uunimäki is located near the NE margin of the intrusion.

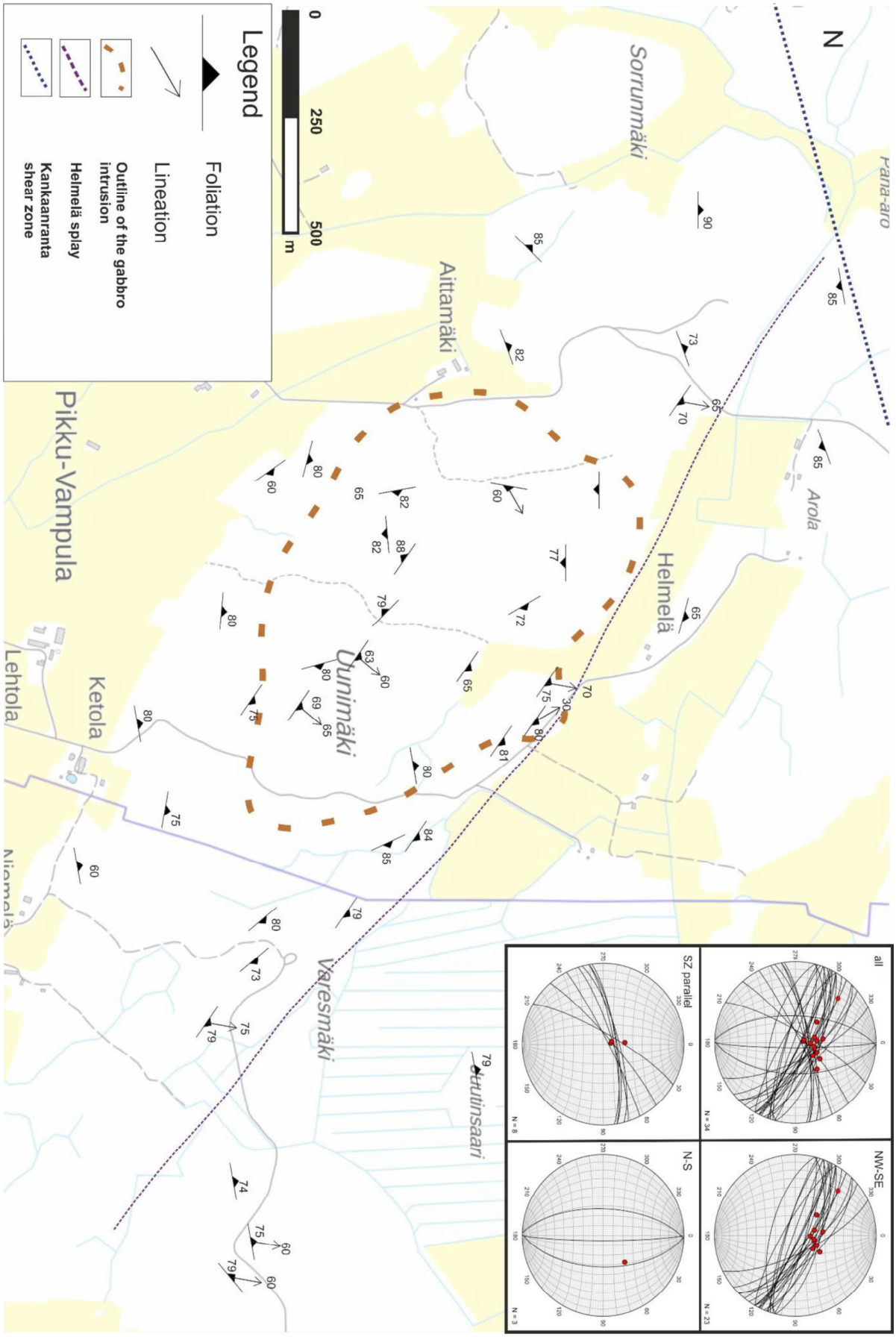

Fig. 40. All structural measurements collected from the Uunimäki area. Measurements include those taken by GTK in 2008-2012. Background map by National Land Survey of Finland.

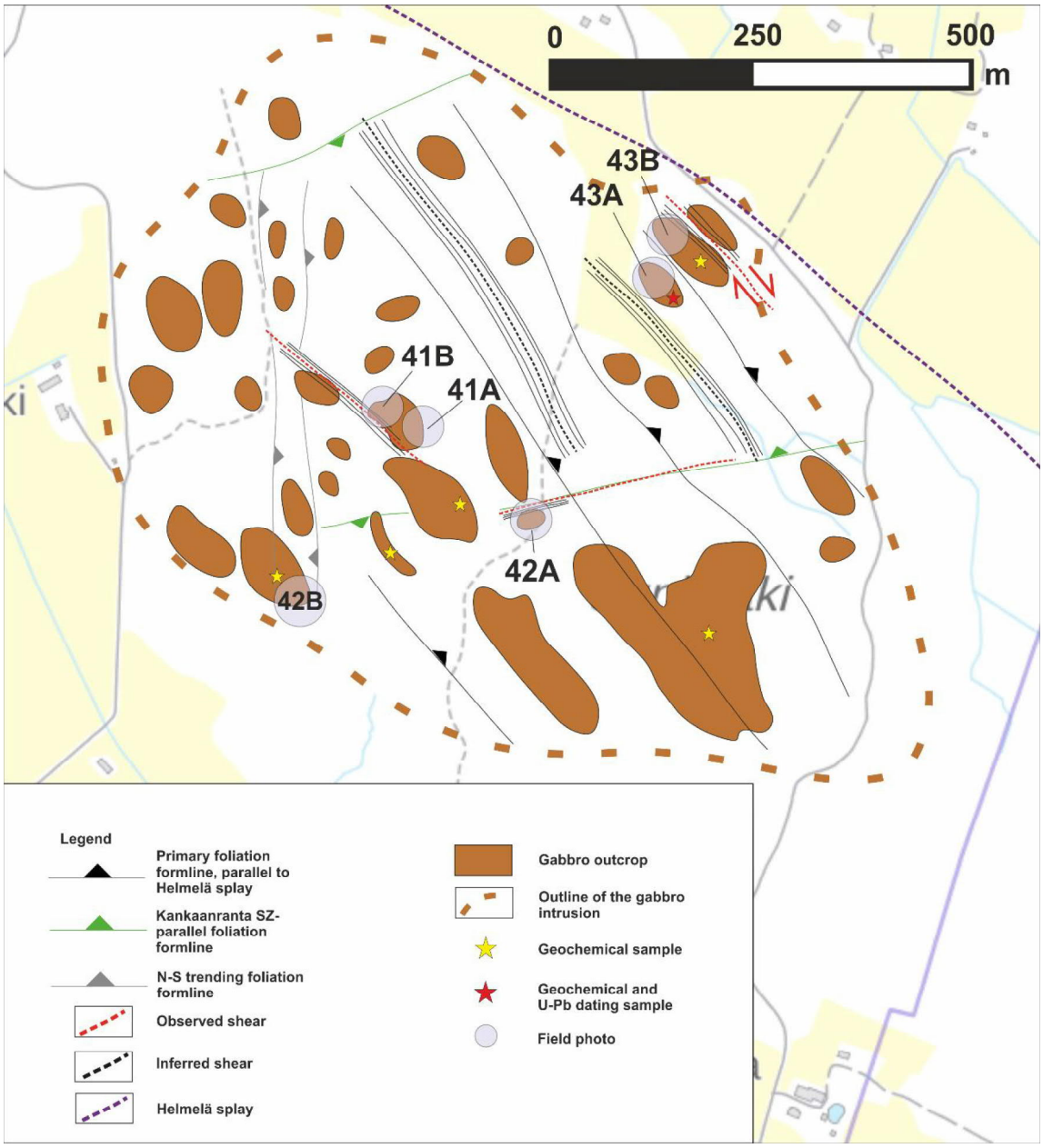

Fig. 41. Structural interpretation of the Uunimäki area. Background map by National Land Survey of Finland.

The predominant structural orientation is NW-SE trending. It can be seen in the oval shaped topography and boundaries of the intrusion itself: NW-SE is the longest axis, while the NE-SW axis is the shortest. The NW-SE orientation is parallel to the orientation of the Helmelä splay that bounds the Uunimäki gabbro from the NE. The dip directions of foliations in this orientation range from 020-050° with dips of 60-75° with the exception of an intensely deformed area in the middle of Uunimäki where the dip direction is flipped to 210-245° with steep dips of 80-85°. Lineations can be divided into two sets. The first is a set of weak lineations that plunge towards NE (20-55°) with angles of 50-60°. Almost all of the lineation measurements from the Uunimäki gabbro belong to

this set. The second set has intense lineations with plunges towards NNW (325-350°) at subhorizontal angles of ~30°. This indicates that the NW-SE oriented deformation in the Uunimäki area is strike-slip partitioned, where weak subvertical movement has accommodated the dip-slip component, and intense subhorizontal movement has accommodated the strike-slip component. Two shear zones with a NW-SE trend were observed within the Uunimäki gabbro, and there are likely more in the NW-SE oriented valleys that dominate the topography of Uunimäki. Though this is the dominant structural orientation of the gabbro, it is not present in most outcrops. The deformation has been concentrated into a series of spaced intensely sheared zones that separate outcrops of weakly foliated or wholly undeformed gabbro.

The second dominant structural trend, ENE-WSW orientation is parallel to the Kankaanranta shear zone located immediately to the north of the Uunimäki gabbro. This orientation is characterized by sub-vertical dips (80-90°) with dip directions either to N-NE (340-360°) or S-SE (140-180°). No lineation measurements were made from the ENE-WSW orientations within the gabbro. These structural orientations are found along the northern margin of the intrusion, as well as a within continuous zone that runs through the middle of the intrusion where one sheared gabbro outcrop was observed. This structural orientation seems to be concentrated into spaced zones.

A N-S trending structural zone can observed in the western part of the Uunimäki gabbro. Foliations from the margin of an individual long, continuous N-S oriented topographic depression have dip directions to the E (80-100°) with dips between 60-85°. Outcrops with this structural orientation are heavily intruded by quartz veins.

3.4.2.1 Mesoscale structures of the Uunimäki gabbro

In some outcrops, the gradual shift from undeformed to heavily deformed gabbro can be seen: the color shifts from dark-gray to pale-gray or greenish, grain size breaks down from medium-grained and equigranular to fine-grained and plagioclase-porphyritic (Fig. 43A). In the N-S trending structures, quartz veins have the same trend as the foliation, though the dip is not always the same (Fig. 43B).

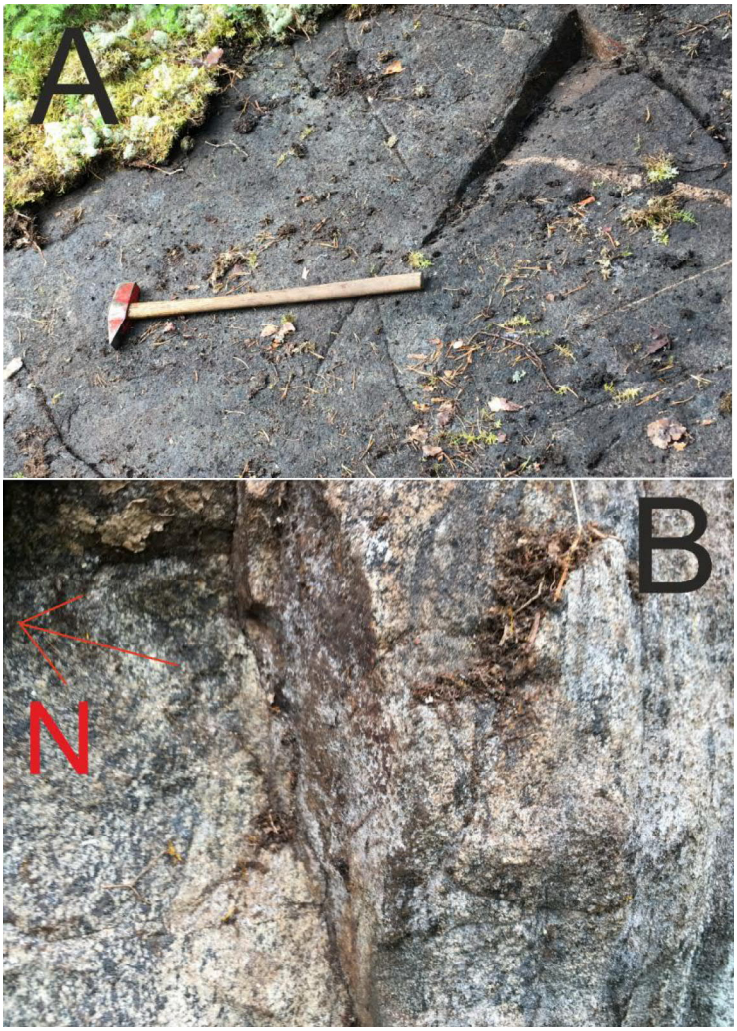

Fig. 42. Undeformed and sheared gabbro from the same outcrop. The distance between the two observations is 50 m (see Fig. 39). The structural orientation is NE-SW. ***A)*** *Relatively underformed equigranular gabbro with some quartz-feldspar veins. Handle of the hammer points to N. TALE-2017-129. N: 6771630, E: 273720.* ***B)*** *Intensely sheared gabbro with reduced grain size and alteration of amphibole to chlorite. TALE-2017-138. N: 6771650, E: 273680*

Fig. 43. ***A)*** *Increase in the strain in a gabbro as a shear is approached is noticeable. Dark and undeformed equigranular gabbro breaks down into pale-green altered gabbro. The orientation of the shear is ENE-WSW (SZ-parallel). TALE-2017-130. N: 6771560, E: 273860.* ***B)*** *Quartz-veins intruded into the same trend as the foliation. The orientation of the structures in the outcrop is N-S. TALE-2017-107. N: 6771445, E: 273605.*

Near the NE margin of the Uunimäki intrusion, the color of the gabbro changes from dark-gray to light-gray. Rusty and sometimes dark-red quartz veins occur as a dense network and have been precipitated into dextral tension gashes within the gabbro (Fig. 44). The quartz veins have broken off into short segments separated by dextral faults in the horizontal plane. Quartz and pegmatite veins outside the most intensely sheared gabbro bend into the direction of the shear. Strain progressively increases towards a valley that separates the outcrop from the next.

Fig. 44. ***A)*** *Undeformed equigranular gabbro from near the NE margin of the intrusion. TALE-2017-17. N: 6771785, E: 274010.* ***B)*** *Heavily deformed gabbro where quartz has precipitated into dextral tension gashes, and is broken off into shorter segments by dextral faults (marked by a red half-arrow) that form a network with antithetic sinistral faults. TALE-2017-203. N: 6771840, E: 274025. The distance between the two observations is 60 m (see Fig. 39).*

3.4.2.2 Microscale structures of the Uunimäki area

Despite several collected samples, kinematic interpretation of the shearing in Uunimäki is based on only one thin section: TALE-2017-18.1 (Fig. 45), as it is the only sample from which kinematic indicators could reliably be interpreted. The sample is taken from a nearly horizontal wall at the edge of a NW-SE oriented valley where shearing is interpreted to have concentrated. The dip of the foliation in the sample site was towards NE (023/80), with lineation towards the NW (324/60). The section has kinematic indicators showing both dextral and sinistral senses of shear. Shear bands follow a general dextral trend through the thin section, though that may vary depending on where in the rock the thin section was prepared from.

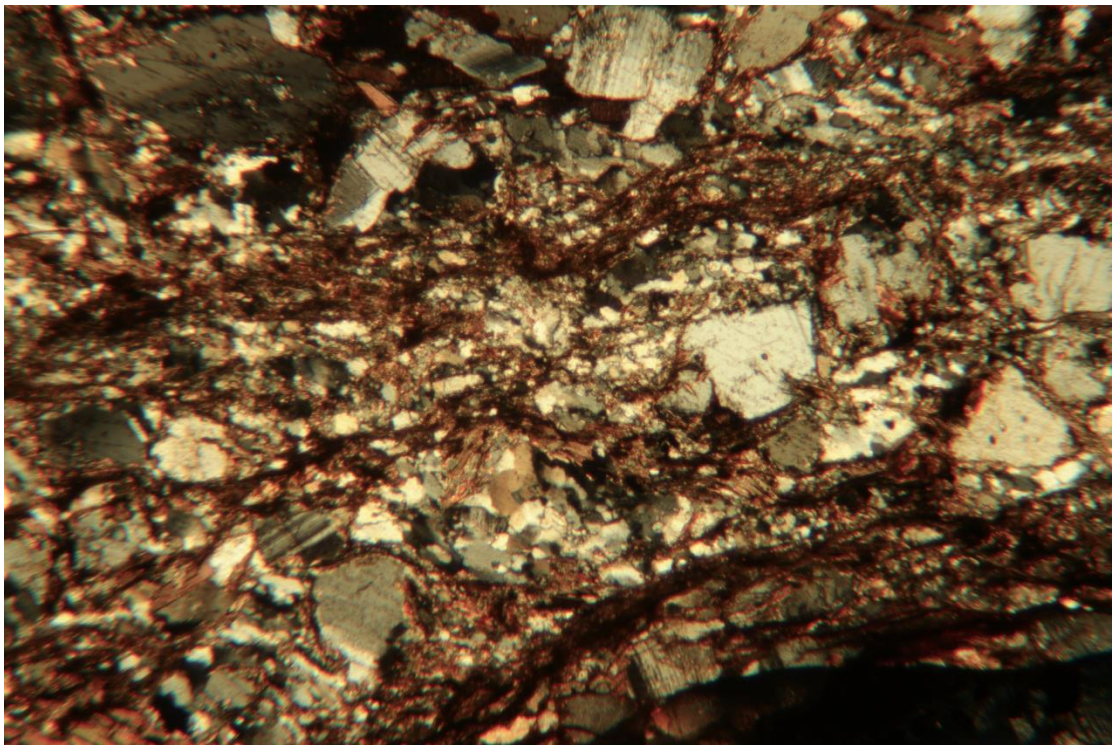

Fig. 45. Intensely sheared network cutting through deformed plagioclase grains in the sheared Uunimäki gabbro. TALE-2017-18.1.

4. Discussion

4.1 Age of the Uunimäki gabbro

The main zircon population yielded an age of 1891 ± 5 Ma which is the best estimate for the age of the Uunimäki gabbro. It can be considered the age of crystallisation of the magma for several reasons. It is unlikely that this age could have been inherited from older rocks, as even the paragneisses have been dated to an age of ~1.92 Ga at the youngest (Lahtinen et al., 2017). Secondly, for it to represent a later, metamorphic event, it would require that the metamorphism in the Häme Belt reached its peak at the time, but the metamorphism in the Häme Belt has been constrained to a later time by several authors (e.g., Nironen 1999; Saalmann et al. 2010). Furthermore, the zircons from the gabbro are mostly acicular grains with no metamorphic rims. The origin of the inherited zircons is unclear, but inherited zircons with similar ages have been described previously in the Svecofennian domain (Claesson et al., 1993; Lahtinen & Huhma, 1997). The two younger populations of zircons, ~1.86 and ~1.84, could be interpreted to represent later metamorphic or Pb-loss events. Amphibolite facies metamorphism at 1.87-1.86 Ga and E-W compressional events coinciding with high-T metamorphism between 1.85 and 1.80 Ga have been previously described in southern Finland (Nironen, 1999; Väisänen, 2002).

They are plausible as explanations for the younger metamorphic ages. Pb-loss caused by the shear activity in Uunimäki is another possible explanation for the younger zircon ages. Even though the age sample was taken from a seemingly undeformed gabbro, observed and inferred shear zones are close enough to the sampling site to have caused Pb-loss in some zircons. It must be noted however, that the different populations of zircons did not show any clear textural differences, and there were no metamorphic rims in the younger populations, making interpretations of their origins speculative.

The 1891 ± 5 age of the Uunimäki gabbro makes it one of the oldest dated rocks in the Häme Belt. The emplacement of plutonic rocks in the Häme Belt is commonly thought to have begun at 1.89 (Lahtinen et al., 2005; Hermansson et al., 2008). Age determinations made for the plutonic rocks of the Häme Belt imply that the time period of synorogenic magmatism at ca. 1886 Ma (Mäkitie et al., 2016) has formed most of the intrusive rocks in the area. One of the other gold deposits hosted by a mafic intrusive, the Jokisivu diorite, yielded a considerably younger age of 1882 ± 4 (Saalmann et al., 2009).

4.2 Geochemistry of the Uunimäki gabbro

It has been established that the Uunimäki gabbro has clear differences in geochemistry compared to the Jokisivu and Palokallio diorites. However, the question arises whether these differences can be explained simply by different levels of differentiation. Looking at the major element diagrams, it seems like a clear explanation, as most major elements form a continuous series when plotted against silica. This is clearest in MgO, Fe_2O_3, CaO, K_2O and TiO_2 contents, though it must be said that the other major elements Al_2O_3, Na_2O, P_2O_5 and minor elements do not imply the same compositional difference by fractionation (Fig. 23). When looking at the trace elements however, major differences between the rocks start to arise (Figs. 25, 26, 27, 28). The Uunimäki gabbro does not have the negative Nb-Ta-anomaly that is often considered a subduction component (Pearce, 1996). Furthermore, Ti and Yb are slightly enriched in the gabbro, elements that are usually not mobile in subduction zone environments. Plotting the Uunimäki gabbro into geotectonic discrimination diagrams, it does not matter which subduction-mobile or subduction-immobile elements we use; the gabbro is clearly separate from the rest of the samples regardless of the diagram chosen. However, it should still be noted that Zr and Hf are slightly depleted in the Uunimäki gabbro (Fig. 26), which is generally considered typical for subduction zone basalts (e.g., Wyman et al., 2002). The multielement-pattern of the

gabbro bears the most resemblance to the pattern of transitional basalts (VAB/WPB) as outlined by Pearce (1996) (Fig. 26).

One possible explanation for the geochemical differences is that the Uunimäki gabbro represents the primitive arc. Primitive arc rocks are rare and appear to occur in areas where the tectonic regime has previously been extensional, allowing the magma to ascend more rapidly (e.g., Smith et al., 1997). This would certainly fit in the tectonic setting of the Svecofennian orogeny at 1.89 Ga. Before 1.89 Ga, the southern margin of the Svecofennian orogeny has been interpreted as extensional, followed by a change to compressional tectonics at ~1.89-1.80 Ga. This would also explain the lack of negative Nb-Ta and Ti anomalies, as the elements have not been repeatedly depleted from the rocks by consecutive ascent through the mantle, and recycling of the sediments into the subducting slab after erosion. Primitive arc rocks should, however, have high magnesium number, and high concentrations of Ni and Cr, as they represent a less evolved mantle-source, but the Uunimäki gabbro does not have abundant Ni or Cr, and has a relatively low magnesium number. In fact, on average, the Uunimäki gabbro has smaller concentrations of Ni and Cr than the Jokisivu and Palokallio diorites, and even the quartz diorites and granodiorites surrounding it.

The lack of Nb-Ta depletion in relation to LREE or Th could be an indicator that the Uunimäki gabbro could have formed in an environment other than a subduction zone. There are, however, alternate explanations for the lack of this depletion. Crustal contamination is a possible, though unlikely, explanation for this. Borisova et al. (2001) discuss a case where crustal contamination with granulites led to depletion of U-Th and Nb-Ta. As Th and U precede Nb and Ta in the MORB-normalized and primitive mantle spider-diagrams respectively, this would create the illusion that there is no negative Nb-Ta-anomaly if all the aforementioned elements are depleted. Compared to the Jokisivu diorite, the Uunimäki gabbro is clearly depleted in U and Th, though the Nb-Ta contents are similar. This explanation seems implausible, however.

If considered in the larger context of the Svecofennian orogeny, the age of the gabbro could represent the latest period of hinge retreat before hinge migration as modeled by Hermansson et al. (2008). The Uunimäki gabbro clearly gives a differing geochemical signature to other mafic intrusives of the area, implying that they have formed in different geotectonic environments. If we consider that the Jokisivu diorite yielded a U-Pb age of

1882 ± 4 (Saalmann et al., 2009) and the geochemical signature is a calc-alkaline arc-type rock, and that the Uunimäki yielded an age of 1891 ± 5 and a geochemical signature more in line of an E-MORB or a within-plate basalt, one could draw the conclusion that the Uunimäki gabbro was formed in an extensional environment, followed by a switch in the sense of the hinge migration, leading to the formation of the Jokisivu diorite in a convergent environment. In the model by Lahtinen et al. (2005), a short-lived period of extension took place due to subduction switchover and reversal between the Lapland-Savo and Fennian orogenies. It is possible that the Uunimäki gabbro was emplaced in this period of extension, as rocks formed during the 1.89-1.88 Fennian orogeny in the Häme Belt are described as volcanic arc-type, a signature that the Uunimäki gabbro clearly does not have.

The most likely possibility seems to be that the Uunimäki gabbro represents the primitive arc. The age of the gabbro compared to its surroundings, as well as the clear geochemical are certainly in support of it. The low Mg# and relatively small concentrations of Ni and Cr are, however, perplexing. It is possible that intensive fractional crystallisation that led to the removal of olivine from the gabbro has caused the low Mg#, Ni and Cr.

4.3 Comparison of the Uunimäki gabbro to mafic volcanics in SW Finland

Since the Uunimäki gabbro differs significantly from the surrounding intrusives, comparison to volcanic rocks in SW Finland is in order. The E-MORB affinity in the Uunimäki gabbro is interestingly only shown in one volcanic suite in the Häme Belt. The Renkajärvi volcanic suite, composed mainly of mafic volcanics, is located in the NE part of the Häme Belt (Sipilä & Kujala, 2014). Intermediate volcanics are sometimes present when moving up the stratigraphy, and felsic volcanics are present only as thin layers among the mafic volcanics. They overlay turbiditic sedimentary sequences that contain layers of volcanic ash, indicating simultaneous extrusive activity and sedimentation. The eruptions of the Renkajärvi suite volcanics are interpreted to have started under water, but gradually developing into subaerial eruptions. Additionally, mafic metavolcanics in the Turku area belonging into the Turku and Pargas groups (Väisänen & Westerlund, 2007) bear geochemical resemblance to the Uunimäki gabbro. The metavolcanics of the Pargas group are a ~500 m thick volcanic layer overlain by marbles and paragneisses with no remaining primary structures, while the Turku group mafic metavolcanics mostly

occur as intercalations of varying sizes within the paragneisses that dominate the bedrock of the Turku area.

The Uunimäki gabbro has some geochemical similarities with the mafic volcanic suites. Not only do they have nearly identical major element concentrations (Fig. 46A), but their trace element geochemistry is similar as well. There is no negative Nb-Ta-anomaly in the Renkajärvi suite volcanics, and only a very minor negative anomaly in the Turku and Pargas group volcanics (Fig. 46C). All of the groups have a moderate LILE-enrichment, a slight negative Zr-Hf anomaly, as well as a very gentle Zr-Y trend in the N-MORB normalized multielement-diagram (Fig. 46C). REE-slopes of all groups are gentle as well, however the REE-slope of the Uunimäki gabbro is a bit steeper than the REE-slope of the Renkajärvi volcanics, while the Turku and Pargas group volcanics have either a flat or only very slightly negative slope (Fig. 46D). In the Nb/Yb vs. Th/Yb -diagram, the samples have significant overlap, and plot close to E-MORB-type rocks (Fig. 46E). There is a slight difference in the rocks in the Zr-Hf-Nb geotectonic diagram (Fig. 46F), as the gabbro has a clear E-MORB/WPT-affinity, while the Renkajärvi volcanics are somewhere between that and a calc-alkaline basalt (CAB)-affinity. Most of the Turku and Pargas group volcanic have a CAB-affinity, though a some of them plot into the N-MORB field.

The geochemical features described above are uncharacteristic traits for subduction zone rocks; Sipilä & Kujala (2014) noted that the Renkajärvi suite volcanics were most likely formed during rifting, as opposed to other suites of volcanics in the Häme Belt that have more arc-type geochemical affinity. Väisänen & Westerlund (2007) interpreted the metavolcanics of the Turku and Pargas groups to have formed in an extensional setting, most likely in a back-arc or intra-arc basin. These comparisons support the idea that the Uunimäki gabbro could have formed in an extensional setting.

It should also be noted, however, that though they are both part of the Häme Belt, the Uunimäki gabbro and the Renkajärvi volcanics are not in spatial vicinity with each other and have different structural features, so they are not directly related. But their geochemical similarity imply that they were both formed before the arc-type volcanism began in the Häme Belt. The Turku and Pargas group volcanics have no spatial connection with the Uunimäki gabbro whatsoever, especially as the Pargas volcanics are associated with marbles and thus connected to the Uusimaa Belt.

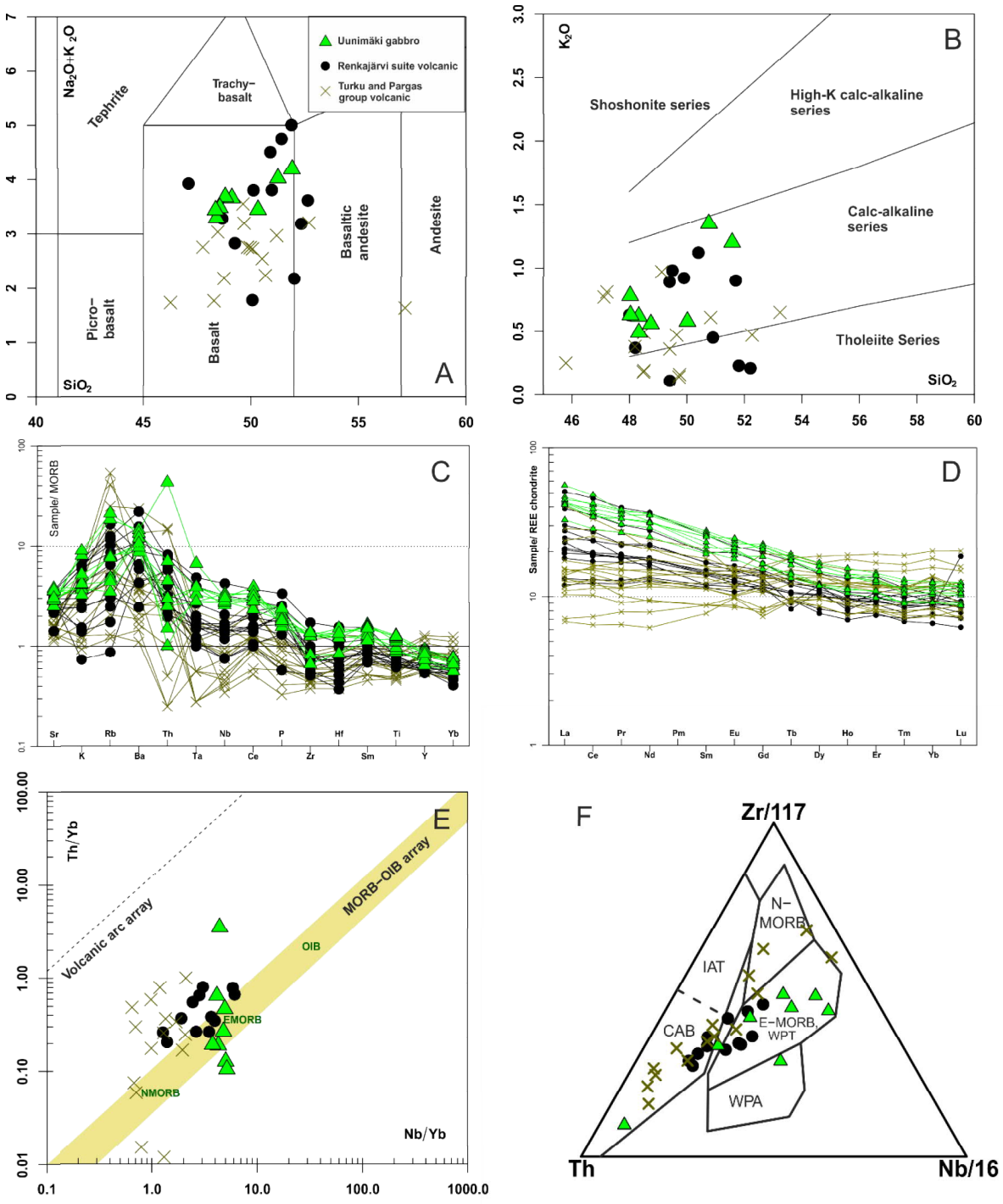

Fig. 46. Geochemical diagrams for the Uunimäki gabbro, Renkajärvi suite volcanics and the Turku and Pargas group volcanics. ***A)*** *TAS-diagram (Middlemost, 1994).* ***B)*** *SiO_2 vs. K_2O –diagram with magma series discrimination according to Peccerillo & Taylor 1976).* ***C)*** *Multielement-diagram normalized to MORB (Pearce, 1983).* ***D)*** *Multielement REE-diagram normalized to chondrite (Boynton, 1984).* ***E)*** *Nb/Yb vs. Th/Yb –geotectonic discrimination diagram (Pearce, 2008).* ***F)*** *Zr-Nb-Th –geotectonic discrimination diagram (Wood, 1979).*

4.4 Structural evolution

The studies of the thin sections from the Kankaanranta shear zone indicate that the relative movement in the shear zone is south-block up which makes the zone a reverse fault. Oblique lineations and outcrops where strike-slip partitioning can be observed indicate that the shear zone has a significant dextral strike-slip component as well. The tectonic regime in the Kankaanranta shear zone has therefore been transpressional, compatible with previously demonstrated NW-SE transpression (e.g. Ehlers et al., 1993).

As previously mentioned, the Uunimäki gabbro is located within the intersection of several regional features with distinct structural orientations. The dominant NW-SE structures are parallel to the Helmelä splay from the the Kankaanranta shear zone. Considering the geometry of the structures between the Kankaanranta shear zone and the Uunimäki area, it is possible that the NW-SE structures were initially formed as fractures caused by the dextral shearing in the Kankaanranta shear zone. The fractures would then have acted as weakness zones where gold-precipitating fluids could move and re-activated as shear zones. Direct age relations that support this can be seen in an outcrop of the Uunimäki gabbro. The ENE-WSW sheared gabbro is located in an outcrop otherwise having a NW-SE orientation (location in Fig. 40, field photo in Fig. 42A). This implies that the NW-SE structures have overprinted older ENE-WSW –trending structures. The sheared gabbro is spatially located within the area where the Kankaanranta shear zone parallel foliations dominate the structural trends outside of the gabbro. Since the gabbro exhibits clear tendency to partition the strain into zones of intense deformation separating undeformed areas, it is possible that the strain placed on the gabbro by the movement in the Kankaanranta shear zone partitioned into thin zone seen in Fig. 42A. The Uunimäki gabbro lies within the influence zone of the Kankaanranta shear zone, when looking at areas where contrasting shear activity (splays) have not deformed the bedrock.

The cause for the relatively thin zone of N-S trending structures is unclear. The Uunimäki gabbro is likely too far away from the influence zone of the Alastaro shear zone to have been deformed in the same event. It is interesting to note that no NW-SE, or any other kinds of structures are present in the Uunimäki gabbro west of the thin zone of N-S structures. It could be that NW-SE trending shears curve from the N-S structures as horsetail splays, but since the N-S shearing is not a dominant feature in the bedrock either

inside or immediately around the Uunimäki gabbro, this is also an unlikely explanation. It is possible for the N-S structures to have formed as secondary structures between zones of dextral NW-SE shearing.

4.5 The gold mineralisation in Uunimäki

The gold has precipitated into areas controlled by the NW-SE-trending shear activity within the Uunimäki gabbro. Considering the age of gold-precipitating fluid movement in the western Häme Belt as constrained by Saalmann et al. (2009), and the spatial vicinity of the Uunimäki area to the Kankaanranta shear zone, the most likely scenario is that the controlling structures of the Uunimäki gold mineralisation are linked to the ENE-WSW-trending shearing in some way. The E-W trending structures that were formed during transpression in 1.83-1.80 Ga have the highest potential to deliver the fluids from which gold precipitated into the Uunimäki gabbro. The most likely timeframe for the mineralisation of gold in the Uunimäki gabbro is the same as interpreted by Saalmann et al. (2010) for the nearby Jokisivu deposit: between 1.82 – 1.79 Ga.

Drawing parallels between the gold mineralisations in Uunimäki, Jokisivu and Palokallio is difficult. The hosting rocks have different geochemical signatures and different ages. It can therefore be said that the chemical attributes and the age of the gold-hosting rocks does not directly determine where gold has been precipitated in the western Häme Belt. It must be noted however, that the mineralisation type in Joksivu (as well as Palokallio) is quite different to that in Uunimäki, as the gold in Jokisivu is enriched in the quartz veins in the shear zones, and in Uunimäki, the gold is not in the shear zone itself, but in small pyrrhotite and quartz veins in the wallrock next to the intensely sheared zones. The difference in mineralisation could be due to different host rock types. Uunimäki is more basic in composition, which likely affects the wallrock interaction during fluid movement. What the deposits have in common is the association with shear activity, though that does not explain why gold does not precipitate into structures inside granodiorites or quartz diorites.

The depth of emplacement for the gold in Uunimäki is most likely hypozonal, meaning a depth of >12 km. Hypozonal orogenic gold deposits have several characteristic features, including enrichment in As, amphibolite facies metamorphism, and deformation in conditions near the brittle-ductile-boundary (Fig. 2). All three of the features are present

in the Uunimäki gabbro, though the timing of the development of these features cannot be perfectly lined up with the actual emplacement of the gold. The amphibolite facies metamorphism is unquestionable, but it is possible that the metamorphic conditions had changed after the peak metamorphism had taken place, but before gold emplacement. The Uunimäki gabbro is deformed by both brittle and ductile features, and the gold concentrations are highest in the 'healthy' wallrocks near the highly deformed zones in the rock. But, it is possible that these features were formed earlier than the gold was precipitated and simply acted as weakness zones through which the gold-forming fluids could move. That leaves local As-enrichment in the gabbro as the last remaining distinguishing feature. As-enrichment is also present in mesozonal (6-12 km) deposits, but at that depth, Te and W are also present. In the Uunimäki gabbro, there is no Te or W enrichment. So, even considering the possibility that metamorphism and deformation took place earlier or later than the gold precipitation, the As-enrichment gives us a good indicator that the formation depth was hypozonal.

4.6 Hydrothermal alteration

Hydrothermal activity concentrated within the Uunimäki area is noticeable in thin sections and geochemistry. Sample TALE-2017-12.1 is a quartz diorite containing garnet from the spatial vicinity of the Uunimäki gabbro. This was already observed in the field, but can be seen in the geochemistry as well, where the quartz diorite has comparatively elevated contents of Al_2O_3, Ta and HREEs, all elements that have high partition coefficients into garnet, while being depleted in MgO, V, Ni and Cr. The thin sections of the Uunimäki gabbro display chloritisation where biotite, and to a lesser extent, amphibole, has altered into chlorite. As a result, the chlorite that has formed is often present as a pseudomorph of biotite or amphibole. Plagioclase has also undergone sericitisation in almost every sample collected. Sulfidisation and garnets are not present in the gabbro samples collected from the surface but have been noted in drill cores (Kärkkäinen et al., 2015). It is clear that alteration related to ore formation has not been significant in outcropped rocks but is only present in drill cores.

5. Conclusions

- The 1891 ± 5 Ma age of the Uunimäki gabbro makes it one of the oldest rocks in the Häme Belt.
- Trace element geochemistry of the Uunimäki gabbro reveals that it does not represent typical arc-magmas. The geochemical signatures are closer to those of rift-related volcanic rocks in SW Finland. The Uunimäki gabbro most likely represents the primitive arc in the early stage of the 1.90-1.88 magmatic phase of the Svecofennian orogeny.
- The ENE-WSW-trending Kankaanranta shear zone is an oblique transpressional reverse fault showcasing south-block up and dextral kinematics.
- The structural orientations of the Uunimäki area have formed in the following order: ENE-WSW, NW-SE, N-S. The ENE-WSW are parallel to the Kankaanranta shear zone and have probably formed in the same event. The NW-SE structures are younger than the ENE-WSW structures, and could represent reactivated weakness zones formed during the ENE-WSW shearing. The N-S structures cannot be directly related to events in a wider tectonic context, but they are likely secondary structures related to NW-SE shearing.
- The Jokisivu and Palokallio diorites have vastly different ages and geochemical signatures than the Uunimäki gabbro. The geochemical attributes and age of emplacement have therefore not played a decisive role in the mineralisation of Au in the western Häme Belt.
- The depth of formation for the Uunimäki Au was hypozonal, and the age of the gold mineralisation is likely related to transpressional events at 1.83-1.80 Ga.
- The hydrothermal alteration present in Au-mineralised parts of the Uunimäki gabbro is not widely visible in outcropped rocks.

6. Acknowledgements

First of all, I'd like to thank the Geological Survey of Finland for funding this project. I'd like to thank geologists Hanna Leväniemi, Markku Tiainen and Janne Hokka for their supervision and support during different phases of the project, and for supplying geophysical and other GIS-material to help during the field season. I'd also like to thank Hugh O'Brien and Yann Lahaye for teaching and supervising the use of the mass spectrometer at the Finnish Geosciences Research Laboratory during the age dating process.

I’d like to thank Professor Pietari Skyttä, university lecturer Markku Väisänen and MSc Jaakko Kara for their guidance and expertise throughout my geology studies at the University of Turku, the field work during this study, and the thesis writing process. I’d also like to thank Jaakko Kara separately for performing the data reduction for the U-Pb geochronological data. I’d like to thank MSc Niklas Tenovuo for preparing the thin sections for this study and laboratory technician Arto Peltola for preparing the zircon-mount for BSE and mass spectrometer studies. I’d like to thank my mapping partner BSc Iiro Pitkälä for his contribution to this study during mapping, structural analysis and thesis writing and BSc Matti Vuorisalo for his help in zircon separation.

References

Belousova, E.A., Griffin, W.L., O'Reilly, S.Y. 2005: Zircon crystal morphology, trace element signatures and Hf isotope composition as a tool for petrogenetic modelling: examples from eastern Australian granitoids. Journal of Petrology, 47, 329-353.

Benning, L.G. & Seward, T.M. 1996: Hydrosulphide complexing of Au (I) in hydrothermal solutions from from 150-400°C and 500-1500 bar. Geochimica et Cosmochimica Acta, 60, 1849-1871.

Bogdanova, S.V., Bingen, B., Gorbatschev, R., Kheraskova, T. N., Kozlov, V. I., Puchkov, V. N., Volozh, Yu. A. 2008: The East European Craton (Baltica) before and during the assembly of Rodinia. Precambrian Research, 160, 23-45.

Borisova, A. Y., Belyatsky, B. V., Portnyagin, M. V., Sushchevskaya, N. M. 2001: Petrogenesis of olivine-phyric basalts from the Aphanasey Nikitin Rise: Evidence for contamination by cratonic lower continental crust. Journal of Petrology, 42, 277-319.

Boynton, W.V. 1984: Cosmochemistry of the rare earth elements: meteorite studies. Developments in geochemistry, 2, 63-114.

Böhlke, J. K. 1982: Orogenic (metamorphic-hosted) gold-quartz veins. US Geological Survey Open-File Report, 795, 70-76.

Cawood, P. A., Kröner, A., Collins, W. J., Kusky, T. M., Mooney, W. D., Windley, B. F. 2009: Accretionary orogens through Earth history. Geological Society, London, Special Publications, 318, 1-36.

Claesson, S., Huhma, H., Kinny, P. D., Williams, I. S., 1993: Svecofennian detrital zircon ages—implications for the Precambrian evolution of the Baltic Shield. Precambrian Research, 64, 109-130.

Corfu, F., Hanchar, J.M., Hoskin, P., Kinny, P. 2003: Atlas of zircon textures. Reviews in mineralogy and geochemistry, 53, 469-500

Ehlers, C., Lindroos, A., Selonen, O. 1993: The late Svecofennian granite-migmatite zone of southern Finland—a belt of transpressive deformation and granite emplacement. Precambrian Research, 64, 295-309.

Eilu, P., Sorjonen-Ward, P., Nurmi, P., Niiranen, T. 2003: A review of gold mineralisation styles in Finland. Economic Geology, 98, 1329-1353.

Fossen, H. 2010: Structural geology. Cambridge University Press. Cambridge. 463 pp.

Gaboury, D. 2013: Does gold in orogenic deposits come from pyrite in deeply buried carbon-rich sediments? Insight from volatiles in fluid inclusions. Geology, 41, 1207-1210.

Gebre-Mariam, M., Hagemann, S. G., Groves, D. I. 1995: A classification scheme for epigenetic Archaean lode-gold deposits. Mineralium Deposita, 30, 408-410.

Goldfarb, R. J., & Groves, D. I. 2015: Orogenic gold: Common or evolving fluid and metal sources through time. Lithos, 233, 2-26.

Goldfarb, R. J., Groves, D. I., Gardoll, S. 2001: Orogenic gold and geologic time: a global synthesis. Ore Geology Reviews, 18, 1-75.

Goldfarb, R. J., Phillips, G. N., Nokleberg, W. J. 1998: Tectonic setting of synorogenic gold deposits of the Pacific Rim. Ore Geology Reviews, 13, 185-218.

Gorbatschev, R. & Bogdanova, S. 1993: Frontiers in the Baltic Shield. Precambrian Research, 64, 3-21

Groves, D. I. 1993: The crustal continuum model for late-Archaean lode-gold deposits of the Yilgarn Block, Western Australia. Mineralium deposita, 28, 366-374.

Groves, D. I., Goldfarb, R. J., Gebre-Mariam, M., Hagemann, S. G., Robert, F. 1998: Orogenic gold deposits: a proposed classification in the context of their crustal distribution and relationship to other gold deposit types. Ore Geology Reviews, 13, 7-27.

Hermansson, T., Stephens, M. B., Corfu, F., Page, L. M., Andersson, J. 2008: Migratory tectonic switching, western Svecofennian orogen, central Sweden: Constraints from U/Pb zircon and titanite geochronology. Precambrian Research, 161, 250-278.

Hodgson, C. J., Chapman, R. S. G., MacGeehan, P. J. 1982: Application of exploration criteria for gold deposits in the Superior Province of the Canadian shield to gold exploration in the Cordillera. Precious metals in the Northern Cordillera, 173-206.

Huhma, H., Mänttäri, I., Peltonen, P., Kontinen, A., Halkoaho, T., Hanski, E., Hokkanen, T., Hölttä, P., Juopperi, H., Konnunaho, J., Lahaye, Y., Luukkonen, E., Pietikäinen, K., Pulkkinen, A., Sorjonen-Ward, P., Vaasjoki, P., Whitehouse, M. 2012: The age of the Archaean greenstone belts in Finland. Geological Survey of Finland, Special Paper, 54, 74-175.

Hölttä, P. & Heilimo, E. 2017: Metamorphic Map of Finland. Bedrock of Finland at the scale 1:1000 000 – Major stratigraphic units, metamorphism and tectonic evolution. Geological Survey of Finland, Special Paper, 60, 77-128.

Kearey, P., Klepeis, K.A., Vine, F.J. 2009: Global Tectonics. Wiley-Blackwell. Oxford. 482 pp.

Korsman, K., Koistinen, T., Kohonen, J., Wennerström, M., Ekdahl, E., Honkamo, M., Idman, H., Pekkala, Y. 1997: Suomen kallioperäkartta–Berggrundskarta över Finland–Bedrock map of Finland. Geological Survey of Finland, Espoo, Finland.

Kähkönen, Y. 2005: Chapter 8: Svecofennian supracrustal rocks. In: Lehtinen, M., Nurmi, E.A. The Precambrian Geology of Finland- Key to the Evolution of the Fennoscandian Shield. Elsevier B.V., Amsterdam, 343–405.

Kärkkäinen, N., Huhta, P., Al-Ani, T. 2015: Uunimäen kultaesiintymän malmimineralogia. Geological Survey of Finland, archive report 76, 15p.

Kärkkäinen, N., Koistinen, E., Huotari-Halkosaari, T., Kuusela, J., Muhammad, S., Huhta, P. 2016: Uunimäki gold prospect, Huittinen, Southwest Finland. Geological Survey of Finland, archive report 77, 55p.

Kärkkäinen, N., Koistinen, E. and Jokinen, T. 2006: Satulinmäki Gold Prospect at Somero SW Finland. Geological Survey of Finland, archive report M19/2024/2006/1/10, 44 p.

Kärkkäinen, N. & Tiainen, M. 2016: Hydroterminen muuttuminen Hämeen kallioperässä, Geological Survey of Finland, archive report 60, 42p.

Lahtinen, R., & Huhma, H. 1997: Isotopic and geochemical constraints on the evolution of the 1.93-1.79 Ga Svecofennian crust and mantle in Finland. Precambrian Research, 82, 13-34.

Lahtinen, R., Huhma, H., Sipilä, P., Vaarma, M. 2017: Geochemistry, U-Pb geochronology and Sm-Nd data from the Paleoproterozoic Western Finland supersuite–A key component in the coupled Bothnian oroclines. Precambrian Research, 299, 264-281.

Lahtinen, R., Korja, A., Nironen, M. 2005: Chapter 11: Paleoproterozoic tectonic evolution. In: Lehtinen, M., Nurmi, E.A. The Precambrian Geology of Finland- Key to the Evolution of the Fennoscandian Shield. Elsevier B.V., Amsterdam, 481-531.

Ludwig, K.R. 2003: User's manual for Isoplot/Ex, Version 3.00. A geochronological toolkit for Microsoft Excel. Berkeley Geochronology Center Special Publication 4, 75p.

McCuaig, T. C. & Kerrich, R. 1998: P—T—t—deformation—fluid characteristics of lode gold deposits: evidence from alteration systematics. Ore Geology Reviews, 12, 381-453.

Mertanen, S. & Karell, F. 2011: Rock magnetic investigations constraining relative timing for gold deposits in Finland. Bulletin of the Geological Society of Finland, 83, 75-94.

Mertanen, S. & Karell, F. 2012: Paleomagnetic and AMS studies on Satulinmäki and Koijärvi fault and shearzones. Gold in Southern Finland: Results of GTK Studies 1998-2011. Geological Survey of Finland, Special Paper, 52, 195-226.

Middlemost, E. A. 1994: Naming materials in the magma/igneous rock system. Earth-Science Reviews, 37, 215–224.

Mikkola, P., Heilimo, E., Luukas, J., Kousa, J., Aatos, S., Makkonen, H., Hokka, J. 2018. Geological evolution and structure along the southeastern border of the Central Finland Granitoid Complex. Development of the Paleoproterozoic Svecofennian orogeny: new constraints from the southeastern boundary of the Central Finland Granitoid Complex. Geological Survey of Finland Bulletin, 407.

Mikucki, E. J. 1998. Hydrothermal transport and depositional processes in Archean lode-gold systems: A review. Ore Geology Reviews, 13, 307–321.

Mäkitie, H., Kärkkäinen, N., Sipilä, P., Tiainen, M., Kujala, H., Klami, J. 2016: Hämeen vyöhykkeen granitoidien luokittelua. Geological Survey of Finland, archive report 33. 146p.

Nironen, M. 2017: Guide to the geological map of Finland – Bedrock 1:1 000 000. Geological Survey of Finland, Special Paper, 60, 41-76.

Nironen, M. 1999: Structural and magmatic evolution in the Loimaa area, southwestern Finland. Bulletin of the Geological Society of Finland, 71, 57-71.

Nironen, M., Kousa, J., Luukas, J., Lahtinen, R. 2016: Geological Map of Finland – Bedrock 1:1 000 000. Geological Survey of Finland.

Pearce, J. A. 1996: A user's guide to basalt discrimination diagrams. Trace element geochemistry of volcanic rocks: applications for massive sulphide exploration. Geological Association of Canada, Short Course Notes, 12, 79-113.

Pearce, J. A. 2008: Geochemical fingerprinting of oceanic basalts with applications to ophiolite classification and the search for Archean oceanic crust. Lithos, 100, 14-48.

Pearce, J. A. 1983: Role of the sub-continental lithosphere in magma genesis at active continental margins. Continental Basalts and Mantle Xenoliths, 230-249.

Peccerillo, A., Taylor, S.R. 1976: Geochemistry of Eocene calc-alkaline volcanic rocks from the Kastamonu area, northern Turkey. Contributions to Mineralogy and Petrology, 58, 63-81.

Peltonen, P. 2005: Chapter 9: Svecofennian mafic-ultramafic intrusions. In: Lehtinen, M., Nurmi, E.A. The Precambrian Geology of Finland- Key to the Evolution of the Fennoscandian Shield. Elsevier B.V., Amsterdam, 407-442.

Phillips, G. N., & Powell, R. 2010: Formation of gold deposits: a metamorphic devolatilization model. Journal of Metamorphic Geology, 28, 689-718.

Pietikäinen, K. J., 1994: The geology of the Paleoproterozoic Pori shear zone, Southwestern Finland, with special reference to the evolution of veined gneisses from tonalitic protoliths. Ph.D. thesis, Michigan Technological University. 129 pp.

Rasilainen, K. & Eilu, P. 2016: Assessment of undiscovered mineral resources of copper, zinc, nickel and gold for the Häme Belt. Geological Survey of Finland, archive report, 94. 58 pp.

Reimers, S., Engström, J., Riller, U. 2018: The Kynsikangas shear zone, Southwest Finland: Importance for understanding deformation kinematics and rheology of lower crustal shear zones. Lithosphere 2018: Tenth Symposium on Structure, Composition and Evolution of the Lithosphere. Programme and Extended Abstracts, Turku, Finland, Nov. 14^{th}-16^{th}. Institute of Seismology, University of Helsinki, Report S-62. 95-99.

Robb, L. 2005: Introduction to ore-forming processes. Blackwell Publishing Ltd. Oxford. 345 pp.

Saalmann, K. 2007: Structural control on gold mineralization in the Satulinmäki and Riukka prospects, Häme Schist Belt, southern Finland. Bulletin of the Geological Society of Finland, 79, 69-93.

Saalmann, K., Mänttäri, I., Peltonen, P., Whitehouse, M. J., Grönholm, P., Talikka, M. 2010: Geochronology and structural relationships of mesothermal gold mineralisation in the Palaeoproterozoic Jokisivu prospect, southern Finland. Geological Magazine 147, 551-569.

Saalmann, K., Mänttäri, I., Ruffet, G., Whitehouse, M. J. 2009: Age and tectonic framework of structurally controlled Palaeoproterozoic gold mineralisation in the Häme Belt of southern Finland. Precambrian Research, 174, 53-77.

Shand, S.J. 1943: Eruptive rocks: their genesis, composition, and classification, with a chapter on meteorites. Wiley, New York, 444 pp.

Sibson, R. H., Robert, F., Poulsen K. H. 1988: High-angle reverse faults, fluid-pressure cycling, and mesothermal gold-quartz deposits. Geology, 16, 551-555.

Sipilä, P., Kujala, H. 2014: Hämeen vyöhykkeen vulkaniittien geokemia. Geological Survey of Finland, archive report 119, 23 p.

Sipiä, P., Mattila, J., Tiainen, M. 2011: Pirkanmaan vyöhykkeen ja Hämeen vyöhykkeen välinen terraanirajatulkinta. Geological Survey of Finland archive report, 2/2011, 27p.

Smith, I. E., Worthington, T. J., Price, R. C., Gamble, J. A. 1997: Primitive magmas in arc-type volcanic associations; examples from the Southwest Pacific. The Canadian Mineralogist, 35, 257-273.

Stipp, M., Stünitz, H., Heilbronner, R., Schmid, S. M. 2002: The eastern Tonale fault zone: a 'natural laboratory'for crystal plastic deformation of quartz over a temperature range from 250 to 700 C. Journal of Structural Geology, 24, 1861-1884.

Tiainen, M., Kujala, S., Ahtola, T., Eilu, P., Grönholm, S., Hakala, O., Istolahti, P., Jumppanen, A., Kärkkäinen, N., Rasilainen, K., Törmä, H. 2017: Summary: Regional economic impacts of potential mining in Kanta-Häme. Geological Survey of Finland research report, 229, 126p.

Tomkins, A.G. 2013: On the source of orogenic gold. Geology, 41, 1255-1256.

Vaasjoki, M., Korsman, K., Koistinen, T., 2005: Chapter 1: Overview. In: Lehtinen, M., Nurmi, E.A. The Precambrian Geology of Finland- Key to the Evolution of the Fennoscandian Shield. Elsevier B.V., Amsterdam, 1-18.

Van Achterbergh, E., Ryan C., Jackson, S., Griffin W., 2001: Data reduction software for LA-ICP-MS, In: Laser-Ablation ICPMS in the Earth Sciences–Principles and applications. Mineralogical Association of Canada short course series, 29, St John, Newfoundland, 239-243.

Voipio, T. 2008: Huittisten Palokallion petrografia, malmimineralogia ja geokemia. MSc Thesis, University of Helsinki. 80 pp.

Väisänen, M. 2002: Tectonic Evolution of the Palaeoproterozoic Svecofennian Orogen in Southwestern Finland. Annales Universitatis Turkuensis, A II, 154, 143 p.

Väisänen, M., Mänttäri, I., Kriegsman, L. M., Hölttä P. 2000: Tectonic setting of postcollisional magmatism in the Palaeoproterozoic Svecofennian Orogen, SW Finland. Lithos, 54, 63-81.

Väisänen, M. & Skyttä, P. 2007: Late Svecofennian shear zones in southwestern Finland. GFF, 129, 55-64.

Väisänen, M. & Westerlund, G. 2007: Palaeoproterozoic mafic and intermediate metavolcanic rocks in the Turku area, SW Finland. Bulletin of the Geological Society of Finland, 79, 127-141.

Wood, D. A., Joron, J. L., Treuil, M. 1979: A re-appraisal of the use of trace elements to classify and discriminate between magma series erupted in different tectonic settings. Earth and Planetary Science Letters, 45, 326-336.

Wyman, D. A., Kerrich, R., Polat, A. 2002: Assembly of Archean cratonic mantle lithosphere and crust: plume–arc interaction in the Abitibi–Wawa subduction–accretion complex. Precambrian Research, 115, 37-62.

Appendix 1. Geochemical analysis results.

Sample	SiO2	Al2O3	Fe2O3	MgO	CaO	Na2O	K2O	TiO2	P2O5	MnO	Cr2O3	Ba	Sc	LOI	Be	Co	Cs	Ga	Hf	Nb	Rb	Sn	Sr	Ta	Th	U	V	W	Zr	Y	As	Au (ppb
IJPI-2017-159.1	59.61	17.25	9.47	1.67	5.9	1.32	1.78	0.71	0.29	0.22	<0.002	390	8	1.6	<1	11.2	5.1	20.1	5.2	15.6	65.4	<1	402.6	0.9	2.2	1.9	31	<0.5	195.8	23.1	12.3	9.7
IJPI-2017-159.2	50.77	17.39	12.15	4.54	8.44	2.64	1.35	1.36	0.21	0.2	0.005	266	25	0.8	<1	29.6	2.5	18.5	3	8.9	42.5	2	302.7	0.7	1.4	1.2	233	1.8	114.1	21.3	65.8	4.2
JKKA-2017-26.1	51.95	18.19	10.69	4.02	8.5	2.76	1.25	1.32	0.23	0.16	0.004	209	25	0.8	<1	26.7	1.7	19.1	2.8	8.4	38.6	1	258.6	0.6	2.2	1.5	235	2.2	88.3	20.3	2.4	58.2
JKKA-2017-26.2	54.8	16.86	10.79	3.53	6.87	3.19	1.65	1.2	0.22	0.17	0.004	317	24	0.5	<1	23.6	2	20.7	5.6	20	49.8	2	261.8	1.2	4.6	2.4	187	1.4	217.8	30.2	2.5	9
JKKA-2017-26.3	56.45	17.16	9.74	3.1	6.4	3.44	1.5	0.97	0.22	0.15	0.003	339	17	0.7	6	22.8	1.8	19.1	6.7	20.4	45.2	1	291.5	1.3	3.6	1.8	123	1.1	258.3	30.9	41.9	4.2
JKKA-2017-27.1	52.7	17.89	11.43	4.04	8.35	3.23	0.49	1.1	0.18	0.19	0.004	112	26	0.2	2	26.3	0.5	18.6	2.7	15.6	9.6	<1	298.1	1.1	1.3	1.2	219	1	118.8	17.2	6.9	13.7
JKKA-2017-27.2	56.25	18.61	9.62	2.69	7.05	3.32	0.71	0.94	0.3	0.23	0.002	177	14	0.1	<1	16.2	1.2	18.9	4.8	26.7	19.8	<1	321.8	1.7	3.8	1.8	70	<0.5	207.6	17.4	2.4	3.3
TALE-2017-107.1	48.33	18.68	11.59	4.67	9.93	3.16	0.49	1.78	0.22	0.17	0.003	268	31	0.7	<1	27.4	0.7	21.2	2	9.7	9.6	<1	435.3	0.6	0.2	0.4	319	<0.5	73.3	21.7	81.8	5.4
TALE-2017-108.1	48.33	17.23	13.59	4.91	9.65	2.85	0.62	1.92	0.23	0.2	0.002	241	32	0.2	<1	38.6	0.9	21.3	3.2	11.2	8.9	<1	358.3	0.7	0.5	0.4	360	<0.5	113.2	27.7	0.9	5.5
TALE-2017-117.1	48.75	17.89	12.73	4.7	9.39	3.08	0.56	1.68	0.25	0.22	<0.002	173	31	0.5	<1	32.4	1.9	20.8	2.9	11.7	7	1	423.9	0.5	0.3	0.3	294	0.7	112.1	25.4	2.1	8.5
TALE-2017-12.1	56.99	19.67	8.49	2.14	4.64	3.86	2.45	0.72	0.27	0.16	<0.002	484	12	0.4	5	15.5	7.6	24.8	6.2	17.4	115.6	3	315.9	2.1	1.6	2.2	77	0.9	240.9	31.9	1.6	8.8
TALE-2017-129.1	48.03	16.86	13.97	5.24	9.41	2.64	0.78	1.88	0.29	0.22	0.004	212	34	0.4	<1	37.3	2.1	22.3	2	10.6	15.2	<1	362.5	0.7	0.6	0.6	333	0.6	59.3	24.8	13.6	5.6
TALE-2017-14.1	58.84	15.35	8.62	4.4	5.17	3.03	2.48	0.98	0.22	0.14	0.018	424	20	0.5	2	24.5	9.3	19.3	4	42.9	127.4	3	370.7	0.9	5	1.9	139	0.6	167.4	15.3	1.5	0.9
TALE-2017-16.1	48.04	16.93	13.76	5.29	9.67	2.64	0.63	1.85	0.22	0.21	0.004	192	37	0.5	<1	35	4	22.3	3.2	9.7	15.7	5	345.3	0.5	0.5	0.6	370	1	122.4	26.2	2	<0.5
TALE-2017-17.1	50.02	17.63	12.36	4.52	9.48	2.85	0.58	1.45	0.28	0.21	0.004	173	25	0.4	<1	30.6	6.9	21.3	2.9	9.4	16.1	1	455.2	0.5	0.9	0.5	257	<0.5	124.5	19.2	1.1	1.3
TALE-2017-18.1	63.68	16.12	7.77	3.66	1.49	2.05	1.85	0.78	0.08	0.06	0.022	405	18	2.2	<1	15.9	2.6	20	4.6	6.3	64.1	<1	253.8	0.5	12.3	2.2	179	1.6	165.7	10.4	1.2	1.2
TALE-2017-182.1	62.56	15.3	7.1	3.44	4.6	2.81	2.14	0.73	0.18	0.09	0.019	574	14	0.8	<1	15.8	3.8	20	4.8	9.6	78.3	1	535.9	0.7	3.4	1.7	114	<0.5	182.7	13.3	1.9	<0.5
TALE-2017-182.2	51.57	17.73	11.65	4.16	8.4	2.97	1.2	1.3	0.19	0.19	0.003	291	26	0.4	<1	26.6	2.4	21.4	3.6	10.8	36.8	2	345.1	1.2	8.7	1.5	256	<0.5	115.7	23.9	1.9	<0.5
TALE-2017-72.1	59.16	16.28	8.28	3.43	5.09	3.06	2.42	1.12	0.23	0.12	0.012	532	18	0.6	3	17.8	4.3	19.5	4.7	13.6	85.3	<1	326.5	0.8	4.5	2.1	134	0.8	188.4	18	1.7	0.9
TALE-2017-79.1	60.14	17.84	6.15	2.43	6.21	3.97	1.67	0.64	0.12	0.09	0.006	460	14	0.5	<1	16.8	1.6	19.2	4.8	10.9	48.7	<1	421.3	0.5	6.1	1.5	105	<0.5	192.9	16.2	2.61	<0.5

Sample	La	Ce	Pr	Nd	Sm	Eu	Gd	Tb	Dy	Ho	Er	Tm	Yb	Lu	F	Mo	Cu	Pb	Zn	Ag	Ni	Cd	Sb	Bi	Cr	B	Na	Hg	Tl	S	Se	Te
IJPI-2017-159.1	23.6	54.4	6.7	27.2	5.69	1.62	4.71	0.73	4.08	0.82	2.3	0.32	2.17	0.34	485	1.1	64.5	4.1	109	0.2	3.4	<0.1	<0.1	0.1	6	<20	0.66	<0.01	0.2	0.79	1.1	<0.2
IJPI-2017-159.2	13.1	29.3	3.75	17.5	3.91	1.31	3.94	0.69	3.92	0.82	2.26	0.29	2.16	0.33	627	0.6	28.3	9.2	55	<0.1	15.5	<0.1	<0.1	<0.1	14	<20	2070	<0.01	0.2	0.06	<0.5	<0.2
JKKA-2017-26.1	13.8	29.5	3.62	16.3	3.77	1.08	3.8	0.62	3.6	0.78	2.09	0.31	1.9	0.29	273	0.9	64.6	3.1	37	0.1	11.2	<0.1	<0.1	0.1	10	<20	0.267	<0.01	0.1	0.1	<0.5	<0.2
JKKA-2017-26.2	26.8	56.5	6.8	27.6	5.73	1.58	5.63	0.9	5.42	1.12	3.14	0.43	3.01	0.48	459	1.3	20.6	50.9	66	<0.1	13	0.1	<0.1	<0.1	16	<20	0.148	<0.01	0.3	<0.05	<0.5	<0.2
JKKA-2017-26.3	25.9	55.7	6.9	29	6.21	1.59	6.12	0.96	5.69	1.19	3.44	0.46	3.08	0.49	359	1.6	9.1	2.5	71	<0.1	13.1	<0.1	<0.1	<0.1	12	<20	0.17	<0.01	0.2	<0.05	<0.5	<0.2
JKKA-2017-27.1	12.5	26.9	3.28	13.9	2.87	1.37	3.15	0.48	3	0.67	2.02	0.26	1.88	0.29	260	0.9	114.6	51.1	34	<0.1	13	<0.1	0.1	<0.1	12	<20	0.22	<0.01	<0.1	0.21	<0.5	<0.2
JKKA-2017-27.2	23.3	43.8	4.7	18.2	3.53	1.33	3.58	0.54	3.2	0.65	2.17	0.29	2	0.34	236	0.8	25.2	2.5	43	<0.1	5.5	<0.1	<0.1	<0.1	8	<20	0.217	<0.01	<0.1	<0.05	<0.5	<0.2
TALE-2017-107.1	10.2	23.1	3.3	15.2	3.76	1.5	4.3	0.67	3.8	0.8	2.3	0.29	1.9	0.28	307	0.4	278.4	1.5	33	0.1	8.6	<0.1	0.1	0.1	10	<20	4370	<0.01	0.1	<0.05	<0.5	<0.2
TALE-2017-108.1	13.9	34.2	4.68	21.5	5.24	1.66	5.86	0.91	5.42	1.11	3.02	0.42	2.64	0.4	432	0.5	125.1	6.8	41	<0.1	7.1	<0.1	<0.1	<0.1	9	<20	4670	<0.01	<0.1	<0.05	<0.5	<0.2
TALE-2017-117.1	14.5	33.3	4.57	21.8	5.41	1.75	5.57	0.86	5.17	1.02	2.76	0.36	2.35	0.36	345	0.2	95.2	1	76	<0.1	5	0.2	<0.1	<0.1	5	<20	3740	<0.01	<0.1	<0.05	<0.5	<0.2
TALE-2017-12.1	15.2	29.7	3.73	15.3	3.74	1.3	4.53	0.78	4.98	1.13	4.09	0.6	4.66	0.8	442	0.6	19.6	10.4	104	<0.1	9.3	<0.1	<0.1	0.1	11	<20	0.131	<0.01	0.7	<0.05	<0.5	<0.2
TALE-2017-129.1	12.8	27.9	4.08	18.8	4.95	1.82	5.36	0.83	4.75	0.98	2.69	0.34	2.23	0.34	257	0.3	71.8	6.5	43	<0.1	8	<0.1	0.1	<0.1	9	<20	3310	<0.01	<0.1	<0.05	<0.5	<0.2
TALE-2017-14.1	24.3	50.2	5.88	23.6	4.13	1.17	3.84	0.51	2.84	0.54	1.64	0.23	1.52	0.22	820	1.2	20.1	3.1	99	<0.1	41.4	<0.1	<0.1	0.4	106	<20	0.157	<0.01	<0.1	<0.05	<0.5	<0.2
TALE-2017-16.1	13.1	31.4	4.35	21.1	5.08	1.56	5.67	0.87	5.15	1.02	2.91	0.4	2.59	0.38	316	0.6	79.9	9.1	34	<0.1	9.2	<0.1	0.1	<0.1	11	<20	3760	<0.01	<0.1	<0.05	<0.5	<0.2
TALE-2017-17.1	13.5	29.7	4.09	19.2	4.22	1.54	4.28	0.63	3.85	0.76	2.06	0.3	1.92	0.29	330	0.5	19.6	1.4	39	<0.1	8.9	<0.1	<0.1	<0.1	13	<20	3780	<0.01	0.1	<0.05	<0.5	<0.2
TALE-2017-18.1	18.7	38.5	4.35	15.5	2.92	0.95	2.4	0.36	2	0.39	1.11	0.16	1	0.16	539	0.8	134.1	9.9	47	<0.1	20.3	<0.1	<0.1	<0.1	58	38	0.058	<0.01	0.1	<0.05	<0.5	<0.2
TALE-2017-182.1	9	21	2.78	12.2	3.1	1.06	2.97	0.43	2.53	0.49	1.4	0.17	1.27	0.17	554	1.7	33.3	4	81	<0.1	42.3	<0.1	<0.1	<0.1	118	<20	0.347	<0.01	0.2	<0.05	<0.5	<0.2
TALE-2017-182.2	17.4	39.1	4.58	19.3	4.54	1.39	4.79	0.77	4.74	0.98	2.61	0.37	2.46	0.38	293	0.4	32.6	2.8	60	<0.1	9.2	<0.1	<0.1	0.1	14	<20	3570	<0.01	0.2	<0.05	<0.5	<0.2
TALE-2017-72.1	17.1	37.8	4.73	19.8	4.11	1.31	3.92	0.56	3.47	0.7	1.95	0.28	1.86	0.27	466	1.4	28.5	3.3	85	<0.1	17.2	<0.1	<0.1	<0.1	73	<20	0.192	<0.01	0.5	<0.05	<0.5	<0.2
TALE-2017-79.1	22.7	42.4	4.89	18.7	3.32	1.06	3.4	0.49	2.94	0.57	1.83	0.23	1.61	0.25	456	0.8	12.4	8.9	40	<0.1	11.7	<0.1	<0.1	<0.1	25	<20	0.145	<0.1	0.2	<0.05	<0.5	<0.2

Appendix 2. U-Pb dating analysis results.

file	sample	comment	Pb^{206}/Pb^{204}	Pb	Th	U	207Pb/206Pb	1s	207Pb/235U	1s	206Pb/238U	1s	r	Concordanc	207Pb/206Pb	1s	207Pb/235U	1s	206Pb/238U	1s
41555_TRA_Data	41555	Uunimaki-158	4023	89	90	203	0.1122	0.0009	5.376	0.145	0.348	0.009	0.96	102	1835	14	1881	23	1923	44
41521_TRA_Data	41521	Uunimaki-125	297007	98	105	239	0.1161	0.0009	5.157	0.139	0.322	0.009	0.96	98	1896	14	1846	23	1801	42
41498_TRA_Data	41498	Uunimaki-19	381966	126	130	302	0.1158	0.0009	5.194	0.140	0.325	0.009	0.96	98	1893	14	1852	23	1815	42
41501_TRA_Data	41501	Uunimaki-26	424963	141	165	336	0.1163	0.0009	5.225	0.141	0.326	0.009	0.96	98	1901	14	1857	23	1818	42
41553_TRA_Data	41553	Uunimaki-156a	308427	101	114	250	0.1157	0.0009	5.168	0.140	0.324	0.009	0.96	98	1891	14	1847	23	1809	42
41518_TRA_Data	41518	Uunimaki-41	389540	130	157	312	0.1157	0.0009	5.162	0.139	0.324	0.009	0.96	98	1890	14	1846	23	1808	42
41504_TRA_Data	41504	Uunimaki-71	275403	92	108	219	0.1164	0.0009	5.214	0.141	0.325	0.009	0.96	98	1902	14	1855	23	1814	42
41522_TRA_Data	41522	Uunimaki-127	4359	163	213	383	0.1139	0.0009	5.126	0.138	0.327	0.009	0.96	99	1862	14	1840	23	1822	42
41523_TRA_Data	41523	Uunimaki-130	8065	137	160	326	0.1141	0.0009	5.148	0.139	0.327	0.009	0.96	99	1866	14	1844	23	1825	43
41505_TRA_Data	41505	Uunimaki-62	2801	92	101	221	0.1128	0.0009	5.019	0.135	0.323	0.009	0.96	99	1845	14	1822	23	1803	42
41496_TRA_Data	41496	Uunimaki-2	379008	124	107	271	0.1159	0.0009	5.742	0.155	0.359	0.010	0.96	102	1894	14	1938	23	1979	46
41497_TRA_Data	41497	Uunimaki-10	397501	132	134	310	0.1176	0.0009	5.354	0.144	0.330	0.009	0.96	98	1920	14	1878	23	1839	43
41499_TRA_Data	41499	Uunimaki-21	272031	89	88	213	0.1157	0.0009	5.242	0.142	0.329	0.009	0.96	99	1891	14	1859	23	1832	43
41500_TRA_Data	41500	Uunimaki-22	362269	121	136	285	0.1168	0.0009	5.269	0.142	0.327	0.009	0.96	98	1908	14	1864	23	1825	43
41502_TRA_Data	41502	Uunimaki-31	5711	112	143	257	0.1147	0.0009	5.230	0.141	0.331	0.009	0.96	99	1875	14	1858	23	1842	43
41503_TRA_Data	41503	Uunimaki-72	455659	149	148	351	0.1157	0.0009	5.334	0.144	0.334	0.009	0.96	99	1891	14	1874	23	1860	43
41514_TRA_Data	41514	Uunimaki-52	279106	92	81	204	0.1157	0.0009	5.647	0.152	0.354	0.009	0.96	102	1891	14	1923	23	1953	45
41515_TRA_Data	41515	Uunimaki-48	5711	167	168	378	0.1137	0.0009	5.438	0.147	0.347	0.009	0.96	102	1859	14	1891	23	1920	44
41516_TRA_Data	41516	Uunimaki-46	436204	142	130	331	0.1159	0.0009	5.458	0.147	0.341	0.009	0.96	100	1894	14	1894	23	1894	44
41517_TRA_Data	41517	Uunimaki-43	1092227	363	411	788	0.1160	0.0009	5.746	0.155	0.359	0.010	0.96	102	1895	13	1938	23	1979	46
41519_TRA_Data	41519	Uunimaki-123	269845	88	87	208	0.1162	0.0009	5.381	0.145	0.336	0.009	0.96	99	1899	14	1882	23	1867	43
41520_TRA_Data	41520	Uunimaki-124	975018	327	393	711	0.1166	0.0009	5.724	0.154	0.356	0.010	0.96	101	1905	13	1935	23	1963	45
41532_TRA_Data	41532	Uunimaki-134	7635	238	304	537	0.1141	0.0009	5.408	0.146	0.344	0.009	0.96	101	1866	14	1886	23	1905	44
41533_TRA_Data	41533	Uunimaki-137	843712	279	307	639	0.1164	0.0009	5.522	0.149	0.344	0.009	0.96	100	1901	13	1904	23	1906	44
41534_TRA_Data	41534	Uunimaki-93	290804	94	86	232	0.1174	0.0009	5.299	0.143	0.327	0.009	0.96	98	1917	14	1869	23	1826	43
41535_TRA_Data	41535	Uunimaki-98	398355	131	129	299	0.1152	0.0009	5.517	0.149	0.347	0.009	0.96	101	1882	14	1903	23	1922	44
41536_TRA_Data	41536	Uunimaki-104	279783	91	97	219	0.1138	0.0009	5.223	0.141	0.333	0.009	0.96	100	1860	14	1856	23	1853	43
41537_TRA_Data	41537	Uunimaki-146	356016	118	128	276	0.1158	0.0009	5.382	0.145	0.337	0.009	0.96	99	1893	14	1882	23	1872	43
41538_TRA_Data	41538	Uunimaki-147	262298	86	89	206	0.1160	0.0009	5.317	0.144	0.333	0.009	0.96	99	1895	14	1872	23	1851	43
41539_TRA_Data	41539	Uunimaki-148a	427699	143	179	342	0.1162	0.0009	5.230	0.141	0.327	0.009	0.96	98	1898	14	1857	23	1821	42
41540_TRA_Data	41540	Uunimaki-148b	401763	134	162	321	0.1148	0.0009	5.183	0.140	0.327	0.009	0.96	99	1877	14	1850	23	1826	43
41541_TRA_Data	41541	Uunimaki-149	272563	88	80	219	0.1169	0.0009	5.241	0.141	0.325	0.009	0.96	98	1909	14	1859	23	1815	42
41552_TRA_Data	41552	Uunimaki-151	389584	129	154	310	0.1153	0.0009	5.247	0.141	0.330	0.009	0.96	99	1885	14	1860	23	1838	43
41554_TRA_Data	41554	Uunimaki-156b	4103	136	131	319	0.1154	0.0009	5.417	0.146	0.340	0.009	0.96	100	1887	14	1888	23	1888	44